

Catalytic membrane reactor-separator for environmental applications.

KAJAMA, M.N.

2016

The author of this thesis retains the right to be identified as such on any occasion in which content from this thesis is referenced or re-used. The licence under which this thesis is distributed applies to the text and any original images only – re-use of any third-party content must still be cleared with the original copyright holder.

Catalytic Membrane Reactor-Separator for Environmental Applications

Mohammed Nasir KAJAMA

A thesis submitted in partial fulfilment of the
requirements of the
Robert Gordon University
for the degree of Doctor of Philosophy

April 2016

Originality Statement

‘I hereby declare that this submission is my own work and to the best of my knowledge it contains no materials previously published or written by another person, or substantial proportions of material which have been accepted for the award of any other degree or diploma at the Robert Gordon University Aberdeen or any other educational institution, except where due acknowledgement is made in the thesis. Any contribution made to the research by others, with whom I have worked at RGU or elsewhere, is explicitly acknowledged in the thesis. I also declare that the intellectual content of this thesis is the product of my own work.’

Dedication

I would like to dedicate this work to Almighty Allah. My parents, and to my beloved wife, Maryam Mohammed Nasir, and my two little kids, Faadil (Kajiyama Mohammed Nasir) and Saabir (Mohammed-Sa'ad Mohammed Nasir).

Acknowledgement

First of all, I would like to express my deepest gratitude to my supervisor Prof. Edward Gobina, for his profound guidance, inspirational support, constructive criticism, and endless injection of both time and energy. His help have been essential to this thesis. It has been under his supervision that I have been allowed to both mature and develop my skills.

I am especially thankful to my colleagues including Dr Abubakar Alkali, Ngozi Nwogu, Habiba Shehu, Edidiong Okon and Ify Orakwe in the Centre for Process Integration and Membrane Technology (CPIMT) for their friendship and making the laboratory such a pleasant place to carry out this work. I would also like to thank Iain Tough, from the School of Pharmacy and life Sciences of RGU for his assistance with SEM and EDX analysis.

My sincere acknowledgements are also due to Bill Walker, Steven Pirie, Alan McLean and David Howie for their ever timely presence where requested for assistance. Special thanks to David Smith and his colleagues at the workshop for their valuable technical assistance.

I would like to acknowledge Petroleum Technology Development Fund (PTDF) for the sponsorship and for making my research experience a rich and beneficial one. I would also like to personally thank Alhaji Ibrahim Tumsah, Alhaji Mohammed Kyari Dikwa, and Yobe State government for the financial assistance, without which I wouldn't have had the opportunity to participate, present and publish my research work.

Finally, I wish to thank my parents for their love and support, and my beloved wife for her love, encouragement and emotional support. I could not have completed the research without them.

Abstract

Flow-through catalytic membrane reactors offer the potential for improved conversions at reduced operating temperature due to product separation and catalyst activity. An experimental work dealing with a forced flow-through membrane reactor is the subject of this thesis. The focus is on the performance and transport characteristics of selective thin supported silica membranes and flow-through catalytic membrane systems. The improvement of VOC-selective, H₂-selective and CO₂-selective membrane properties by the use of systematic dip-coating techniques and the application of the technique in a bi-layer membrane repair concept for gas separation membranes has been studied. In addition, several methods were used to characterize the membranes including scanning electron microscopy, energy diffraction X-ray, nitrogen adsorption, and gas permeation. In the first part of this work CO₂ permeance $3.39 \times 10^{-8} \text{ mol m}^{-2} \text{ s}^{-1} \text{ Pa}^{-1}$ at 25 °C for γ -Al₂O₃ membrane after exposing boehmite to the support was mainly attributed to the Knudsen diffusion mechanism. CO₂/CH₄ selectivity of 24.07 was obtained from silica membrane at 25 °C and 0.7 bar. Such a selectivity value could be useful in small-scale carbon dioxide removal unit for natural gas treatment processes. In addition, H₂/N₂ selectivity of 1.36 and 2.72 at 1 bar were obtained from macro and meso porous membranes at 25 °C. The selectivity of propylene (C₃H₆) over N₂ was also obtained. Higher selectivity of 1.79 at 0.05 bar was obtained. This selectivity increased by a factor of 2 compared to the ideal Knudsen selectivity (0.82).

Remarkable propane conversion of 95.47% on 3.52 wt% platinum (Pt) catalyst at different total flow rates ranging from 166 to 270ml/min was achieved at a temperature of 378 °C. The temperature at which the catalytic combustion takes place for the VOC corroborates if not lower than the one obtained from the literature for the same VOC on 5 wt% Pt/ γ -Al₂O₃ catalysts.

List of Publications and conference proceedings

M. N. Kajama, N. C. Nwogu, E. Gobina. (2016). Catalytic membrane reactor for VOC destruction 1. To be published by Springer (Accepted Book Chapter).

M. N. Kajama, H. Shehu, E. Okon, I. Orakwe, E. Gobina. (2016). VOC oxidation in excess of oxygen using flow-through catalytic membrane reactor. *International Journal of Hydrogen Energy*. doi:10.1016/j.ijhydene.2016.04.164. Accepted on 22/04/2016. (Journal Paper).

Kajama, M., Nwogu, N & Gobina, E. (2016). Preparation and Characterization of Inorganic Membranes for Hydrogen Separation. *International Journal of Hydrogen Energy*, 41(19), 8221-8227. (Journal Paper).

Shehu, H., Okon, E., **Kajama, M. N.** & Gobina, E. (2015). Characterization of Y-type zeolite membrane using the fickian approach for VOC recovery from shuttle tankers, *American International Journal of Research in Science, Technology, Engineering & Mathematics*, 1(11), 19-22. (Journal Paper).

Okon, E., Shehu, H., Nwogu, N., **Kajama, M.**, Orakwe, I. & Gobina, E. (2015). Resin characterization and tubular membrane transport with single gases for ethyl lactate separations for industrial purposes, *Journal of Material Science and Chemical Engineering*. 3(8); 8-14. (Journal Paper).

Nwogu, N. C., **Kajama, M.** & Gobina, E. (2015). A study of gas diffusion characteristics on a micro porous composite silica ceramic membrane. *Composite Structures*. 134, 1044-1050, (Journal Paper).

Kajama, M. N., Nwogu, N. C., Okon, E. O., Shehu, H., Orakwe, I. & Gobina, E. (2015). Hydrogen separation using Pt-alumina impregnated membrane. *Energy and Power Engineering*, 7, 412-417. (Journal Paper).

Nwogu, N. C., **Kajama, M. N.**, Orakwe, I. & Gobina, E. (2015). High molecular permeance dual-layer ceramic membrane for capturing CO₂ from flue gas stream. *Energy and Power Engineering*, 7, 418-425. (Journal Paper).

Nwogu, N. C., **Kajama, M. N.**, Osueke, G. & Gobina, E. (2015). Structural characteristic and permeation of gases through a supported silica inorganic ceramic membrane, *In Proceedings of The World Congress on Engineering*, (1), 245-248. (Proceedings).

Nwogu, N. C., **Kajama, M. N.**, Osueke, G. & Gobina, E. (2015). High performance valuation of CO₂ gas separation ceramic membrane system, *In Proceedings of The World Congress on Engineering*, (2), 824-827. (Proceedings).

Okon, E., Shehu, H., **Kajama, M.**, Adesola, O., Nwogu, N., Orakwe, I. & Gobina, E. (2015). Hydrodynamic Performance in Mesoporous Silica Membrane for Lactic Acid and Esterification. *In Proceedings of The World Congress on Engineering*, (2), 781-784. (Proceedings).

Orakwe, I. R., Nwogu, N. C., **Kajama, M.**, Shehu, H., Okon, E. & Gobina, E. (2015). An initial study of single gas permeation using a commercial alumina membrane. *In Proceedings of The World Congress on Engineering*, (2), 737-739. (Proceedings).

Kajama, M., Nwogu, N. & Gobina, E. (2015). Propylene oxidation using Pt-alumina impregnated catalytic membrane reactor. *In Proceedings of The World Congress on Engineering*, (2), 900-903. (Proceedings).

Nwogu, N., **Kajama, M.** & Gobina, E. (2015). Performance evaluation of an inventive CO₂ gas separation inorganic ceramic membrane. *International Journal of Chemical, Molecular, Nuclear, Materials and Metallurgical Engineering*, 9(6), 568-571. (Proceedings).

Kajama, M. N., Nwogu, N. C. & Gobina, E. (2015). Volatile organic compounds destruction by catalytic oxidation for environmental applications. *International Journal of Environmental, Chemical, Ecological, Geological and Geophysical Engineering*, 9(6), 613-616. (Proceedings).

Kajama, M. N., Shehu, H., Okon, E. & Gobina, E. (2015). Preparation and characterization of inorganic membranes for hydrocarbon separation from N₂ for environmental applications. *Energy and Environment Research*, 5(1) 110-120. (Journal Paper).

Kajama, M. N., Nwogu, N. C. & Gobina, E. (2015). Effect of gas permeation temperature on gamma-alumina ceramic membranes. Presented at the 3rd International Conference on Challenges in Environmental Science and Computer Engineering. 21st–22nd June 2014, London, United Kingdom, - atlantis-press.com (Proceedings).

Kajama, M. N., Nwogu, N. C. & Gobina, E. (2015). Hydrogen permeation using nanostructured silica membranes. In Proceedings Sustainable Development and

Planning VII (Book), WIT Transactions on Ecology and The Environment, 193, pp. 447-456. (Proceedings).

Shehu, H., Okon, E., **Kajama, M.**, Nwogu, N., Orakwe, I. & Gobina, E. (2015). An initial study of the selectivity of methane over carbon dioxide and inert gases using a Y-type zeolite membrane. *International Journal of Current Research*, 7(4), 14986-14990. (Journal Paper).

Okon, E., Shehu, H., **Kajama, M.** & Gobina, E. (2015). Investigation of carrier gas transport through silica membrane for ethyl lactate separation and VOC emission applications. *International Journal of Current Research*, 7(4), 14975-14979. (Journal Paper).

Okon, E., Shehu, H., **Kajama, M.**, Nwogu, N., Orakwe, I. & Gobina, E. (2015). Cation-exchange resin characterisation and carrier gas performance with mesoporous silica membranes for ethyl lactate separation. *International Journal of Engineering Research & Technology*, 4(4), 465-469. (Journal Paper).

Kajama, M. N., Nwogu, N. C. & Gobina, E. (2015). Hydrogen separation using inorganic membranes. *In Proceedings Advanced Materials Research © Trans Tech Publications, Switzerland*, Vol. 1102, 91-94. (Proceedings).

Nwogu, N. C., **Kajama M. N.**, & Gobina, E. (2015). Validation of a novel approach for CO₂/N₂ gas separations by means of a hybrid ceramic membrane. *In Proceedings Advanced Materials Research © Trans Tech Publications, Switzerland*. Vol. 1102, 73-76. (Proceedings).

Kajama, M. N., Nwogu, N. C. & Gobina, E. (2014). Experimental study of carbon dioxide separation with nanoporous ceramic membranes. *In Proceedings Energy and Sustainability V (Book), WIT Transactions on Ecology and The Environment*, Vol. 186, pp. 625-633. (Proceedings).

Okon, E., **Kajama, M. N.** & Gobina, E. (2014). Gas permeation on silica membrane for lactic acid esterification applications. *J. Energy Power Sources*, 1(5), 265-269. (Journal Paper).

Okon, E., **Kajama, M. N.**, Shehu, H., Nwogu, N. & Gobina, E. (2014). Surface area analysis and gas transport properties with inorganic ceramic membranes. *International Journal of Current Research*, 6(11), 9569-9575. (Journal Paper).

Kajama, M. N., Nwogu, N. C. & Gobina, E. (2014). Hydrogen separation using silica-based composite membranes. *In Proceedings Advanced Materials Research © Trans Tech Publications, Switzerland*. Vol. 1051, pp. 107-111. (Proceedings).

Nwogu, N. C., **Kajama M. N.**, Okon, E. P., Shehu, H. & Gobina, E. (2014). Testing of gas permeance techniques of a fabricated CO₂ permeable ceramic membrane for gas separation purposes. *International Journal of Advance Research in Computer Science and Management Studies*. 2(9), 429-436. (Journal Paper).

Nwogu, N. C., **Kajama M. N.**, Okon, E. P., Shehu, H. & Gobina, E. (2014). A novel performance of ordered porous ceramic materials in hydrogen recovery processes for sustainable energy potential. *International Journal of Advance Research in Computer Science and Management Studies*. 2(9), 44-50. (Journal Paper).

Nwogu, N. C., **Kajama M. N.**, & Gobina, E. (2014). Experimental study of gas flux characteristics in a CO₂ selective silica based modified membrane. *International Journal of Advanced Research In Engineering And Technology (IJARET)*. 5(8), 01-09. (Journal Paper).

Shehu, H., **Kajama, M. N.** & Gobina, E. (2014). Effect of temperature on gas separations using porous alumina membranes. *International Journal of Modern Science and Engineering Technology (IJMSET)*. 1(5), 22-29. (Journal Paper).

Kajama, M. N., Shehu, H. & Gobina, E. Purification of gases using nanoporous inorganic membranes. *International Journal of Scientific Engineering and Technology*, 3(9) 1156-1159. (Journal Paper).

Kajama, M. N., Nwogu, N. C. & Gobina, E. (2014). Gas permeation study using porous ceramic membranes. *Energy and Environment Research*, 4(3) 43-49. (Journal Paper).

Nwogu, N. C., **Kajama M. N.**, Dedekuma, K. & Gobina, E. (2014). An experimental analysis of a nano structured inorganic ceramic membrane for carbon capture applications in energy security challenges. *Energy and Environment Research*, 4(3) 1-8. (Journal Paper).

Nwogu, N. C., Gobina, E. & **Kajama, M. N.** (2013). Improved carbon dioxide capture using nanostructured ceramic membranes. *Low carbon economy*, 4(3) 125-128. (Journal Paper).

Kajama, M. N. & Gobina, E. (2013). Experimental study of membrane properties on gas permeation in γ -alumina macroporous ceramic membranes. *In Proceedings International Nanotechnology Conference and Exhibition, Nanotech Dubai 2013, 28th – 30th October 2013.* (Proceedings).

Kajama, M. N. & Gobina, E. (2013). Gas transport characteristics in membrane reactors for environmental applications. *In Proceedings 13th Health, Safety, Security & Environmental Conference, SPE Americas E&P. Galveston, Texas, USA. 18th-20th March 2013.* (Proceedings).

Conferences Attended and Presented

2016 Emerging and Hybrid Membrane Technologies. Organised by; IChemE Fluid Separations Special Interest Group. Swansea, United Kingdom (10th June 2016). Tubular Hybrid Membrane Reactor for Gas Separation/Purification and Reaction Applications. **Mohammed Nasir Kajama**, Habiba Shehu, Edidiong Okon, Ify Orakwe and Edward Gobina (Oral presentation).

The 2015 International Conference of Manufacturing Engineering and Engineering Management, World Congress for Engineers. 1st - 3rd July 2015 London, United Kingdom. Propylene Oxidation Using Pt-alumina Impregnated Catalytic Membrane Reactor. **Mohammed N. Kajama**, Ngozi C. Nwogu and Edward Gobina (Oral presentation).

7th International Conference on Sustainable Development and Planning, 19th – 21st May 2015 Istanbul, Turkey. Hydrogen Permeation Using Nanostructured Silica Membranes. **M. N. Kajama**, N. C. Nwogu and E. Gobina, (Oral presentation).

6th International Conference on Hydrogen Production (ICH₂P-2015), May 3rd – 6th 2015, UOIT, Oshawa/Ontario, Canada. Hydrogen Permeation Using Macroporous and Mesoporous Inorganic Membranes. **Kajama Mohammed Nasir**, Nwogu Ngozi Claribelle, Gobina Edward (Oral presentation).

The 2nd International Conference on Sensors and Materials Manufacturing Science 2015 (2nd ICSMMS2015) 17th-18th January 2015. Paris, France. Hydrogen Separation Using Inorganic Membranes. **M. N. Kajama**, N. C. Nwogu and E. Gobina (Oral presentation).

2014 3rd International Conference on Challenges in Environmental Science and Computer Engineering. 21st-22nd June 2014, London, United Kingdom. Effect of gas

permeation temperature on γ -alumina ceramic membranes. **Mohammed Nasir Kajama**, Ngozi Claribelle Nwogu, Edward Gobina (Oral presentation).

Energy Quest 2014, 23rd–25th April 2014, Ekaterinburg, Russia. Experimental study of carbon dioxide separation with nanoporous ceramic membranes. **M. N. Kajama** and E. Gobina (Oral presentation).

8th IMSTEC 2013, 25th–29th November 2013, Melbourne, Australia. The Effects of membrane properties on gas permeation in γ -alumina mesoporous ceramic membranes for natural gas separation E. Gobina and **M. N. Kajama** (Oral presentation).

International Nanotechnology Conference and Exhibition, Nanotech Dubai 2013, 28th–30th October 2013. Experimental study of membrane properties on gas permeation in γ -alumina macroporous ceramic membranes. **M. N. Kajama** and E. Gobina (Oral Presentation).

Engineering with Membranes towards a sustainable future, Saint-Pierre d'Oleron, France. 3rd–7th September 2013. Effect of Gas Permeation Temperature On γ -Alumina Ceramic Membranes. E. Gobina, **M. N. Kajama** (Poster Presentation).

11th International Conference on Catalysis in Membrane Reactors. Porto, Portugal. 7th–11th July 2013. Gas Permeation Properties on γ -Alumina Ceramic Membranes at High Temperature. **M. N. Kajama**, E. Gobina (Poster Presentation).

13th Health, Safety, Security & Environmental Conference, SPE Americas E&P. Galveston, Texas, USA. 18th–20th March 2013. Gas Transport Characteristics in Membrane Reactors for Environmental Applications. **M. N. Kajama**, E. Gobina (e-Poster Presentation).

Nomenclature

A	surface area of the membrane	(m ²)
<i>c</i>	coefficient of adsorption energy	-
<i>d_p</i>	pore diameter	(m)
<i>d</i>	diameter	(m)
F	permeation flux	(mol m ⁻² s ⁻¹ Pa ⁻¹)
<i>K_n</i>	Knudsen number	-
L	thickness	(m)
M	molecular weight of gas	(g/mol)
<i>n_{ads}</i>	amount of gas adsorbed by unit mass of adsorbent	(cc.mg ⁻¹)
<i>n_m</i>	volume of gas adsorbed when the adsorbent surface is covered by monolayer	(cc.mg ⁻¹)
<i>N_A</i>	avogadro's number	(6.02214129×10 ²³ mol ⁻¹)
P	gas pressure	(Pa)
<i>P_{av}</i>	average pressure	(Pa)
<i>P_e</i>	permeability	(mol-m/m ² s ⁻¹ Pa ⁻¹)
<i>P_{kn}</i>	Knudsen diffusion	(mol m ⁻² s ⁻¹ Pa ⁻¹)
<i>P₀</i>	saturation pressures of the adsorptive at the adsorption temperature	(atm)
<i>P_t</i>	total permeance	(mol m ⁻² s ⁻¹ Pa ⁻¹)
<i>P_v</i>	viscous flow	(mol m ⁻² s ⁻¹ Pa ⁻¹)
<i>P_y</i>	permeability of y component	(mol-m/m ² s ⁻¹ Pa ⁻¹)
<i>P_z</i>	permeability of z component	(mol-m/m ² s ⁻¹ Pa ⁻¹)
ΔP	pressure difference	(Pa)
q	molar flow	(mol/sec)
r	mean pore radius	(m)
R	gas constant	(8.314 J.K ⁻¹ .mol ⁻¹)
T	temperature	(K)
<i>W₁</i>	weight of the alumina support before coating	(g)
<i>W₂</i>	total weight of the support and the membrane	(g)

Greek Symbols

ε	porosity	-
μ	viscosity	(Pa-s)
τ	tortuosity	-
λ	mean free path	(m)

ρ	density	(kg.m ⁻³)
$\alpha_{y,z}$	selectivity	-

Table of Contents

<i>Originality Statement</i>	<i>i</i>
<i>Dedication</i>	<i>ii</i>
<i>Acknowledgement</i>	<i>iii</i>
<i>Abstract</i>	<i>iv</i>
<i>List of Publications and conference proceedings</i>	<i>v</i>
<i>Nomenclature</i>	<i>xi</i>
<i>Table of Contents</i>	<i>xiii</i>
<i>List of Figures</i>	<i>xvii</i>
<i>List of Tables</i>	<i>xx</i>
1. Introduction	1
1.1 Problem Statement and Aim	1
1.2 Research objectives of the present study	1
1.3 Structure of This Thesis	2
2 Literature Review	3
2.1 Background	3
2.2 VOCs emissions regulation.....	4
2.3 Technologies for VOCs control	5
2.3.1 Process and equipment optimization methods/techniques	5
2.3.2 End-of-the-pipe methods/techniques	6
2.4 VOCs destruction.....	7
2.4.1 Thermal Oxidation	8
2.4.2 Catalytic Oxidation	8
2.4.2.1 Catalyst life	11
2.5 Recent Development in VOC Conversion Technology	12
2.5.1 Concepts of a membrane reactor.....	12
2.6 Inorganic Membranes for Gas Separation and Recovery.....	19
2.6.1 Gas Transport Mechanism in Membrane	21
2.6.1.1 Viscous Flow.....	22
2.6.1.2 Knudsen Diffusion	23
2.6.1.3 Surface Diffusion	23
2.6.1.4 Multi-Layer Diffusion.....	23
2.6.1.5 Molecular sieving.....	23
2.6.1.6 Solution-Diffusion	24
2.6.1.7 Combined Transport.....	24
2.6.2 Factors That Influence Operating Variables	24

2.6.2.1	Feed Concentration	24
2.6.2.2	Transmembrane Pressure	25
2.6.2.3	Temperature	25
3	<i>Experimental Procedure and Equipment Setup</i>	26
3.1	Introduction	26
3.2	Equipment Setup	26
3.2.1	Membrane Reactor	27
3.2.2	Alumina Ceramic Membrane	28
3.2.3	Pressure Gauges/Manometers	29
3.2.4	Thermocouple	29
3.2.5	Thermometer	29
3.2.6	CO ₂ analyser (CT2100-Emissions Sensor)	30
3.2.7	Propane Gas	30
3.2.8	Propylene Gas	30
3.2.9	N-butane Gas.....	30
3.2.10	Oxygen Gas.....	30
3.2.11	Nitrogen Gas	30
3.2.12	Methane Gas	31
3.2.13	Carbon Dioxide Gas.....	31
3.2.14	Hydrogen Gas	31
3.2.15	Helium Gas	31
3.2.16	Sylgard(R) 184 Silicone Elastomer Kit.....	31
3.2.17	2-Methylbutane (Iso-pentane).....	31
3.2.18	Boehmite Powder	31
3.2.19	Platinum Metal Solution	31
3.2.20	Silica Membrane Preparation.....	32
3.2.21	Catalytic Membrane Preparation.....	32
3.2.22	Membrane Reactor Operation Procedure.....	32
3.2.23	Procedure of CO ₂ Analyser Calibration and VOCs Conversion.....	35
3.3	Membrane Characterization Methods and Gas Transport Measurement.....	39
3.3.1	BET Surface Area, Pore Size and Pore Size Distribution.....	39
3.3.2	Gas Permeability Measurements	43
3.4	Support and Membrane Characterization Methods.....	45
3.4.1	Scanning Electron Microscopy (SEM)	45
3.4.2	Energy Dispersive X-ray Analysis (EDXA)	47

3.4.3	BET Surface Area and Pore Size Distribution Determination	48
3.4.4	BET Surface Area Determination	50
3.5	Safety	50
3.5.1	Overview of Ethical Issues.....	50
3.5.2	Minimising Risk.....	50
3.5.3	Health and Safety	50
4	<i>Results</i>	52
4.1	Membrane Characterization	52
4.1.1	BET Surface Area, Pore Size and Porosity of Alumina Membrane	52
4.2	Catalyst Characterization	55
4.2.1	BET Surface Area	55
4.2.2	SEM and EDXA of Silica-alumina Membrane.....	56
4.2.3	SEM and EDXA of Pt-alumina Membrane.....	58
4.3	Gas Permeability Study.....	64
4.3.1	Defect Repair of Composite Membrane.....	64
4.3.2	Experimental Procedure	65
4.3.3	Results and Discussion.....	68
4.4	CO ₂ Recovery from Natural Gas by Modifying 30nm Support.....	71
4.4.1	Introduction.....	71
4.4.2	Experimental Procedure	72
4.4.3	Results and Discussion.....	72
4.4.3.1	Effect of Gas Permeation and Selectivity at Room Temperature	72
4.5	CO ₂ Recovery from Natural Gas by Modifying 15nm Support.....	76
4.5.1	Introduction.....	76
4.5.2	Experimental Procedure	77
4.5.3	Results and Discussion.....	78
4.5.3.1	Gas permeation	78
4.6	H ₂ Separation Using Inorganic Membranes.....	83
4.6.1	Introduction.....	83
4.6.2	Experimental Procedure	84
4.6.3	Results and Discussion.....	85
4.7	H ₂ Recovery Using Silica-Based Membrane	89
4.7.1	Introduction.....	89
4.7.2	Experimental Procedure	90
4.7.3	Results and Discussion.....	90
4.7.3.1	H ₂ Permeation and Selectivity.....	90

4.8	VOC Recovery Using Silica-Based Membrane	94
4.8.1	Introduction.....	94
4.8.2	Experimental Procedure	95
4.8.3	Results and Discussion.....	96
4.8.3.1	Propylene and nitrogen permeation and selectivity	96
5	<i>VOC Destruction in a Flow-Through Membrane Reactor</i>	99
5.1	Introduction.....	99
5.2	Experimental Procedure	99
5.2.1	Performance/Characteristics of the Membrane Reactor.....	100
5.3	Results and Discussion.....	101
5.3.1	Gas Permeation	101
5.3.2	Propane Conversion	102
5.3.3	N-butane Conversion	106
5.3.4	Propylene Conversion	110
6	<i>Conclusions and Recommendation for Future Work</i>	114
6.1	Conclusions.....	114
6.2	Recommendations for Future Work.....	115
7	<i>References</i>	116

List of Figures

Figure 2.1 - VOC control techniques.	7
Figure 2.2 - Forced flow-through Contactor Configuration for Catalytic Membrane Reactor Process.	10
Figure 2.3 - The extractor mode membrane reactors.	14
Figure 2.4 - The distributor mode membrane reactors.	15
Figure 2.5 - The active contactor mode membrane reactors.	17
Figure 2.6 - Membrane design.	20
Figure 2.7 - Gas Transport Mechanism for Membrane.	22
Figure 3.1 - Schematic diagram of the feed, membrane reactor and analytical systems.	27
Figure 3.2 - Pictorial view of the experimental rig.	28
Figure 3.3 - Pictorial view of commercial tubular ceramic support.	29
Figure 3.4 - Pictorial view of the reactor section.	34
Figure 3.5 - Calibration curve of the CO ₂ analyser.	36
Figure 3.6 - Classification of absorption-desorption isotherm.	40
Figure 3.7 - BET plot and relation between c and n_m to slope and intercept of y-axis.	41
Figure 3.8 - Schematic diagram of the experimental setup.	44
Figure 3.9 - SEM image of the alumina support inner surface.	46
Figure 3.10 - SEM image of the alumina support outer surface.	46
Figure 3.11 - SEM image of the alumina support cross-sectional area.	47
Figure 3.12 - N ₂ adsorption/desorption isotherm of the alumina support.	49
Figure 3.13 - Pore-size distribution of the alumina support measured by N ₂ adsorption.	49
Figure 4.1 - N ₂ adsorption/desorption isotherm of silica membrane.	53
Figure 4.2 - Pore-size distribution of silica membrane measured by N ₂ adsorption.	53
Figure 4.3 - N ₂ adsorption/desorption isotherm of Pt membrane.	54
Figure 4.4 - Pore-size distribution of Pt membrane measured by N ₂ adsorption.	55
Figure 4.5 - SEM image of the inner surface of the silica membrane.	56
Figure 4.6 - SEM image of the outer surface of the silica membrane.	57
Figure 4.7 - EDXA of the silica membrane outer surface.	58
Figure 4.8 - SEM image of the Pt membrane inner surface.	59
Figure 4.9 - SEM image of the Pt membrane outer surface.	60
Figure 4.10 - SEM image of the Pt membrane cross-sectional area.	60
Figure 4.11 - SEM image of the Pt membrane edge surface.	61
Figure 4.12 - EDXA image of the Pt membrane inner surface.	62
Figure 4.13 - EDXA image of the Pt membrane outer surface.	63
Figure 4.14 - EDXA image of the Pt membrane cross-section.	64

Figure 4.15 - Pictorial view of the cracked membrane.	66
Figure 4.16 - Membrane's heat-treatment profile.	67
Figure 4.17 - Pictorial view of membrane with the stainless steel reactor showing the graphite ring seals.	67
Figure 4.18 - CO ₂ permeance against average pressure across tubular membrane at room temperature.	69
Figure 4.19 - CO ₂ /H ₂ selectivity against average pressure across tubular membrane at room temperature.	70
Figure 4.20 - N ₂ permeance across non-modified (alumina support) and modified (silica) membrane against average pressure at 298 K.	73
Figure 4.21 - Methane permeance across alumina support and silica membrane against average pressure at 298 K.	74
Figure 4.22 - Gas flow rate across silica membrane after fifth dip-coating against feed pressure at 298 K.	75
Figure 4.23 - CO ₂ selectivity against feed pressure across silica membrane at room temperature.	76
Figure 4.24 - Silica membrane thickness per dip against number of dips.	78
Figure 4.25 - Gas permeates flux across alumina support against feed pressure at 298 K (fully opened retentate).	79
Figure 4.26 - Flow rate of CO ₂ and CH ₄ across alumina support and silica membrane against feed pressure at 298 K.	80
Figure 4.27 - CO ₂ flow rate against feed pressure across alumina support & silica membrane at 298 K.	81
Figure 4.28 - CO ₂ and CH ₄ permeance across silica membrane against average pressure at 298 K.	82
Figure 4.29 - Helium permeation across silica membrane against temperature at different feed pressures.	83
Figure 4.30 - Gas permeation across mesoporous membrane against mean pressure at 298 K.	85
Figure 4.31 - Hydrogen permeation across macro- and meso porous membranes against feed pressure at 298 K.	86
Figure 4.32 - Gas permeation against temperature across mesoporous membrane at 1.5 barg.	87
Figure 4.33 - H ₂ /He Selectivity across mesoporous membrane against temperature at 1.6 barg.	88

Figure 4.34 - H ₂ /N ₂ Selectivity against feed pressure across macro- and meso porous membranes at 298 K.	88
Figure 4.35 - Gas permeate flux across silica membrane against feed pressure at 298 K.	90
Figure 4.36 - H ₂ permeation across alumina support and silica membrane against feed pressure at 298 K.....	91
Figure 4.37 - H ₂ /N ₂ selectivity across silica membrane against temperature at 0.9 barg.....	92
Figure 4.38 - H ₂ /CH ₄ selectivity against temperature across silica membrane at 0.9 barg.	93
Figure 4.39 - H ₂ /Ar selectivity against temperature across silica membrane at 0.9 barg.....	94
Figure 4.40 - (a): Crushed sample of the alumina support, (b): Crushed sample of silica membrane.....	96
Figure 4.41 - Nitrogen and propylene gas flow rates against feed pressure across silica membrane at 298 K.	97
Figure 4.42 - C ₃ H ₆ /N ₂ selectivity across silica membrane against feed pressure at 298 K.....	97
Figure 5.1 - Schematic cross-section of flow-through tubular membrane reactor.....	100
Figure 5.2 - Permeation flux across alumina support and platinum membrane against average pressure at 298 K.	102
Figure 5.3 - Propane conversion against reaction temperature (194 to 232 °C).....	103
Figure 5.4 - Propane conversion against reaction temperature (235 to 427 °C).....	104
Figure 5.5 - Propane conversion against reaction temperature (225 to 333 °C).....	105
Figure 5.6 - Propane conversion against reaction temperature (226 to 378 °C).....	106
Figure 5.7 - N-butane conversion against reaction temperature (242 to 273 °C).....	107
Figure 5.8 - N-butane conversion against reaction temperature (195 to 259 °C).....	108
Figure 5.9 - N-butane conversion against reaction temperature (200 to 244 °C).....	109
Figure 5.10 - N-butane conversion against reaction temperature (183 to 245 °C).....	110
Figure 5.11 - Propylene conversion against reaction temperature (174 to 220 °C).	111
Figure 5.12 - Propylene conversion against reaction temperature (187 to 331 °C).	112
Figure 5.13 - Propylene conversion against reaction temperature (190 to 420 °C).	113

List of Tables

Table 2.1 Some common VOCs	4
Table 3.1- Characteristics of the gases uses for the experiments.....	26
Table 3.2- N-butane conversion.....	37
Table 3.3- Propane conversion.....	38
Table 3.4- Propylene conversion.....	39
Table 4.1 - BET surface area and average pore diameter measurements of the silica membrane.....	52
Table 4.2 - BET surface area, average pore diameter and pore volume measurements of the Pt-alumina membrane.	56
Table 4.3 - Outer surface EDX analysis of silica membrane.....	58
Table 4.4 - Inner surface EDX analysis of Pt membrane.....	62
Table 4.5 - Outer surface EDX analysis of Pt membrane.	63
Table 4.6 - Cross-section EDX analysis of Pt membrane.	64
Table 4.7 - H ₂ selectivity at room temperature and 0.9 bar.	92

1. Introduction

1.1 Problem Statement and Aim

A large amount of volatile organic compounds (VOCs) are released into the atmosphere from chemical plants, petroleum refineries, pharmaceutical plants, automobile manufacturers, airplane manufacturers, food manufacturers, textile manufacturers, printing plants, can coating plants, painting facilities, wood stoves, etc. Catalytic destruction of VOCs has recently attracted attention because of the economic and environmental advantages that include:

(1) Catalytic combustion can be accomplished with less input energy as well as cost. In this case, the same reaction occurs in a catalyst bed with an activation energy barrier thus significantly reducing the temperature of operation (Rusu & Dumitriu, 2003; Saracco & Specchia, 2000; Khan & Ghoshal, 2000; Ruddy & Carroll, 1993).

(2) VOC molecules are transformed into carbon dioxide (CO₂) and water (H₂O) which are less environmentally toxic (Rusu & Dumitriu, 2003).

Catalytic oxidation combust VOCs in a similar way that thermal oxidation does. As its name implies, catalytic oxidation uses a catalyst in order to facilitate the rate of a chemical reaction without itself being consumed. The main difference between thermal and catalytic oxidation is that catalytic oxidation operates at a lower temperature typically between 371 °C to 482 °C (Khan & Ghoshal, 2000; Ruddy & Carroll, 1993); 260 °C to 482 °C (Rusu & Dumitriu, 2003; www.meca.org/galleries/files/hapwp.pdf 1995). They offer many advantages for the appropriate application. The present study proposes a novel technology for the process reactor using flow-through contactor reaction and membrane separation of the CO₂ product.

The main aim of this research is to develop, test and utilise both catalytic membranes for VOC destruction and non-catalytic (selective) membranes in product recovery for environmental applications in order to optimize raw materials utilization and energy efficiency.

1.2 Research objectives of the present study

- ❖ To prepare the membrane with bohemite solution and silicone elastomer using dip coating method and test for gas separation.
- ❖ To incorporate low-content platinum (Pt) catalysts in ceramic membranes.
- ❖ To test the catalytic oxidation in a flow-through contactor configuration in order to create intimate contact between the target VOC and the catalyst which enables complete destruction.

- ❖ To test the permeation properties on both the selective and catalytic membranes in order to examine the influence of the flow rate, kinetic diameter, molecular weight of different gases through the membrane reactor for VOC abatement.
- ❖ To confirm that the membrane reactor is a promising alternative for VOC destruction with a low overall catalyst loading and moderate temperature.

The application of a catalytic membrane reactor is a relatively new area of research in reaction engineering. The ultimate goal of commercializing this technology will further strengthen application to waste treatment technologies. This study will serve as an example for many other important reactions in the process industries to mitigate or enhance waste stream pollution.

1.3 Structure of This Thesis

The thesis is divided into 6 chapters. In chapter 1, VOC destruction in a porous membrane reactor is introduced. Chapter 2 provides the literature review on the significance of the existing problem, and the conventional method used to tackle the problem. It describes the membrane reactor and its construction including its stability at high temperature and corrosive resistant material to tackle the challenge of enhancing VOC destruction. In chapter 3, the experimental set-up description and methodology are presented, including a description of the reactor fabrication and material selection. Chapter 4 describes the results obtained from gas permeation experiments, VOC recovery experiment, silica membrane characterization (SEM-EDXA, N₂ adsorption/desorption) and gas permeability studies, the catalysts were also characterized by the same methods. Chapter 5 presents the VOCs destruction experimental study using the membrane reactor. Governing parameters such feed pressure, permeation rate, and temperature were investigated. Chapter 5 describes the performance of the reactor. The conclusions of the study are detailed in Chapter 6 together with recommendations for future research.

2 Literature Review

2.1 Background

Volatile organic compounds (VOCs) encompass all organic compounds that boil at 50 - 260 °C excluding pesticides but includes dichloromethane (which boils at 41°C) (Aguado, Coronas & Santamaría, 2005). VOCs are grouped as aliphatic hydrocarbons (compounds containing carbon and hydrogen joined together in straight chains, such as propene and ethane), aromatic hydrocarbons (toluene and benzene), aldehydes (formaldehyde), ketones (acetone), halogenated hydrocarbons, alcohols (ethanol, methanol and n-propanol), and esters (ethylacetate) among others (Pina *et al.*, 1997). VOCs are extremely harmful when emitted to the environment. Toluene and propylene in particular are acknowledged as vastly polluting molecules due to their elevated photochemical ozone creativity potential (Liotta, 2010).

VOCs are mostly generated from industrial processes (petroleum refineries, chemical and pharmaceutical plants, automobile manufacturers, food processors), transport (at variable degrees) and also from household products. Some common VOCs listed in Table 2.1 include; ethane, acetaldehyde, benzene, carbon tetrachloride, toluene, and naphthalene among others (Khan & Ghoshal, 2000; Buzcu-Guven & Harriss, 2012; Ruddy & Carroll, 1993). Additionally, VOCs have many health and adverse impacts on plants which are associated with the pollution they produced. Some symptoms associated with short term exposure of VOCs include; allergic skin reaction, headaches, dizziness, coughing, visual disorders, eye and respiratory tract irritation and fatigue. Similarly, kidney, brain damage, liver, damage to the nervous, reproductive and immune systems are associated with long term exposure (Rusu & Dumitriu, 2003). Emissions of VOCs could be a result of natural sources, although most VOCs emissions result from anthropogenic sources. About 235 million tonnes of VOCs are released annually worldwide into the atmosphere from man-made sources (Rusu & Dumitriu, 2003). From an environmental point of view, it is necessary to reduce these vapour emissions which may lead to a significant milestone in the oil and process industries.

Table 2.1 Some common VOCs (Khan & Ghoshal, 2000; Ruddy & Carroll, 1993)

Number	VOCs
1	Acetaldehyde
2	Acetamide
3	Acetone
4	Acetonitrile
5	Benzene
6	Benzyl chloride
7	Carbon tetrachloride
8	Cyclohexane
9	Ethyl acetate
10	Ethylene glycol
11	Formaldehyde
12	Heptane
13	Hexane
14	Isopropyl alcohol
15	Methyl ethyl ketone
16	Methylene chloride
17	Naphthalene
18	Propylene
19	Styrene
20	Toluene

2.2 VOCs emissions regulation

The release of VOCs into the environment will be harnessed by imposing strict regulations (Liotta, 2010). In recent years, VOC emissions have been strictly regulated in different countries around the globe. For example, in the air quality standards developed by the United States Environmental Protection Agency (USEPA) the maximum 3-hour concentration of 1.6×10^{-4} kg/m³ (0.24 ppm) hydrocarbon content should not be exceeded for a period of more than a year (Tamaddoni *et al.*, 2014). However, reduction of VOC emissions that exceed the current national air quality standard for ozone of 0.12 ppm is mandated under Title I of the US Clean Air Act Amendment (USCAAA) of 1990. Also, Title III of the amendments requires 90% reduction in emissions of 189 toxic pollutants, of which 70% are VOCs (Hubbell *et al.*, 2010; Rusu & Dumitriu, 2003).

The recently passed European Community emissions limit is 35 g total organic compounds (TOC) per cubic meter gasoline loaded likewise the US Environmental Protection Agency Standard (USEPAS) established an emission limit of 10 g TOC/m³. The German TA-Luft Standard has also set an emissions limit of 0.15 g TOC/m³ (Tamaddoni *et al.*, 2014). The Gothenburg protocol states that by 2020 the European Union (EU) should reduce VOC emission levels by 50% compared to the year 2000.

In African countries, VOC legislation is not a very common practice but VOC regulations can be found for example in North Africa. Morocco has approved a draft decree which sets standards for air quality and the manner of installation of monitoring networks (Ojala *et al.*, 2011). The decree is similar to the National Ambient Air Quality Standards (NAAQS) in South Africa and includes regulations for benzene (Ojala *et al.*, 2011). Most sections of the National Environmental Management: Air Quality Act (NEMAQA) in South Africa have been brought into effect. The legislative reform in the form of the National Environmental Management: Air Quality Act (No. 39 of 2004) (NEMAQA) in 2004 replaced the outdated Atmospheric Pollution Prevention Act from the year 1965 (No. 45 of 1965) (APPA). The act provides the basis for setting standards for ambient air quality and emissions respectively. Some initiatives to counter emissions problems including the National Framework for Air Quality Management (2007) (NFAQM) sets plans for achieving the objectives of the NEMAQA. The national framework provides systems and procedures for attaining compliance with AAQS and establishes national standards on how provinces will monitor air quality. In March 2010, the Department of Environmental Affairs (DEA) published national air quality standards which included regulations for benzene emissions (Ojala *et al.*, 2011).

After considering the detailed analysis of an emission inventory, therefore, it is essential to select the appropriate and cost-effective technique of air pollution control.

2.3 Technologies for VOCs control

Different methods/techniques are available to control VOCs emissions. These methods/techniques are: process and equipment optimizations (Khan & Ghoshal, 2000; Ruddy & Carroll, 1993), add-on or end-of-the-pipe control techniques, absorption, adsorption and condensation (Rusu & Dumitriu, 2003). These techniques are categorised under either destruction and/or recovery of the pollutants. Contaminants can be destroyed by either oxidation/incineration or by biodegradation. However, methods like absorption, adsorption and condensation are candidates for VOC recovery which will not be further discussed in this thesis.

2.3.1 Process and equipment optimization methods/techniques

Process optimizations are usually preferred as the alternative method for reducing VOC emissions. Optimizations comprise the replacement of materials to reduce VOC input to the process, changes in operating conditions to limit the volatilization of VOCs, as well as the optimization of equipment to reduce the opportunities for VOC escape into the atmosphere (Khan & Ghoshal, 2000; Ruddy & Carroll, 1993).

The objective of equipment optimization is to avert the escape of VOCs. VOCs can be emitted through vents, or leaks at valves, or as a result of process conditions such as spray painting. Monitoring and repair programs can be instituted to reduce emissions due to leaks from valves, pumps, and process piping connections in order to curtail the emissions. Likewise, design of process enclosures can also reduce emissions. A positive means of collecting the emissions can also be provided by enclosing the source. On the other hand, by simply employing an enclosure might not be sufficient to reduce emissions. For example, if the emissions are captured in the enclosure and no additional measures are taken, the toxic pollutants will eventually escape into the atmosphere. Typically, this situation is handled by end-of-pipe means (William & Lead, 1997; Chadha & Parmele, 1993). An overall approach to develop collection and control measures to reduce VOC emissions is through a stepwise analysis. The first step is to quantify the air pollutants by developing and understanding the process steps, followed by sampling and measuring the vent flows (Khan & Ghoshal, 2000).

2.3.2 End-of-the-pipe methods/techniques

End-of-the-pipe methods are often used for emission control instead of process optimization. End-of-the-pipe methods can be classified into either; destruction or recovery methods. The destruction method is further divided into oxidation and bio-filtration, while the recovery method is divided into absorption, condensation, membrane separation and adsorption methods (Fig. 2.1) which will be discussed later in this chapter (Khan & Ghoshal, 2000; Rusu & Dumitriu, 2003).

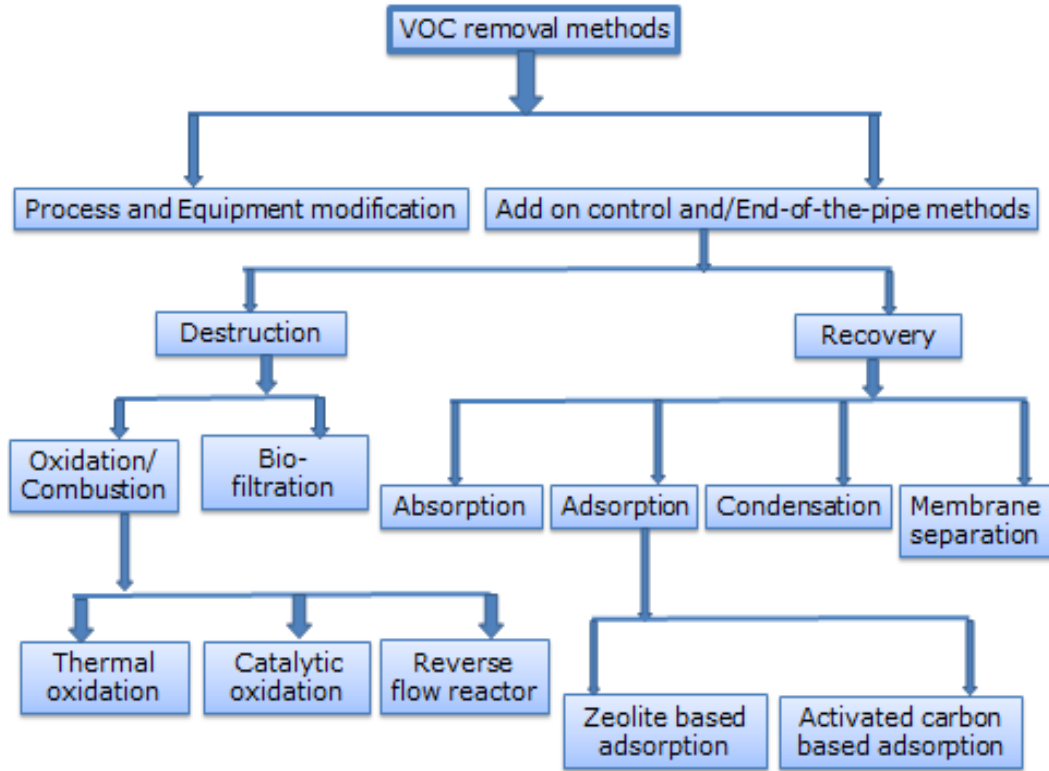


Figure 2.1 - VOC control techniques (Khan & Ghoshal, 2000).

A number of parameters need to be considered when selecting the most appropriate VOC emission control equipment. These include; desired control efficiency, air stream properties such as concentration, heat content, flow rate, vapour pressure, moisture content, temperature; contaminant properties such as volatility, molecular weight, solubility in water, pH among others; safety issues like flammability as well as the value of the material that would be recovered (Rusu & Dumitriu, 2003).

2.4 VOCs destruction

Among the VOC abatement technologies mentioned above, the most widely implemented VOC destruction methods are thermal and catalytic oxidation in which VOCs are combined with oxygen at specific temperatures and yield carbon dioxide (CO₂) and water (H₂O). In general, the chemical reaction takes the form:



2.4.1 Thermal Oxidation

Thermal oxidation or thermal incineration is the process of oxidizing combustible materials (VOCs) by increasing their temperature above the auto-ignition point and when combined with oxygen at a high temperature yields carbon dioxide and water. At present, modern thermal oxidisers are simply designed to achieve 95 to 99+% VOC destruction. Thermal oxidisers can be designed to handle a capacity of 1,000 to 500,000 cfm (cubic feet per minute) and a VOC concentration of 100 to 2,000 parts per million (ppm). Nominal residence time is between 0.5 to 1.0 second (Khan & Ghoshal, 2000; Ruddy & Carroll, 1993). Thermal oxidisers are very popular for VOC combustion (Khan & Ghoshal, 2000; Ruddy & Carroll, 1993; Marks & Rhoads, 1991; William & Lead, 1997).

The temperature range used to achieve VOC combustion for thermal oxidation systems is typically between 704 °C to 982 °C (1,300 °F to 1,800 °F) (Khan & Ghoshal, 2000). The actual operating temperature however is a function of the type and concentration of the material within the exhaust stream and the desired destruction and removal efficiency (DRE). Some compounds that are difficult to combust or are present at low inlet concentrations will need greater heat input and retention time in the combustion zone. Inlet concentrations above 25% of the lower explosive limits (LEL) are avoided due to explosion hazards (Khan & Ghoshal, 2000; Mukhopadhyay, Moretti & Nilson, 1993).

The disadvantage of thermal oxidisers when operating at temperatures near 982 °C is that they produce higher levels of nitrogen oxides, which is a secondary pollutant that may require further treatment. Halogenated compounds in the exhaust stream are converted to acidic compounds. These quantities may require the use of highly expensive corrosion resistant materials of construction as well as the use of additional acid gas controls, such as scrubbing, as a follow-up treatment (Ruddy & Carroll, 1993).

2.4.2 Catalytic Oxidation

Catalytic oxidation or catalytic incineration systems also combust VOCs in a similar way that thermal oxidation does. As its name implies, catalytic oxidation uses a catalyst in order to facilitate the rate of a chemical reaction without itself being consumed. The main difference between thermal and catalytic oxidation is that catalytic oxidation operates at a lower temperature typically between 371 °C to 482 °C (Khan & Ghoshal, 2000); 260 °C to 482 °C (Rusu & Dumitriu, 2003; www.meca.org/galleries/files/hapwp.pdf 1995). They offer many advantages for the appropriate application. The required energy for catalytic oxidation is lower

than that for thermal oxidation due to the presence of the catalyst resulting in lower operating and/or capital cost (Rusu & Dumitriu, 2003).

Catalytic systems can be designed to handle a throughput capacity of 1,000 to 100,000 cfm and a VOC concentration of 100 to 2,000 ppm. Destruction efficiencies in excess of 90% with a higher DRE of 95% are common (Khan & Ghoshal, 2000; Patkar & Laznow, 1992). Catalytic oxidation can be applied to the abatement of VOCs at low concentrations at a higher range of total gas flow rate (Benard *et al.*, 2009; Liotta *et al.*, 2009). Catalytic oxidizers are usually applied to mitigate emissions from VOCs sources, including process vents, solvent evaporation processes as well as gasoline bulk-loading operations (Moretti, 2002). Catalytic oxidation can also be used in mobile sources. For example, the automotive exhaust gases formed in gasoline engines contain a lot of environmentally unfriendly compounds as a result of incomplete oxidation, such as hydrocarbons (HC), carbon monoxide (CO) and oxides of nitrogen (NO_x) which necessitate the introduction of a catalytic converter in order to treat the exhaust gas (Nice & Bryant, 2000; Rusu & Dumitriu, 2003). A catalytic converter converts three regulated emissions which are VOCs, CO and NO_x, and known as the *Three Way Catalyst (TWC)* to CO₂, H₂O and N₂. The introduction of the TWCs started in the 1970s (Heck & Farrauto, 2009) and now almost 85% of the world's cars are fitted with the TWC (Rusu & Dumitriu, 2003).

The well recognized catalysts for VOC destruction are the supported noble metal catalysts which are famous in oxidation reactions because of their high activity (Santos *et al.*, 2010). However, the most efficient catalytic system for VOC destruction is the platinum supported on gamma-alumina (Pt/γ-Al₂O₃) which can operate at a lower temperature and achieve total VOC conversion (Saracco & Specchia, 1995; Saracco, Specchia & Specchia, 1996; Saracco & Specchia, 2000; Pina, Menéndez & Santamaria, 1996; Pina *et al.*, 1997; Benard *et al.*, 2009; Liotta *et al.*, 2009; Marécot *et al.*, 1994; Benard *et al.*, 2010; Paulis *et al.*, 2000; Müller *et al.*, 1993; Tahir & Koh, 1999). For example, in the case of flow-through membrane contactor configuration, the reactants gas mixtures (VOC and oxygen) are forced to go through the catalytic pores from the reactor entrance after being heated to the desired temperature. The catalysts (Pt) lower the reaction's activation energy and the membrane provides a wide dispersion of the catalytically active metal and creates a large surface area so that oxidation of the reactants will occur on the catalyst surface. Heat will be released as the VOCs are converted and yield the product from the exit side of the reactor as shown in Figure 2.2.

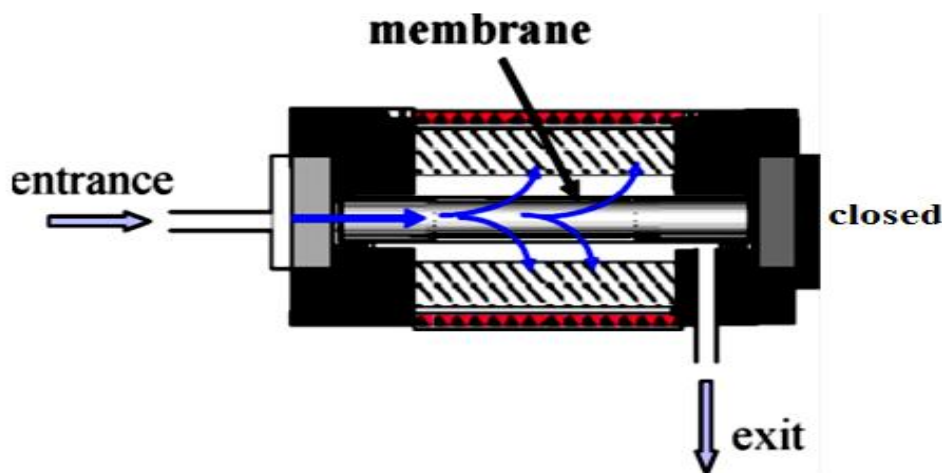


Figure 2.2 - Forced flow-through Contactor Configuration for Catalytic Membrane Reactor Process (Benard *et al.*, 2010).

Generally, VOC conversion can be achieved on the following categories of catalyst:

- ❖ Noble metals (platinum (Pt), titanium (Ti), palladium (Pd)) and copper (Cu), among others which can be supported on e.g. aluminium oxide Al_2O_3 , silicon dioxide SiO_2 , among others or may not be supported, and
- ❖ Transition metal oxides (e.g. iron-III oxides Fe_2O_3 , chromium-III oxides Cr_2O_3 , vanadium-V oxides V_2O_5 , among others).

The most commonly applied catalysts include noble metals (e.g. Pt, Rh, Pd) supported on oxide supports (e.g. Al_2O_3 , SiO_2). Due to their high intrinsic action for VOC destruction (Benard *et al.*, 2009; Paulis *et al.*, 2000; Paulis, Peyrard & Montes, 2001; Papaefthimiou, Ioannides & Verykios, 1997; Rusu & Dumitriu, 2003) than less expensive base-metal catalysts such as manganese dioxide (Moretti, 2002) they also offer longer service life (Moretti, 2002) which will be discussed later. It is indeed for this reason that to achieve total combustion in for example toluene, n-butane and propane, supported noble metals on alumina are more frequently used than transition metal catalysts (Benard *et al.*, 2009; Everaert & Baeyens, 2004).

Nonetheless, literature disclosed that platinum supported on alumina are more superior for the catalytic combustion of toluene and propene (Benard *et al.*, 2009; Paulis *et al.*, 2000; Paulis, Peyrard & Montes, 2001; Radic, Grbic & Terlecki-Baricevic, 2004; Kim *et al.*, 2004; Tahir & Koh, 1999; Gluhoi, Bogdanchikova & Nieuwenhuys, 2006; Pina, Menéndez & Santamaria, 1996). Noble-metal based catalysts are mostly obtained with γ - Al_2O_3 as a support with over 65% dispersion (Benard *et al.*, 2009). Performance of catalysts robustly relies on the method of preparation. This will dictate the degree of metal dispersion on the surface of the support and the

metallic nano-particles size. The content of the noble metal should be low due to its high cost. Consequently, particle size and dispersion are among the key parameters ensuing in preparing such catalysts for VOC abatement (Benard *et al.*, 2009).

This approach was employed in a sequence of work by Saracco & Specchia, (1995); Saracco, Specchia & Specchia, (1996) who used catalytically modified fly-ash filters for alcohol dehydration and for the reduction of nitrogen oxides with ammonia. A step further was taken in previous work by Pina, Menéndez & Santamaria, (1996) in which toluene combustion was proposed using a Pt/Al₂O₃ catalytic membrane operating in the Knudsen diffusion regime (Pina *et al.*, 1997). Since the probability of collisions between the molecules and the wall of the pores is maximised in the Knudsen diffusion regime, this type of membrane was expected to give a significantly higher efficiency in the reaction of dilute streams such as those commonly encountered in VOC removal.

Gluhoi, Bogdanchikova & Nieuwenhuys, (2006) compared the oxidation of propene and propane over gold-copper oxide (Au/Al₂O₃) and (Pt/Al₂O₃) catalysts. Propene conversion for gold-alumina (Au/Al₂O₃) was obtained at nearly 450 °C compared to (Pt/Al₂O₃) below 300 °C. Their findings exhibited that Pt/Al₂O₃ has higher activity than the Au containing catalysts for propene and propane conversion.

2.4.2.1 Catalyst life

Theoretically, the life of catalysts is ageless but is practically reduced due to deactivation caused by fouling and other contaminants (Rusu & Dumitriu, 2003; Cooley, 2002). Catalytic activity of a catalyst on VOC incineration studies is evaluated by the light-off curves i.e. the relationship of VOC conversion and reaction temperature (Paulis *et al.*, 2000; Wilburg & Young, 1991). This curve may show a loss of activity (deactivation) after some time of operation.

Three main reasons for catalyst deactivation include; fouling, poisoning and thermal deactivation:

- ❖ Fouling deactivation occurs if the active sites or the catalyst's pores are blocked by the deposited material (Rusu & Dumitriu, 2003). Coke (carbonaceous deposits) is the most common foulant (Rusu & Dumitriu, 2003). Coke is formed by undesired reactions of the organic compounds over catalyst. Such deactivation mostly occurs on zeolite catalysts (Rusu & Dumitriu, 2003).
- ❖ Deactivation caused by poisoning phenomenon deactivation causes catalytic activity to decrease if the active sites of the catalyst react with another chemical, and if the catalytic

activity enhances the phenomenon it is known as doping (Rusu & Dumitriu, 2003; Thomas, Thomas & Salzberg, 1967). Examples of these chemicals include halogens, phosphorus, mercury, silicones, sulphur and lead (Wilburg & Young, 1991; Cooley, 2002; Rusu & Dumitriu, 2003). If chlorinated compounds are converted over the catalysts (Sinquin *et al.*, 2001; Rusu & Dumitriu, 2003) the presence of chlorine may block the active sites and hydrochloride may react with the carrier and may vaporize metal-chlorine species (Spivey & Butt, 1992; Rusu & Dumitriu, 2003). A VOC stream containing more than 10 ppm of halogenated compounds degrades up to 43% of the catalyst activity (Wilburg & Young, 1991; Rusu & Dumitriu, 2003). However, a good catalyst for chlorinated compounds incineration may not be affected by the above mentioned degradation phenomena (Rusu & Dumitriu, 2003).

- ❖ Thermal deactivation occurs if the active metal exceeds the catalyst operational temperature (Trimm, 1991; Rusu & Dumitriu, 2003). High temperature induces solid state reactions between the components of the catalyst. Crystal growth at high temperature leads to a loss of surface area. Therefore, it is significant to develop a low-temperature catalyst which is one of the main aims of researchers in the minimization of the cold-start period (Rusu & Dumitriu, 2003).

2.5 Recent Development in VOC Conversion Technology

Besides the industrialized VOCs abatement processes, destruction of VOC into CO₂ and H₂O has been widely studied using membrane reactors (Benard *et al.*, 2009; Paulis *et al.*, 2000; Paulis, Peyrard & Montes, 2001; Radic, Grbic & Terlecki-Baricevic, 2004; Kim *et al.*, 2004; Tahir & Koh, 1999; Gluhoi, Bogdanchikova & Nieuwenhuys, 2006; Pina, Menéndez & Santamaria, 1996).

2.5.1 Concepts of a membrane reactor

A membrane reactor is a process which combines reaction and separation in a single unit (Sanchez Marcano & Tsotsis, 2002). They can be made from different materials such as metals, ceramics and polymers. Different definitions exist for membrane reactors (MRs) (Westermann & Melin, 2009).

The International Union of Pure and Applied Chemistry (IUPAC) defines a membrane reactor as a device for simultaneously carrying out a reaction and membrane-based separation in the same physical enclosure (Koros, Ma & Shimidzu, 1996). According to a wider definition, any reactor in which a chemical reaction is performed in the presence of a membrane is called membrane reactor (Saracco & Specchia, 1994). The application of membrane reactors has received

attention over five decades and quite a lot of papers have been published on the subject of catalysis, membrane science and chemical engineering (Julbe, Farrusseng & Guizard, 2001; Julbe & Ayrál, (2007); Coronas & Santamaria, 1999; Hwang, 2001; Lu *et al.*, 2007; Uemiya, 2004). The membrane is used as an active candidate in a chemical conversion for increasing the reaction rate, selectivity and yield (Julbe, Farrusseng & Guizard, 2001). The interest of membrane reactors has been demonstrated on the laboratory scale for dehydrogenation, hydrogenation, decomposition and oxidation reactions among others (Julbe, Farrusseng & Guizard, 2001). The concept has yet to be commissioned widespread for industrial application although some small industrial installations already exist (Julbe, Farrusseng & Guizard, 2001).

The drawback for commercial development of membrane reactors are the membrane themselves, their support and issues such as performance, cost and stability among others which still need to be optimized (Julbe, Farrusseng & Guizard, 2001).

In recent years, the concept applied to the combination of membranes and reactors is being proposed. The concept is classified into three groups namely; extractor, distributor and contactor which are related to the role of the membrane in the process (Julbe, Farrusseng & Guizard, 2001).

- ❖ ‘*Extractor*’ this type of concept is used to selectively remove the product(s) from the reaction mixture.
- ❖ ‘*Distributor*’ this type of concept is used to control the addition of reactants to the reaction mixture.
- ❖ ‘*Contactor*’ this type of concept is used to intensify the contact between reactants and the catalyst.

Extractor mode membrane reactors (Fig. 2.3) are applied to enhance conversion if there is limitation due to thermodynamic equilibrium. For example, by using catalytic dehydrogenation of alkanes which occurs by selectively extracting the hydrogen being produced (Dittmeyer, Höllein & Daub, 2001). Steam reforming of methane, water gas shift and the decomposition of H₂S have also been demonstrated on the laboratory scale with membrane using the reactor extractor mode (Westermann & Melin, 2009). Two main factors controlling the efficiency of this particular process are the hydrogen permeability of the membrane and its permselectivity. But most extractors feature the removal of hydrogen while some decomposition reactions consider oxygen removal (Julbe, Farrusseng & Guizard, 2001).

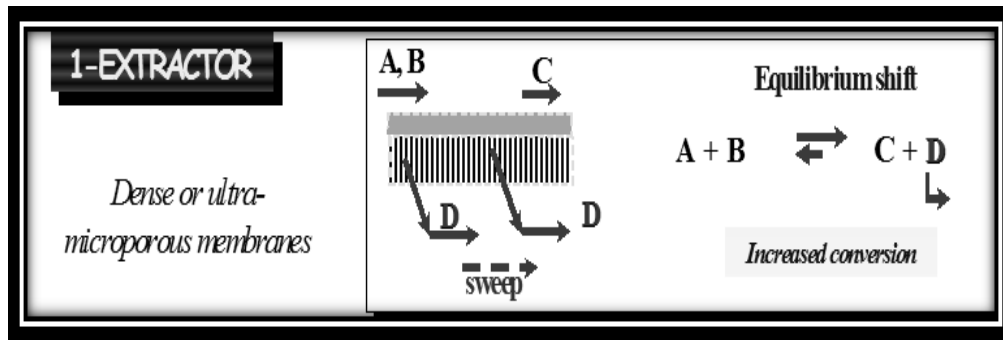
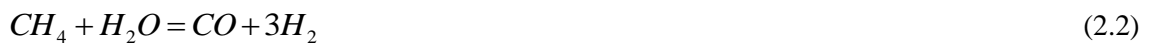


Figure 2.3 - The extractor mode membrane reactors (Julbe, Farrusseng & Guizard, 2001).

In 2002, the New Energy and Industrial Technology Development Organization (NEDO) and Japan Gas Association (Julbe, Farrusseng & Guizard, 2001) developed a compact and economical on-site hydrogen production unit based on steam methane reforming coupled with membrane technology. This system operated between 500-550 °C instead of 800 °C in classical methane reformers (Julbe, Farrusseng & Guizard, 2001). Hydrogen is selectively extracted by the Pd-based membrane, and the equilibrium is shifted to the production side;



Residual CO separated from H₂ is burned to CO₂. The CO in the newly developed systems is used in the water gas shift reaction in order to increase the H₂ yield (Julbe, Farrusseng & Guizard, 2001);



Gobina & Hughes, (1996) investigated the catalytic dehydrogenation of n-butane in a membrane reactor. They used palladium and gold (Pd/Ag) catalysts membrane with a thickness of 6µm. The use of inert nitrogen and reactive sweep gases nitrogen/carbon monoxide and nitrogen/oxygen enhanced their conversion of n-butane.

Dehydrogenation of cyclohexane to benzene has been investigated by Tiscarño-Lechuga, Hill & Anderson, (1996). A comparison between a pure membrane reactor, a conventional packed bed reactor, and a hybrid membrane reactors consisting of a packed bed reactor segment followed by a membrane reactor segment was carried out. The conversion obtained in a pure membrane reactor was 60 to 128% higher than that obtained in a conventional packed bed reactor. However, the increases in the conversion level obtained are not primarily attributed to the selective removal of hydrogen through the membrane but to the reduction of the partial pressures of the reactants in the retentate stream.

A *distributor mode* membrane reactor is the second mode of application for permselective membranes (Fig. 2.4). This mode is typically tailored in partial oxidation or oxy-dehydrogenation of hydrocarbons (Julbe, Farrusseng & Guizard, 2001). For example, in reacting an alkane with oxygen, a distributor is used to control the supply of oxygen in a fixed bed of catalysts. The supply of the oxygen by-passes the explosive zone in order to optimize the oxygen concentration and maximize the selectivity in the desired product (Coronas & Santamaria, 1999; Julbe, Farrusseng & Guizard, 2001). The oxygen permselectivity of the membrane is a significant factor since air can also be used rather than pure oxygen in the oxygen supply side (Coronas & Santamaria, 1999; Julbe, Farrusseng & Guizard, 2001).

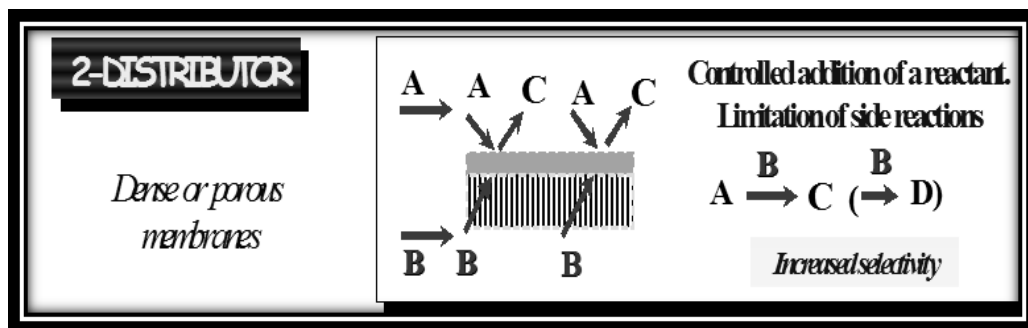
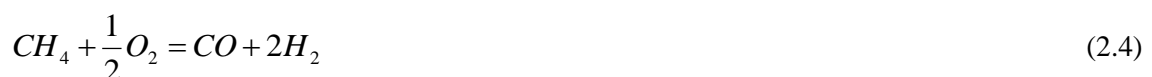


Figure 2.4 - The distributor mode membrane reactors (Julbe, Farrusseng & Guizard, 2001).

However, the main concern in this type of mode is that commercially available oxygen selective membranes being developed have low permeability (e.g. dense oxygen permselective membranes) and can only operate at relatively high temperatures $> 800\text{ }^{\circ}\text{C}$. Also, there are issues of long term stability (Julbe, Farrusseng & Guizard, 2001). Due to these constraints, some authors have applied macroporous and mesoporous membranes as oxygen distributors for oxidative reactions at temperatures $< 700\text{ }^{\circ}\text{C}$ (Coronas & Santamaria, 1999; Julbe, Farrusseng & Guizard, 2001). Air Products and Chemicals, Inc. conducted a research for converting methane to syngas by partial oxidation;



The membrane is able to transport oxygen at temperatures $> 700\text{ }^{\circ}\text{C}$ (Coronas & Santamaria, 1999; Julbe, Farrusseng & Guizard, 2001; Christopher, 2003). The membrane is also able to deliver highly reactive oxygen on the reaction side (Julbe, Farrusseng & Guizard, 2001).

Guanzhong, Shoucang & Ren, (1996) prepared SiO₂ (I) and Mo-Co-O/SiO₂ (II) microporous membranes. The catalytic membrane reactor (CMR) and the reactant-swept catalytic membrane reactor (RSCMR) have been proposed to investigate the oxidation of methane to methanol by air at atmospheric pressure and at 500-700 °C. They obtained a yield 0.5 g/m² h in CMR and 0.9 g/m² h in RSCMR of methanol. Also, the CMR using (II) microporous membrane supported on (I) of pore radius larger than 4nm resulted in poor catalytic activity. Under similar reaction conditions at 1.0% methane conversion, the methanol selectivity is 11.2% in CMR and 4.5% in a fixed bed reactor (FBR).

Coronas, Menendez & Santamaria, (1995) used a fixed bed of Li/MgO catalyst deposited on a porous ceramic membrane. Oxygen was permeated through the membrane while ethane was fed axially. They used two different configurations; a homogeneous wall membrane reactor and a mixed system equivalent to a membrane reactor followed by a conventional fixed bed reactor. They obtained high conversions of ethane, while maintaining good selectivity. The yield to ethylene and higher hydrocarbons of up to 57% was reported.

Tonkovich *et al.*, (1996b) also investigated the oxidative dehydrogenation of ethane to ethylene. They used a magnesium oxide catalyst which was doped with lithium and samarium oxide. Their findings showed that a membrane reactor outperforms a fixed-bed reactor in both ethylene conversion as well as selectivity to ethylene respectively.

The investigation of oxidative coupling of methane to improve yields over a fixed-bed reactor was proposed by Tonkovich *et al.*, (1996a). They obtained slight yield improvements with a samarium oxide doped magnesium oxide catalyst for oxidative coupling of methane.

In general, inorganic membrane reactors have been used successfully and proposed by many literatures (Capannelli *et al.*, 1996; Ramachandra *et al.*, 1996; Saracco *et al.*, 1995a; Saracco *et al.*, 1995b; Peureux *et al.*, 1995).

Finally, the active contactor mode membrane reactor involves a forced flow-through membrane reactor, where the membrane acts as a diffusion barrier and is catalytically active (Coronas & Santamaria, 1999; Julbe, Farrusseng & Guizard, 2001).

This type of membrane is used to provide a reaction space where the catalyst is deposited inside the membrane pores. The catalyst-membrane arrangement leads to high catalytic activity (Fig. 2.5) (Coronas & Santamaria, 1999; Julbe, Farrusseng & Guizard, 2001).

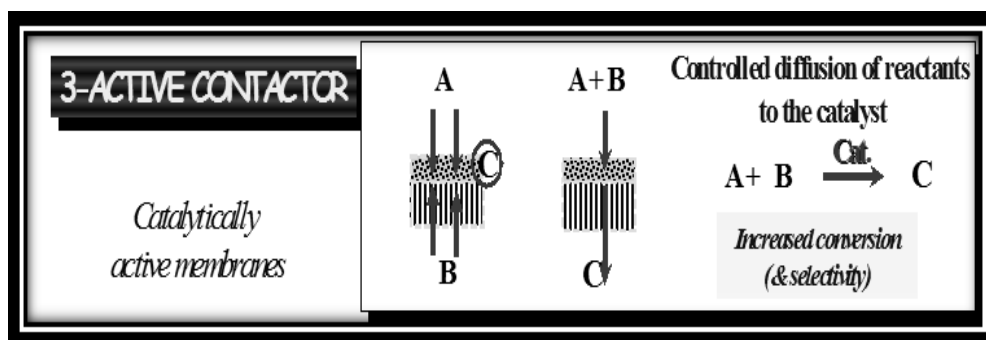


Figure 2.5 - The active contactor mode membrane reactors (Julbe, Farrusseng & Guizard, 2001).

The forced flow-through contactor mode has been widely employed by many researchers in the total oxidation of VOCs (Irusta *et al.*, 1998; Dittmeyer, Höllein & Daub, 2001; Lange *et al.*, 1998; Yamada *et al.*, 1988; Splinter *et al.*, 2002; Saracco & Specchia, 1995; Zalamea *et al.*, 1999; Maira *et al.*, 2003; Tsuru *et al.*, 2003).

Saracco & Specchia, (1995) prepared and then characterized ceramic porous filters used in their previous work (Saracco & Montanaro, 1995). The filters were deposited with a $\gamma\text{-Al}_2\text{O}_3$ layer via urea method for potential application in flue gas cleaning according to a combined action: mechanical particulate removal as well as catalytic abatement of chemical pollutants (nitrogen oxides, volatile organic compounds, etc.). They used isopropyl alcohol dehydration as a model reaction since it is directly catalyzed by $\gamma\text{-Al}_2\text{O}_3$ with no need of further catalytic activation. They proposed a reaction mechanism for their test reaction and the proposed kinetic rate expression was developed on the basis of experimental runs performed on a batch-operated differential reactor. The urea method was demonstrated to be a reliable tool to deposit a $\gamma\text{-Al}_2\text{O}_3$ layer uniformly over the pore walls of the filter, markedly increasing its specific surface area. The drawbacks of the procedure employed are the occurrence of pore blocking after a few deposition cycles and the occasional presence of cracks in the deposited layer.

The development and application of perovskite-based catalytic membrane reactors was proposed by Irusta *et al.*, 1998. They prepared and characterized catalytic membranes containing La-based perovskites. The membranes were prepared by *in-situ* crystallization of different perovskites inside a porous α -alumina matrix. The dominance of the Knudsen diffusion regime was obtained with perovskite loads of 2 wt% and higher. The catalytic membranes obtained were used as combustors of VOCs (toluene and methyl ethyl ketone) contained in air streams, at concentrations between 875 and 3450 ppm V, and space velocities of up to 27200 h^{-1} . The membranes were operated in the flow-through mode, which resulted in total VOC combustion at moderate temperatures. Their main concern with the preparation of the perovskite membranes

was the low surface area obtained, especially in the membranes prepared at the higher temperatures. Their recommendation to overcome this difficulty was to reduce the number of high temperature steps required.

Splinter *et al.*, (2002) in their work used a flow-through membrane for gas pre-combustion based on porous silicon technology combined with anisotropic silicon etching. They were able to adjust the active area and retention time in order to achieve nearly 100% CO conversion.

Zalamea *et al.*, (1999) also developed catalytic membranes operating in a mixed permeation regime i.e. Knudsen and laminar contributions. The membranes prepared had wide pores and presented a low pressure drop. The Pt/ γ -Al₂O₃ were active for VOC combustion. They achieved complete n-hexane conversion at 300 °C with 2 wt.% γ -Al₂O₃ and 0.15 wt.% Pt.

Pina *et al.*, (1997) investigated the combustion of VOCs over platinum-based catalytic membranes in a porous catalytic membrane using toluene and methyl ethyl ketone (MEK) as representatives of VOCs. The Pt loading used was between 0.016 and 0.45 wt % as a catalyst and the membrane operating under the Knudsen diffusion regime. The two methods used were impregnation and chemical vapour deposition (CVD). The membrane performed efficiently allowing total VOC destruction at low temperatures below 300 °C.

Saracco & Specchia, (2000) also investigated VOC abatement with catalytic filters using Pt/ γ -Al₂O₃ catalyst by the wet impregnation method. However, they also used naphthalene representing PAH, propylene representing alkenes, propane representing alkanes and methane well-known refractoriness to catalytic combustion as VOCs at a temperature of up to 600 °C.

Tahir & Koh, (1999) extended the development of noble metal catalysts by depositing a low Pt loading on the external surface of the Al₂O₃ support for the removal of traces of various VOCs. They applied a series of Pt loadings (0.05, 0.1, 0.2, 0.3 and 0.4 wt. %) for methanol, toluene, n-butyl-amine and n-hexane destruction. The authors observed a 50% increase of the temperature during toluene conversion from 180 °C to 263 °C when Pt loading decreased from 0.4 to 0.05 wt. %.

Benard *et al.*, (2009) investigated the conversion of propene and toluene. They applied a series of Pt catalysts loadings 0.56, 0.9 and 1.5 wt. % respectively. Complete conversion of propene occurs at 140 °C for 1.5 wt. %, at 152 °C for 0.9 wt. % and at 175 °C for 0.56 wt. %. In the case of toluene conversion, the catalytic activity also increased with the Pt loading. Complete

conversion occurred at 227 °C for 0.9 wt. %, while the temperature slightly rose to 250 °C when Pt content decreased to 0.56 wt. %.

Within the last few decades, systematic research was undertaken with a membrane reactor which confirms that forced flow-through contactor membrane reactor is a promising alternative technology for the combustion of VOCs. Also, the flow-through membrane reactor may lead to decreased light-off and total VOC combustion temperature in addition to a lower overall Pt loading.

2.6 Inorganic Membranes for Gas Separation and Recovery

Gas separation processes started in 1829 when Thomas Graham conducted his first experiment on gas and vapour transport with polymeric membranes. Later in 1866, he also reported ideas for gas permeation with regard to a solution-diffusion mechanism (Sanders *et al.*, 2013). A quantitative explanation for the transport of material via boundary coatings was suggested by Fick in 1855 (Pandey & Chauhan, 2001). Both concepts have significantly contributed to the knowledge of gas-diffusion phenomena across membranes. Widespread work on the development of membranes and membrane processes for gas separation has been done in many literatures. Several books have also been published on membrane science and technology which includes membrane material selection, process principles, process design and applications among others (Mulder, 1996; Baker, 2004; Bose, 2009; Li, 2007; Yampolskii & Freeman, 2010; Hsieh, 1996).

In the last five decades, modern membrane science and technology has advanced and sufficient knowledge between their structures and function in gas-separation has been presented (Smart *et al.*, 2013). In the late 1980s, small membrane units for organic vapour separation from air were first installed. Around the mid-1990s, some million-dollar systems were sold by Membrane Technology and Research, Inc. (MTR) to petrochemical plants for the recovery of olefins from polyolefin manufacture. At that time, the European GKSS technology started installing large systems for gasoline vapour capture from fuel terminals and tank farms (Baker, 2001). The market of vapour separation systems is growing at about \$20-30 million per annum. Almost 500 small scale systems are now in operation with a value of \$10,000-\$100,000 each for vapour emissions captured from petrochemical process vents, retail gasoline stations and industrial refrigerator units (Baker, 2001). Gas separation using membranes later emerged as a commercial process on a large scale where significant improvements were achieved. These included; membrane formation processes, chemical and physical structures, as well as configuration and applications (Smart *et al.*, 2013).

A membrane is basically a barrier that is selective to specific component and hinders others to pass (Fig. 2.6) and is driven by a concentration difference across the membrane. Membranes are widely used for purification in industry e.g. waste water treatment, pharmaceuticals, food, and biochemistry (Jin, Yiqun & Nanping, 2010) among others. Membrane technology has gained acceptance for gas separation and recovery. This includes carbon dioxide separation from fuel gas (Luebke, Pennline & Myers, 2005), hydrogen separation/recovery for fuel cell application (Shah *et al.*, 2011), hydrogen separation from natural gas (Kajama *et al.*, 2014), ethylene recovery in ethylene oxide, gasoline vapour recovery (Baker, 2001) and recovery of methane from bio-gas (Othman, Mukhtar & Ahmad, 2004).

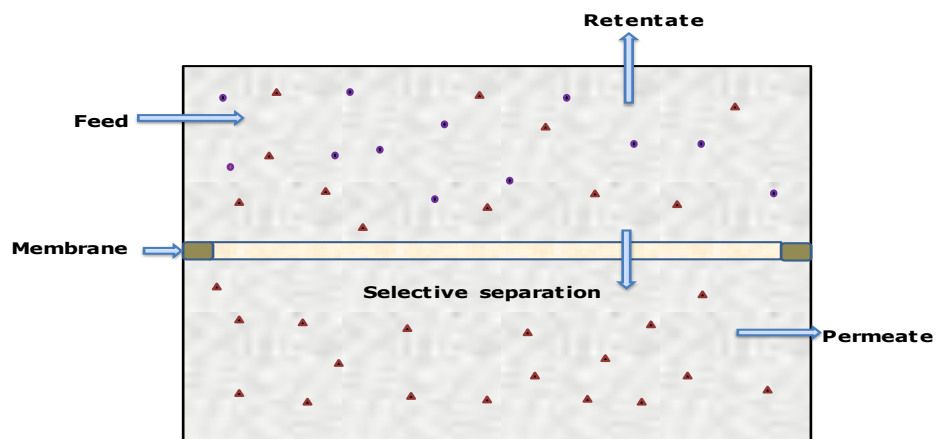


Figure 2.6 - Membrane design.

Membrane gas separation possesses several advantages when compared to other gas separation processes such as adsorption, absorption, cryogenic distillation. The advantages of membrane separation includes; compact and light, easy to operate and maintain, does not involve phase change, environmentally benign, cost-effective and energy efficient (Kajama *et al.*, 2014; Ohwoka, Ogbuke & Gobina, 2012a).

Membranes can be classified into inorganic, organic and organic/inorganic (hybrid) systems. The organic ones are further divided into biological and polymeric constituents, while the inorganic membranes can be divided into metallic and ceramic (porous and non-porous) membranes (Lu *et al.*, 2007). According to IUPAC, porous membranes are classified as; Micropores < 2 nm where separation is based on molecular sieving mechanism, mesopores 2 - 50 nm where the Knudsen flow mechanism is the dominant flow but multilayer flow and/or capillary condensation and viscous flow can also take place, and macropores > 50 nm where there is no separation and the

flow mechanism is basically influenced by viscous flow (Zhang *et al.*, 2009; Ahmad & Mustafa, 2007; Carlos & Joaquin, 1999). In all cases, some considerations on productivity and separation selectivity, mechanical integrity, and membrane durability at the operating conditions needs to be taken into account against cost issues (Lu *et al.*, 2007) because the importance of each of these requirements differs with their applications. In fact, permeability and selectivity are the main basic properties of a membrane. It can be elaborated that the higher the permeability, the lower the membrane area is required. Also, the higher the selectivity, the more efficient the process, the lower the driving force required to attain a separation and therefore the lesser the operating cost of the separation (Lu *et al.*, 2007). On the one hand, the technical merits of inorganic membranes include chemical stability over wide pH, high thermal stability, long term durability as well as high structural integrity. Some of the demerits include the fact that they are expensive, and have low hydrothermal stability. On the other hand, the technical merits of polymeric membranes include the fact that they are cheap. The demerit of polymeric membranes is that they are prone to denature and being contaminated, they are structurally weak, and they are not stable (Lu *et al.*, 2007) which hinders the use of such membranes for gas separation at high temperature. It is for these reasons that the inorganic material membrane is receiving an ever increasing attention (Adom *et al.*, 2012). Inorganic membranes are commonly made from metal oxide or sintered metal, palladium metal, zeolite among others (Lu *et al.*, 2007).

Lin & Burggraaf, (1991) prepared and characterized crack and pinhole-free composite alumina membranes consisting of an alpha-alumina support and a modified gamma-alumina top layer. The membrane was prepared via the sol-gel method and was thermally stable up to 1100 °C. The supported thermally stable top layer was made by dip-coating the support with a boehmite solution doped with lanthanum nitrate. The average pore diameter of the La-doped alumina top layer was 17 nm after sintering at 1100 °C for 30 hours compared to 109 nm for the common alumina top layer.

2.6.1 Gas Transport Mechanism in Membrane

Gas transport mechanisms through porous membranes are influenced by viscous flow, Knudsen diffusion, surface flow, multi-layer diffusion, capillary condensation, molecular sieving and solution-diffusion (Ohwoka, Ogbuke & Gobina, 2012b; Kentish, Scholes & Stevens, 2008; Kim *et al.*, 2001).

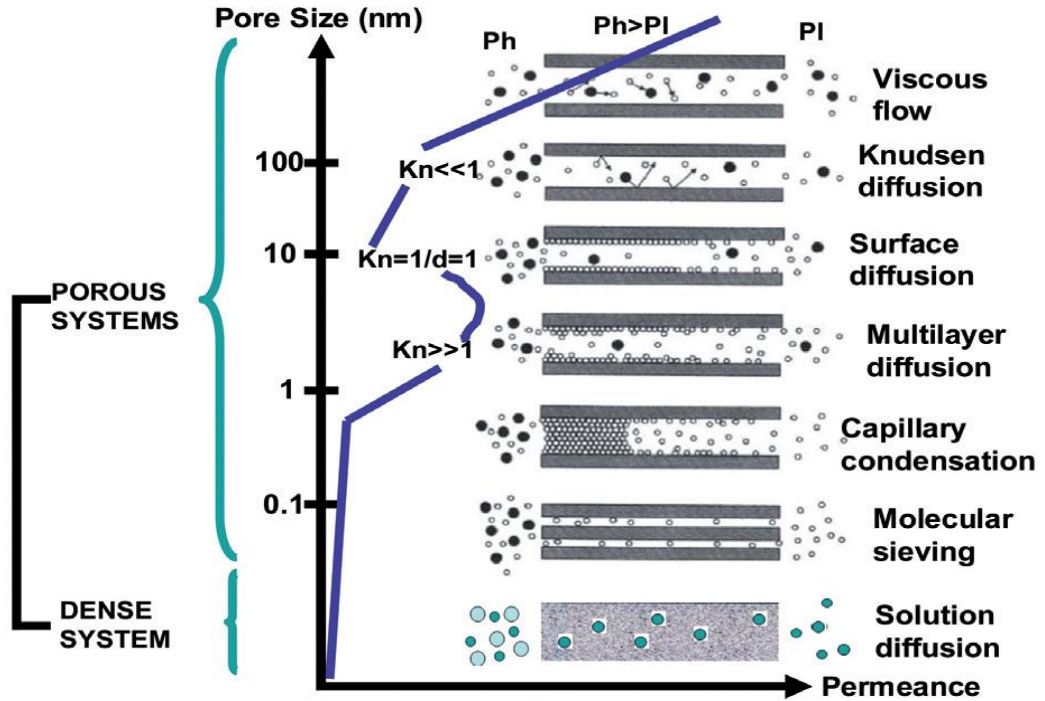


Figure 2.7 - Gas Transport Mechanism for Membrane (Ohwoka, Ogbuke & Gobina, 2012b).

2.6.1.1 Viscous Flow

This is also known as Poiseuille flow and occurs if the mean free path (average distance travelled by a gas molecule from one collision to the other) is much smaller than the pore diameter. The flow characteristics are determined primarily by collisions among the molecules and no separation is obtained between the different gaseous components. In gas membrane separation processes, viscous flow mechanism is an unwanted transport mode because it is non-selective. In viscous flow, the flux can be written as (Wall, Braun & Brunner, 2010);

$$P_v = \left(\frac{\varepsilon r^2 P_{av} \Delta P}{8\pi\mu RTL} \right) \quad (2.5)$$

where;

$$P_{av} = \frac{P_1 + P_2}{2} \quad (2.6)$$

Where ε is the porosity of the membrane, r is the mean pore radius (m), P_{av} is the average pressure (Pa), ΔP ($P_1 - P_2$) is the pressure difference (Pa) between the high pressure side and low pressure side, μ is the viscosity (Pa-s), R gas constant ($8.314 \text{ J.K}^{-1}.\text{mol}^{-1}$) and T is the permeation temperature (K) and L is the thickness of the membrane (m).

2.6.1.2 Knudsen Diffusion

Transport of gases through Knudsen diffusion occurs if the mean free path is effectively larger than the pore diameter. If the collisions among the permeating molecules and the pore wall of the membrane are more frequent than intermolecular collisions, the separation is based on molecular weight difference (Ohwoka, Ogbuke & Gobina, 2012b; Wall, Braun & Brunner, 2010; Kim *et al.*, 2001). Thus, Knudsen permeance states that the permeation flux is proportional to the inverse square root of both molecular weights of gases and temperature which can be written as;

$$P_{kn} = \frac{\varepsilon 8r_p \Delta P}{3\tau L (2\pi RTM)^{0.5}} \quad (2.7)$$

Where τ is the tortuosity which describes the geometry and transport properties of porous media and M is the molecular weight of the diffusing gas (g/mol).

2.6.1.3 Surface Diffusion

Transport through surface diffusion occurs if the diffusing molecules exhibit strong attraction (adsorbed) with the pore walls of the membrane and migrates along the pore surface and desorbs on the permeate site of the membrane. In surface diffusion, the main driving force is the chemical potential. Surface diffusion can occur in parallel with Knudsen diffusion (Sotirchos & Burganos, 1999).

2.6.1.4 Multi-Layer Diffusion

Multi-layer diffusion occurs if the flow of gas molecules is adsorbed in the membrane at a different number of layers. Gas mixture permeates through the pores of the membrane at a given pressure and temperature.

2.6.1.5 Molecular sieving

Molecular sieving is used to separate gas molecules which differ in kinetic diameter. It enables the permeation of gases which have lower kinetic diameter to pass through the membrane “sieve” than the larger ones (Ohwoka, Ogbuke & Gobina, 2012b). Zeolite membranes possess pore sizes that are of the same size of the gas molecules and can result in very high separation factors (Khan & Ghoshal, 2000).

2.6.1.6 Solution-Diffusion

Solution-diffusion separation relies on the physical-chemical interaction of gases and the dense membrane that determine the amount of gas which accumulates in the membrane matrix (Kentish, Scholes & Stevens, 2008).

2.6.1.7 Combined Transport

The property of gas diffusion is influenced by the ratio of the molecule-molecule collision to the number of molecule-wall collisions. The so-called Knudsen number is used to classify gas flow in a porous media which is written as (Ohwoka, Ogbuke & Gobina, 2012b; Wall, Braun & Brunner, 2010);

$$K_n = \frac{\lambda}{d_p} \quad (2.8)$$

Where λ is the mean free path of gas molecules, and d_p is the pore diameter.

Also the mean free path can be defined as the distance traversed by a gas molecule from one collision to the other and is given as (Wall, Braun & Brunner, 2010; Mulder, 1996);

$$\lambda = \frac{RT}{\sqrt{2}\pi d^2 N_A P} \quad (2.9)$$

where N_A is the Avogadro's number ($6.02214129 \times 10^{23} \text{ mol}^{-1}$), d diameter (m).

2.6.2 Factors That Influence Operating Variables

Among the several factors which influence membranes operating parameters are; feed concentration, transmembrane pressure and temperature (Othman, Mukhtar & Ahmad, 2004; Hsieh, 1996).

2.6.2.1 Feed Concentration

The increase of feed concentration increases the permeate flux (Othman, Mukhtar & Ahmad, 2004). Also, higher feed concentration raises the fluid viscosity (Hsieh, 1996). Separation of a gas tends to increase owing to the concentration of lighter gas species in the feed stream is increased due to the more impetus that the lighter gas species gain from collision between its own molecules (Othman, Mukhtar & Ahmad, 2004).

2.6.2.2 Transmembrane Pressure

As stated by Hsieh, (1996), transmembrane pressure is the driving force for permeation to occur along the membrane. A linear function of the transmembrane pressure is normally obtained as pure fluid permeates through the membrane. Similarly, for example, if a mixture is passed through the membrane, the permeate flux is lower than that of pure feed due to concentration polarization (Hsieh, 1996). Separation of gases is normally attributed to Knudsen diffusion mechanism at relatively low pressure. However, by increasing pressure substantially, separation of gases can exceed the boundary of Knudsen separation factor shifting towards surface diffusion mechanism (Othman, Mukhtar & Ahmad, 2004).

2.6.2.3 Temperature

Fluid viscosity is usually affected by changes in temperature. Therefore, the influence of temperature on permeation is important. Gas viscosity at low density increases with temperature, and thus if temperature rises, gas permeate flux becomes lower (Hsieh, 1996; Othman, Mukhtar & Ahmad, 2004).

A brief literature review covering membranes and methods for catalytic VOC destruction in order to yield CO₂ and H₂O is presented here.

3 Experimental Procedure and Equipment Setup

3.1 Introduction

This chapter presents a detailed description of the design, fabrication, and operation method of a tubular membrane reactor for separation and reaction. This tubular membrane reactor, employs a commercially available alumina membrane which possesses high temperature and chemical poisoning resistance. The quality of the membrane is important particularly when applying alumina membrane for gas permeation, CO₂ recovery, H₂ recovery, VOC recovery and VOC destruction.

The membrane preparation and characterization technique used in this study is presented in this chapter. In addition, the experimental procedure of silica membrane and the reactions of the VOCs destruction process are also presented. The details of the gases used are presented in table 3.1.

Table 3.1- Characteristics of the gases uses for the experiments.

Gas	Outlet pressure (bar)	Purity (% vol.)
Argon	230	99.97
Carbon dioxide	230	99.95
Helium	200	99.90
Hydrogen	200	99.90
Methatne	230	99.90
N-butane	14	99.97
Nitrogen	230	99.97
Oxygen	14	99.99
Propane	5	99.50
Propylene	5	99.50

3.2 Equipment Setup

The experimental rig consisted of feed delivery, reaction, and analytical systems. It was designed for the purpose of fundamental study. This chapter provides details of the experimental apparatus.

3.2.1 Membrane Reactor

The schematic diagram of the experimental rig is illustrated in Figure 3.1. It consisted of the feed delivery system, the membrane contactor/separator and the analytical system. The reactor used was a tubular membrane reactor in a shell configuration. The shell was made from stainless steel material and has 28mm I.D., 36mm O.D., 395mm long, 5mm thick that can withstand high temperatures. The stainless steel shell was covered with heating tapes in order to maintain the heating of the reactor system. The two ends were removable for membrane replacement purpose. Gas tightness between the shell was maintained by graphite O-rings and gaskets. Two graphite rings (one at each end) were used as sealing for the alumina tube ends to withstand high temperature as well as allowing for thermal expansion of the alumina membrane.

The reactants were introduced into the reactor entrance (feed) using mass flow controllers. The reaction experiments occurred at atmospheric pressure within the stainless steel reactor. The product (permeate) was analysed by a CO₂ analyser. The water formed in the reaction was removed from the effluent in a moisture trap at room temperature. A pictorial view of the entire experimental rig is depicted in Figure 3.2.

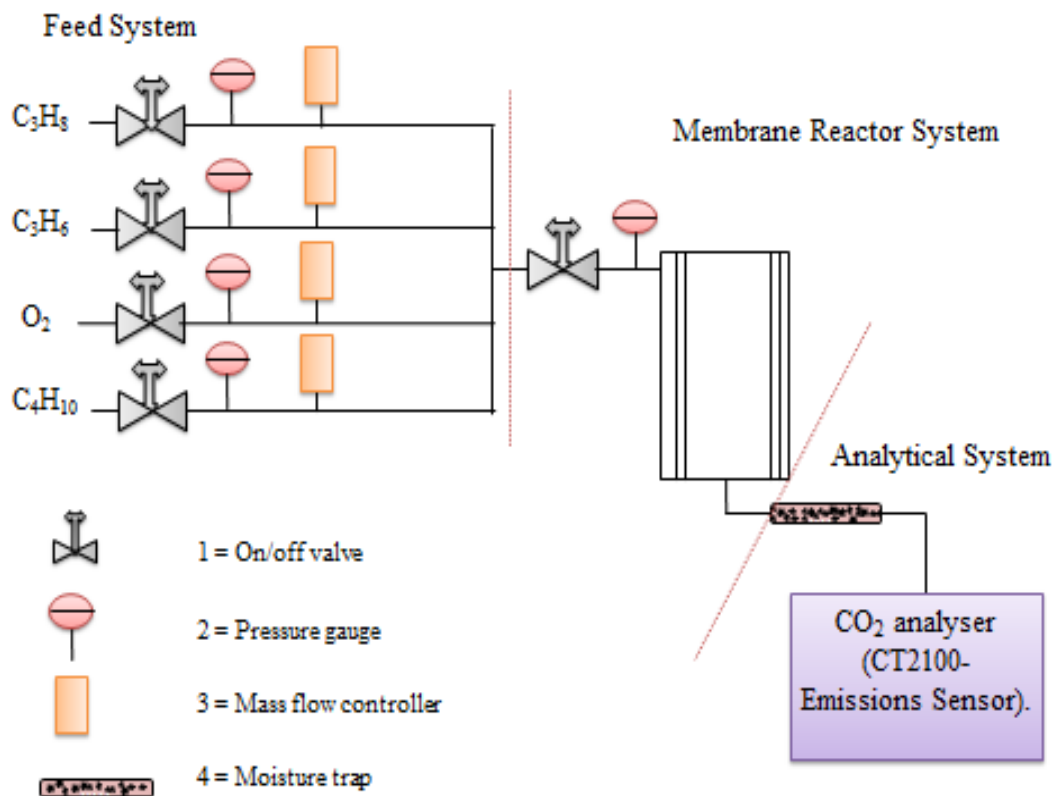


Figure 3.1 - Schematic diagram of the feed, membrane reactor and analytical systems.

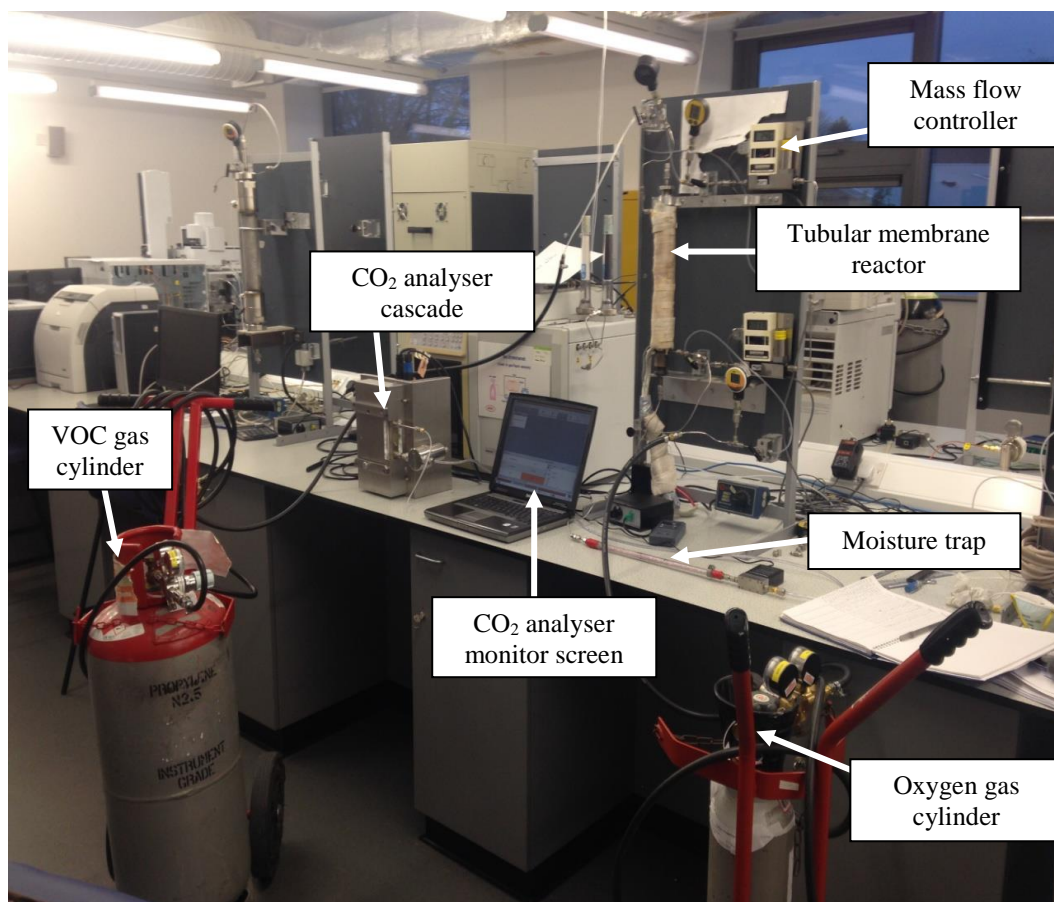


Figure 3.2 - Pictorial view of the experimental rig.

3.2.2 Alumina Ceramic Membrane

Several factors were considered in selecting the membrane for this experiment. An alumina support was chosen because of its lower maintenance cost, although its permselectivity is slightly low. Platinum supported on γ -alumina was demonstrated as the most efficient catalytic system for VOC destruction (Liotta *et al.*, 2009; Marécot *et al.*, 1994; Paulis, Peyrard & Montes, 2001; Benard *et al.*, 2009) leading to the lowest operating temperature.

The alumina tube supplied by Ceramiques Techniques et Industrielles (CTI SA) France composed of 77% alumina + 23% TiO_2 possesses an internal and outer diameter of 7 and 10 mm respectively. The alumina support consisted of a permeable length of 348 mm and a porosity of 45%. This alumina support was chosen because it possesses good resistance to corrosion and oxidation, as well as chemical and mechanical stability at high temperature, and it is commercially available in different shapes and sizes. The tubular alumina membrane used for this experiment is depicted in Figure 3.3.



Figure 3.3 - Pictorial view of commercial tubular ceramic support.

3.2.3 Pressure Gauges/Manometers

The inlet pressure of the reactor were measured with highly accurate and versatile digital pressure measuring gauges (Keller Druckmesstechnik, Winterthur, Switzerland) with an accuracy of 0.1% factory setting at room temperature. The gauge has two operating keys. The left key is used to turn the instrument on, which allows selection of the pressure unit, while the right key allows execution of the selected unit/function. The right key also allows switching between the maximum and minimum value. The working pressure range of this pressure gauge is between -1 to 30 bar.

3.2.4 Thermocouple

The K type 6-way switch box bench selector (RS components) in a moulded housing with aluminium front and rear panels were employed as temperature sensors for the reactor's shell and tube. The 6 rear inputs are switched through a front mounted rotary selector switched to the single output socket.

3.2.5 Thermometer

Temperatures were measured using intrinsically safe digital thermometers Digitron (Sifam Instruments Ltd, Torquay UK). This instrument is certified for use in flammable environments. The working temperature ranges between -50 to 950 °C.

3.2.6 CO₂ analyser (CT2100-Emissions Sensor)

Cascade's CT2100 sensors monitor the amount of CO₂ from ambient environments of up to 70 °C and gas temperatures of 450 °C. The sensor is installed at the measurement point (in a stack) and configured to maintain a flow of gas at constant temperature and pressure within the sample cell. The capability measurement is in (%). A 240V-AC/DC convertor was connected to the sensor. A PC was also connected to the sensor port in order to record the conversion %. This system is applied in places such as power plant emissions monitoring, engine combustion tools, ship emissions monitoring, carbon trading among others.

3.2.7 Propane Gas

Propane gas with 99.5% purity was supplied in cylinders by BOC (UK) with maximum pressure at 288.15 K of 5 bar, and has an outlet connection of ¼" compression Swagelok (standard outlet connection). A flashback arrestor was connected to the hose of the regulator for safety reasons.

3.2.8 Propylene Gas

N2.5 grade propylene gas with 99.5% purity was supplied in cylinders by BOC (UK) with a maximum working pressure at 288.15K of 5 bar, and has an outlet connection of ¼" compression Swagelok (standard outlet connection). A flashback arrestor was connected to the hose of the regulator for safety reasons.

3.2.9 N-butane Gas

N-butane gas with 99.97% purity was supplied in cylinders by BOC (UK) with maximum working pressure at 288.15K of 14 bar, and has an outlet connection of ¼" compression Swagelok (standard outlet connection). A flashback arrestor was connected to the regulator for safety reasons.

3.2.10 Oxygen Gas

N5.0 grade oxygen gas with 99.999% purity was supplied in cylinders by BOC (UK) with maximum working pressure at 288.15K of 14 bar, and has an outlet connection of ¼" compression Swagelok (standard outlet connection).

3.2.11 Nitrogen Gas

Nitrogen gas with 99.97% purity was supplied in cylinders by BOC (UK) with maximum pressure at 288.15 K of 230 bar. Additional purification was unnecessary.

3.2.12 Methane Gas

Methane gas with 99.9% purity was supplied in cylinders by BOC (UK) with maximum pressure at 288.15 K of 200 bar.

3.2.13 Carbon Dioxide Gas

Carbon dioxide gas with 99.95% purity was supplied in cylinders by BOC (UK) with maximum pressure at 288.15 K of 230 bar.

3.2.14 Hydrogen Gas

Hydrogen gas with 99.9% purity was supplied in cylinders by BOC (UK) with maximum pressure at 288.15 K of 200 bar. A flashback arrestor was connected to the hose of the regulator for safety reasons.

3.2.15 Helium Gas

Helium gas with 99.9% purity was supplied in cylinders by BOC (UK) with maximum pressure at 288.15 K of 200 bar.

3.2.16 Sylgard(R) 184 Silicone Elastomer Kit

Sylgard(R) 184 silicone elastomer kit was supplied from Dow Corning Corporation (U.S.A). The silicone is in liquid form, colourless with some odour. The complete kit comes with a 50ml bottle of curing agent. No health effect is expected in case of contact with skin.

3.2.17 2-Methylbutane (Iso-pentane)

2-Methylbutane (Iso-pentane) was supplied in 500ml glass bottle from Sigma-Aldrich (UK).

3.2.18 Boehmite Powder

Alumina monohydrate (AlO(OH)) Boehmite powder was supplied by Alcan Chemicals Europe. Boehmite is a non-hazardous product.

3.2.19 Platinum Metal Solution

Chloroplatinic acid solution (H_2PtCl_6), 8 wt% in water was supplied by Sigma-Aldrich (UK) in 50ml glass bottle.

3.2.20 Silica Membrane Preparation

Commercially available porous alumina support of tubular configuration (Figure 3.3) with an average pore diameter of 30 nm was employed to obtain a silica membrane. The alumina support consisted of an internal and outer diameter of 7 and 10 mm respectively. The support possesses a permeable length of 348 mm and a porosity of 45%.

The Si/ γ -Al₂O₃ membrane was prepared by the repeated dip-coating technique proposed by (Gobina, 2006; Nwogu, Gobina & Kajama, 2013). The solution was prepared by mixing 50ml of silicon elastomer (Sylgard[®]) and nine parts of isopentane contained in a glass tube to obtain a clear and colourless solution. A curing agent (Sylgard[®]) equivalent to one-tenth of the elastomer was added and the resulting solution was mixed at room temperature. The solution was then allowed to age for 30 minutes after which the ceramic support was immersed in the solution for 30 minutes. The membrane was then oven dried at 65 °C for 24 hours (Gobina, 2006) to form an ultra-thin layer on the support. The same procedure was repeated for subsequent coatings. Up to five coatings were prepared and evaluated at room temperature in this experiment.

3.2.21 Catalytic Membrane Preparation

The Pt/ γ -Al₂O₃ membrane was prepared by the repeated dip-coating technique. Chloroplatinic acid solution (H₂PtCl₆) has been used as a platinum precursor. The tubular support was first dried at 65 °C. After weighing, it was dipped for 2 hours in deionised water before Pt introduction. The deposition method used was based on evaporation-crystallization steps.

This method was based on the so-called “reservoir” method proposed by (Uzio, Miachon & Dalmon, 2003; Iojoiu *et al.*, 2003). The tube was first dipped for 2 hours in deionised water afterwards the tube was dipped in a 10g/l H₂PtCl₆ precursor solution for 10 hours. The sample was then dried at room temperature for 24 hours to favour evaporation from the inner side and deposition in the top layer.

Metallic platinum was obtained after thermal treatment of the sample under flowing hydrogen at 400 °C for at least 10 min followed by nitrogen flow for 10 min at 400 °C. After the above processes the membrane could be used as a reactor.

3.2.22 Membrane Reactor Operation Procedure

Leak test was carried out by flowing N₂ through the system prior to the experiment. Permeate was measured to ensure the system was leak-free. The reactor was then heated up to experimental temperature.

The temperature in the reactor was regulated by an electro thermal power regulator (ETPR Figure 3.4). Temperatures in the tube side were measured using a k-type thermocouples located axially in the membrane tube (TM Figure 3.4). Also, pressures were measured by pressure gauges along the reactor (P1 to P3 Figure 3.4).

The reactants (VOCs and oxygen) were fed through the mass flow controllers (MFC1 and MFC2 Figure 3.4) to the feed side (F1 Figure 3.4) of the membrane reactor. Products (CO_2 and H_2O) flows from the permeate stream (PM Figure 3.4) through the moisture trap where the moisture trap absorbs the H_2O , and the CO_2 flows through the digital flowmeter (FM Figure 3.4) to the CO_2 analyser. The retentate stream (RTN Figure 3.4) was closed.

After each experiment, the reactor was cooled down. Before starting each experiment, N_2 gas was purged through the system and hoses to remove residual reaction gases from the system. This was used in order to minimize error that any residual gases may cause.

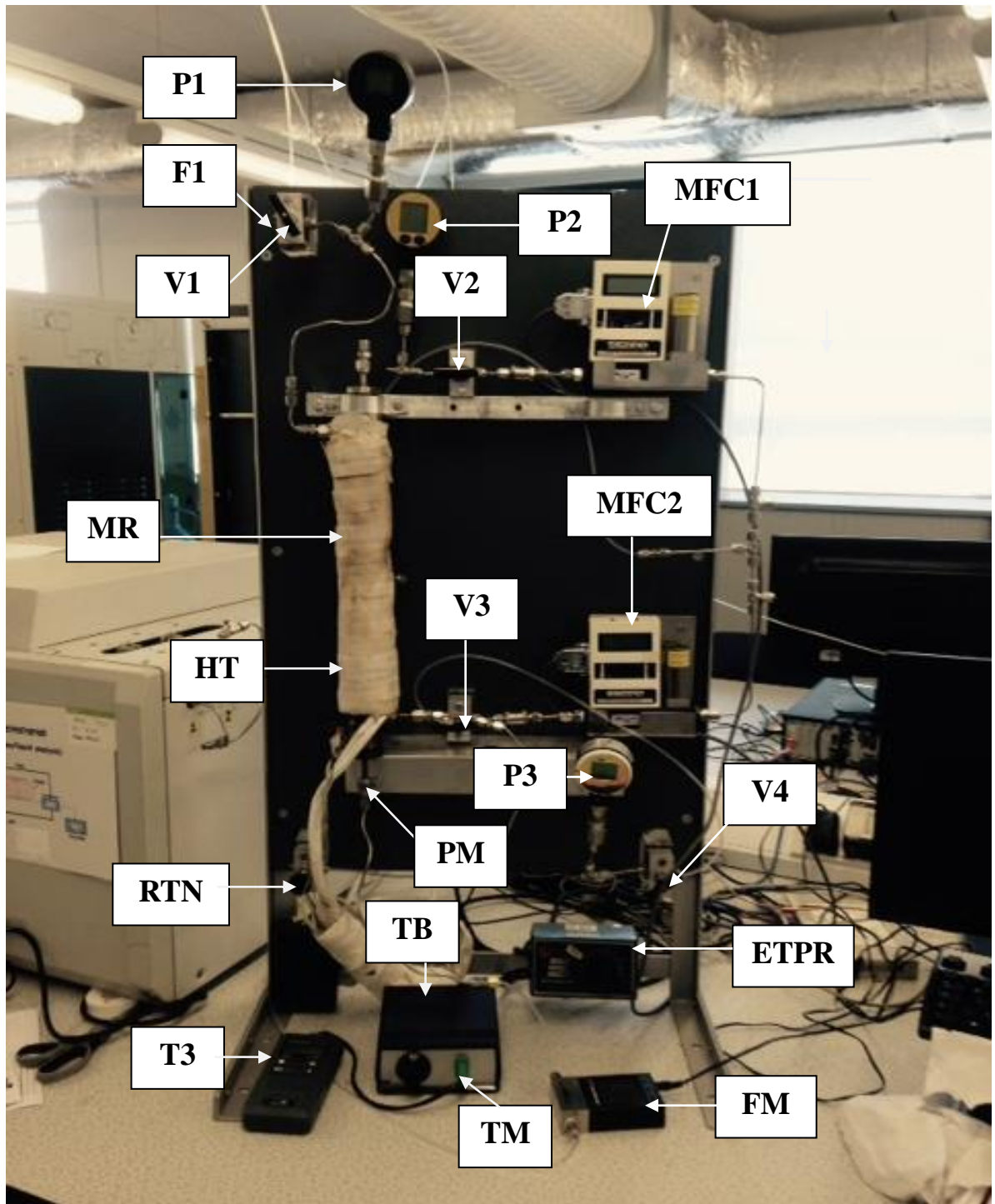


Figure 3.4 - Pictorial view of the reactor section.

NOTE:

TM = Thermocouple
 FM = Flowmeter
 PM = Permeate
 RTN = Retentate
 HT = Heating tape
 MR = Membrane reactor

TB = Thermocouple box
 ETPR = Electro thermal power regulator
 P = Pressure gauge
 V = Valve
 F1 = Feed side
 MFC = Mass flow controller

3.2.23 Procedure of CO₂ Analyser Calibration and VOCs Conversion

3.2.23.1 CO₂ Analyser Calibration Procedure

CO₂ analyser (Cascade's CT2100 sensors) was connected from the catalytic membrane reactor permeate side. As the reactants (VOCs and O₂) fed into the feed side of the catalytic membrane reactor, combustion/conversion occurs at different flow rates, pressures and reaction temperatures, were the products (CO₂ and H₂O) permeated through the permeate side of the membrane reactor, passing through the moisture trap (where the H₂O is been absorbed) through the digital flowmeter to the CO₂ analyser in order to record the % concentration of the product CO₂.

The CO₂ analyser was calibrated before the experiment. CO₂ gas cylinder with 99.95 % vol. was connected to the cascade analyser. The CO₂ value to be calibrated was set from 0-3.5% at temperatures between 88-89°C and pressures between 0-7600 Torr. Shakya, Deegan & Hegarty, (2015) in their work calibrated 5% CO₂ gas using the static calibration method were they claimed that the method used as the current technique for calibrating CO₂ analysers, because it is widely accepted as a valid technique for such gas analysers (Shakya, Deegan & Hegarty, 2015).

Infrared detectors are built inside the cascade were the CO₂ % are measured. The IR Quantum Cascade Lasers (QCL) is highly sensitive detectors which senses the changing light intensity as the laser beam passes through the gas (CO₂). When a current pulse of sub-microsecond duration is applied, the QCL exhibits a nearly linear wavelength scan. Cascade have patented this novel approach and refined the use of this phenomenon to produce instantaneous wavelength tuning across the absorption lines of the gas (CO₂).

In this experiment, after setting the calibration inputs, carbonTrustB was selected for low CO₂ concentration value. Work icon from the tool bar was selected to start the calibration, where data obtained are shown on Fig. 3.5. The response of the CO₂ analyser between the real and speculated data was obtained to be nearly identical as seen from the curve. The calibration response from the CO₂ analyser was not linear, but the concentration of the speculated data agreed with the calibration curve.

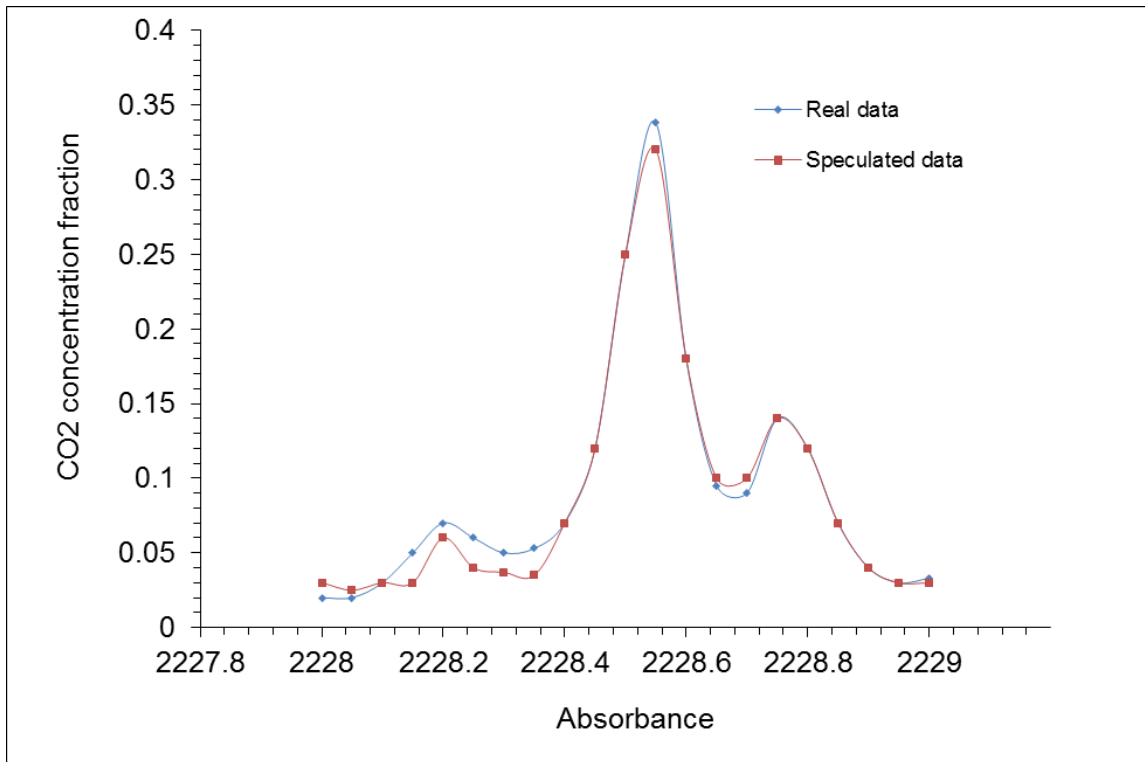


Figure 3.5 - Calibration curve of the CO₂ analyser.

3.2.23.2 VOC Conversion Calculation

The conversion of VOCs was calculated using equation (3.1) (Delimaris & Ioannides, 2008; Delagrange, Pinard & Tatibouet, 2006).

$$X_{VOC}(\%) = \frac{VOC_i - VOC_o}{VOC_i} \times 100 \quad (3.1)$$

where VOC_i is the flow rate of VOC at the feed recorded from the flow meter, and VOC_o is the permeate flow rate of VOC at the permeate recorded from the flow meter respectively.

As seen in Tables 3.2, 3.3 and 3.4, the obtained value for conversion from each VOC at different temperature is presented. The CO₂ analyser (%) values are the concentration of CO₂ obtained from the analyser after combustion, whereas the VOC conversion (%) obtained from the calculation made using eqn. 3.1. Only 2 decimal places were used because the obtained data from the CO₂ analyser were set at 2 decimal places.

Table 3.2- N-butane conversion

Temperature (°C)	VOC conversion (%)	CO₂ analyser (%)
242	3.64	3.48
242	4.20	4.05
247	6.40	6.31
251	9.71	9.51
252	13.71	13.58
255	16.77	16.94
255	17.52	17.48
255	24.93	24.90
256	27.35	27.31
258	30.36	30.29
260	35.78	35.74
261	39.21	39.20
263	43.15	43.11
273	45.51	45.50
273	46.14	46.05

Table 3.3- Propane conversion

Temperature (°C)	VOC conversion (%)	CO₂ analyser (%)
226	0.37	0.30
226	0.37	0.37
230	0.73	0.60
233	1.10	1.02
238	1.87	1.63
244	2.27	2.08
248	2.92	2.90
254	3.45	3.75
254	4.54	4.44
257	6.67	6.48
260	11.29	11.16
260	13.33	13.34
263	16.75	16.96
265	23.18	23.05
266	26.52	26.49
269	30.34	30.30
270	37.55	37.47
272	43.67	43.58
274	49.25	49.22
278	51.58	51.43
279	54.18	54.13
282	55.70	55.63
286	66.47	66.41
318	71.97	71.95
334	74.33	74.33
378	95.48	95.47

Table 3.4- Propylene conversion

Temperature (°C)	VOC conversion (%)	CO ₂ analyser (%)
202	3.88	3.82
203	4.21	4.25
210	6.37	6.38
216	8.54	8.29
218	10.40	10.22
221	15.15	15.01
221	17.95	17.88
223	21.95	21.86
227	26.56	26.34
228	30.22	30.23
228	34.71	34.65
231	40.58	40.51
233	46.05	46.06
235	51.88	51.88
239	56.10	56.09
241	60.21	60.19
247	66.90	66.90
249	69.33	69.36
250	70.85	70.82
255	71.08	71.01
262	75.62	75.62
372	79.88	79.88
420	82.18	82.17

3.3 Membrane Characterization Methods and Gas Transport Measurement

3.3.1 BET Surface Area, Pore Size and Pore Size Distribution Determination

Physical gas adsorption is a standard technique employed to characterize the pore structure and network of a material. It is perhaps simple and the most widely used method to determine the specific surface area, pore size and pore size distribution of a nano-sized porous adsorbents (Smart *et al.*, 2013; Choma, Kloske & Jaroniec, 2003). The gas adsorption isotherm is divided into six categories (Smart *et al.*, 2013; Choma, Kloske & Jaroniec, 2003; Weidenthaler, 2011) as

depicted on Figure 3.5. Five of the six categories are mentioned in the IUPAC recommendations (Choma, Kloske & Jaroniec, 2003).

Type I isotherm is governed by adsorption in micropores sample (with < 2nm pore size) at low relative pressure, while the Type II isotherm is regarded as non-porous or macroporous (with > 50nm pore size) adsorbents formation of multilayers of adsorbate on surfaces of adsorbent, knee at point B (Figure 3.6) indicates completion of monolayer coverage. Type III isotherm is also a non-porous or macroporous adsorbents with weak adsorbent-adsorbate interactions. Type IV isotherm is a typical mesoporous adsorbents with initial monolayer-multilayer coverage on external and mesopore surface and is followed by capillary condensation in mesopores with different types of hysteresis loops which are observed depending on the shape of pores. A Type V isotherm is also a mesoporous adsorbent with weak adsorbent-adsorbate interaction. An example of this uncommon isotherm is observed in water adsorption on activated carbon (Weidenthaler, 2011). Type VI isotherm is a highly uniform surface which shows a layer-by-layer adsorption (Smart *et al.*, 2013; Choma, Kloske & Jaroniec, 2003; Weidenthaler, 2011).

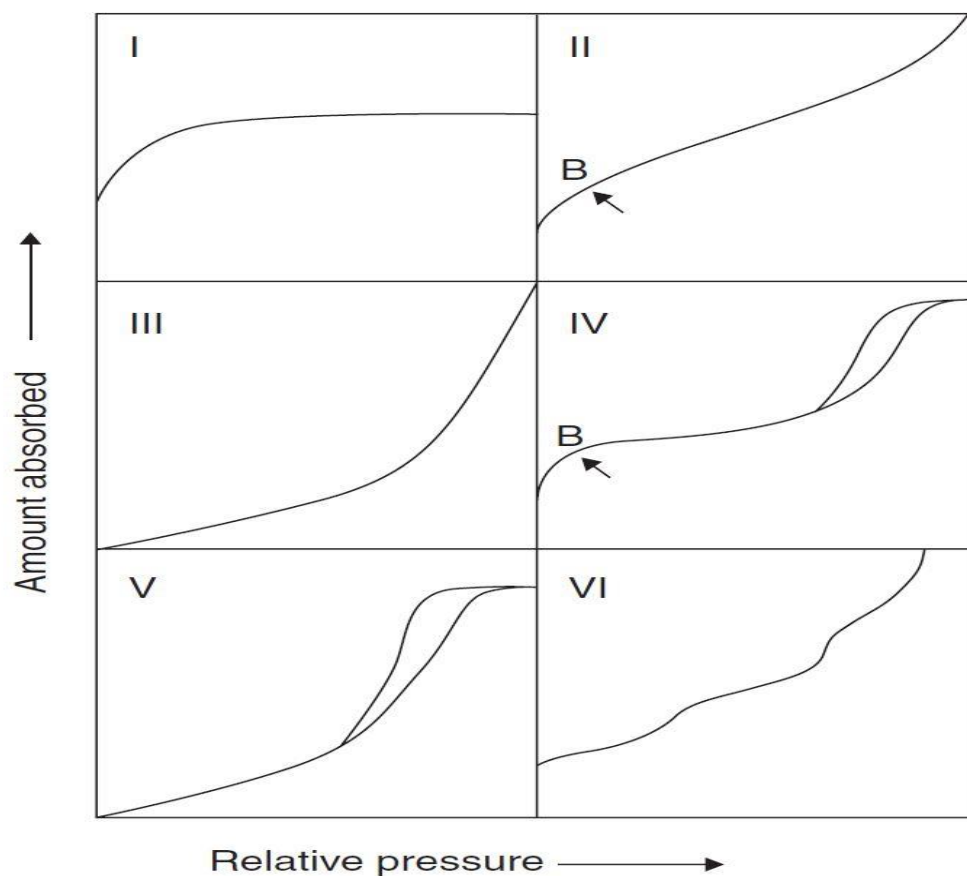


Figure 3.6 - Classification of absorption-desorption isotherm (Smart *et al.*, 2013; Weidenthaler, 2011).

The specific surface area of a given material can be assessed if the number of molecules in a monolayer of the adsorbate and the occupied space by one molecule are known. Therefore, models have been developed to assess the monolayer capacity of a given adsorbent. The BET model developed by Brunauer, Emmett, and Teller is the most commonly used based on a simplified model of monolayer-multilayer adsorption that represents an extension of the Langmuir model which is used as a kind of universal method for the determination of specific surface areas of the catalyst (Weidenthaler, 2011). The BET surface area can be expressed in equation (3.2) as;

$$\frac{P}{n_{ads}(P_0 - P)} = \frac{1}{cn_m} + \frac{(c-1)}{cn_m} \times \frac{P}{P_0} \quad (3.2)$$

where p and p_0 as equilibrium and saturation pressures of the adsorptive at the adsorption temperature, n_{ads} amount of gas adsorbed by unit mass of adsorbent, c is an empirical constant related to the heat of adsorption and indicating the magnitude of adsorbent-adsorbate interaction energy, and n_m the monolayer capacity (Weidenthaler, 2011).

The BET equation requires a linear relationship between $p/n_{ads}(p_0 - p)$ and p/p_0 as shown in the BET plot (Figure 3.7). Linearity is typically observed only in the range of the relative pressure (p/p_0) between 0.05 and 0.3. At higher p/p_0 values capillary condensation occurs and the BET equation is no longer valid. Nitrogen gas is the most frequently employed for BET surface measurement.

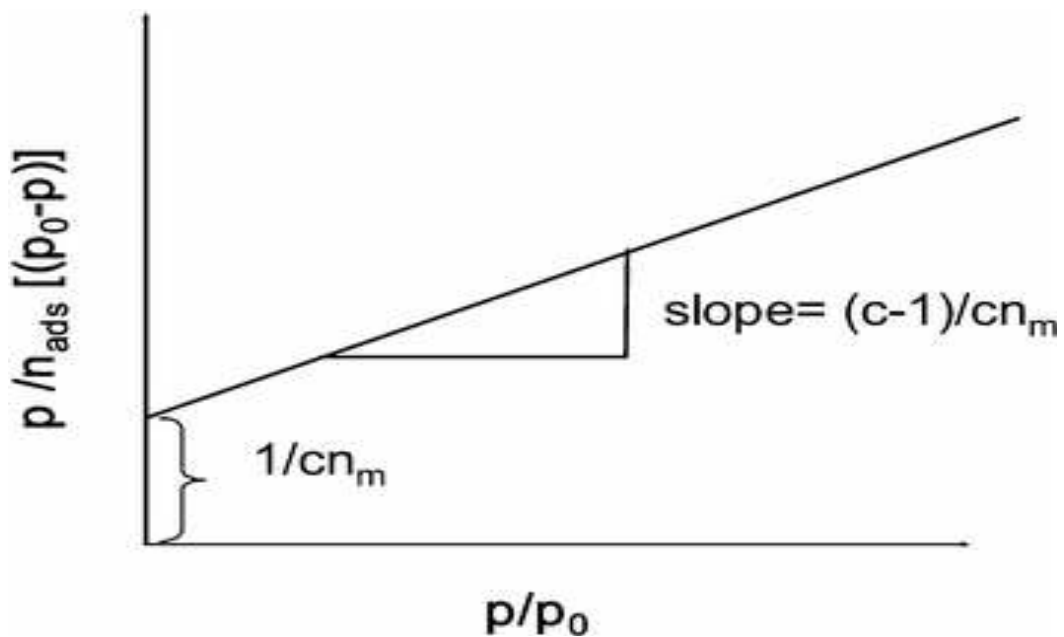


Figure 3.7 - BET plot and relation between c and n_m to slope and intercept of y-axis (Weidenthaler, 2011).

The adsorption behaviour of mesoporous materials is determined by both, adsorbent-adsorbate interactions and interactions between the adsorbent molecules. This leads to pore condensation in addition to multilayer adsorption. For pore condensation, a gas condenses in a pore to a liquid-like phase at pressures below the saturation pressure p_0 of the bulk liquid. Adsorption in mesoporous materials is represented by type IV and V adsorption isotherms. In the region of low p/p_0 values, the type IV isotherm is similar to the isotherms of non-porous materials (type II). Monolayer adsorption and the initial steps of multilayer formation are similar on an external surface of a particle and on the walls of mesopores. At higher p/p_0 , a deviation of the type IV isotherm from the type II isotherm is visible which is caused by capillary condensation in the mesopores. Capillary condensation occurs in mesopores when multilayer adsorption in such pores proceeds to a point at which adsorbed layers from opposing walls meet each other and form a concave meniscus. Adsorption on concave adsorbate films is strongly enhanced and therefore rapid filling of the mesopores is observed which is characterized by a distinct step in the isotherm (Weidenthaler, 2011).

The Barrett-Joyner-Halenda (BJH) method is used to determine the pore size distribution of mesoporous materials. Kelvin equation (eqn. 3.3) is used to describe the relation between the change in vapour pressure and the curvature of a meniscus with radius r .

$$r_k = -\frac{2\gamma V_m}{RT} \ln\left(\frac{P_0}{P}\right) \quad (3.3)$$

where r_K is the Kelvin radius (radius of curvature of hemispherical meniscus), γ the surface tension, and V_m the molar volume of adsorbate in liquid (Weidenthaler, 2011). Equation (3.4) is obtained in considering the thickness t of a multilayer film for the calculation of the pore radius r_p of cylindrical pores.

$$r_p = r_k + t \quad (3.4)$$

The Kelvin equation is therefore describes the interaction of a meniscus of liquid-like adsorbate with an adsorptive in the gas phase at equilibrium and hence applies correctly only for the desorption process since the capillary filling upon adsorption is no equilibrium process. The Kelvin equation based on cylindrical pores is used for the evaluation of the pore size distribution of mesopores by the BJH method (Weidenthaler, 2011).

The relationship between the Kelvin equation, Kelvin radius and real pore size of a membrane and the Knudsen diffusion equation (2.7) in chapter 2, the pore size and pore size distribution of a membrane can be obtained with a stepwise reduction (or increase) of relative pressure (Smart

et al., 2013; Weidenthaler, 2011). Pore size determination of materials with small mesopores and materials with both meso- and micropores can be influenced by a tensile strength effect. The tensile strength effect causes a characteristic step-down in the hysteresis loop which is related to the instability of the meniscus of the liquid-gas interface rather than to properties of the pore structure of the material (Weidenthaler, 2011).

The pore volumes of the membranes were measured by (Quantachrome instrument version 3.0) adsorption apparatus where nitrogen gas was used for adsorption at 77 K. The pore volumes were determined by BET and BJH methods. The BET isotherm obtained was employed to determine the size range of pores present in the membrane. Also, visual examination of the membrane structure was conducted using Zeiss EVO LS10 scanning electron microscopy.

3.3.2 Gas Permeability Measurements

There are three parameters which determine the performance of an efficient membrane. These parameters are permeability, selectivity and service life of a membrane. It can be elaborated that the higher the permeability, the lower the membrane area required. Also, the higher the selectivity, the more efficient the process, the lower the driving force required to attain a separation and therefore the less the operating cost of the separation system (Lu *et al.*, 2007).

The permeability of the gases in the support, silica membrane, boehmite membrane and platinum membrane at various temperatures and pressures were investigated. Figure 3.8 depicts a schematic diagram of the apparatus employed for gas permeability measurement. Similar experiment system was employed in the reactor performance experiment except that the reactor was empty.

In a typical experiment, the gas was passed into the shell-side and permeated through the support/coated membrane at the desired temperatures and pressures. The permeate was connected to the flowmeter to measure the flow rates (l/min). The measured flow rate was converted to molar flow (mole/sec) and normalized by dividing it with the active membrane area to determine the permeation rate (i.e. gas fluxes, permeances and permeabilities) for each component. The membrane possesses resistance to the flowing component. Transmembrane pressure was measured using the pressure gauge. Gas permeation experimental temperature ranged from 298 to 923 K. The membrane area was 0.00602 m².

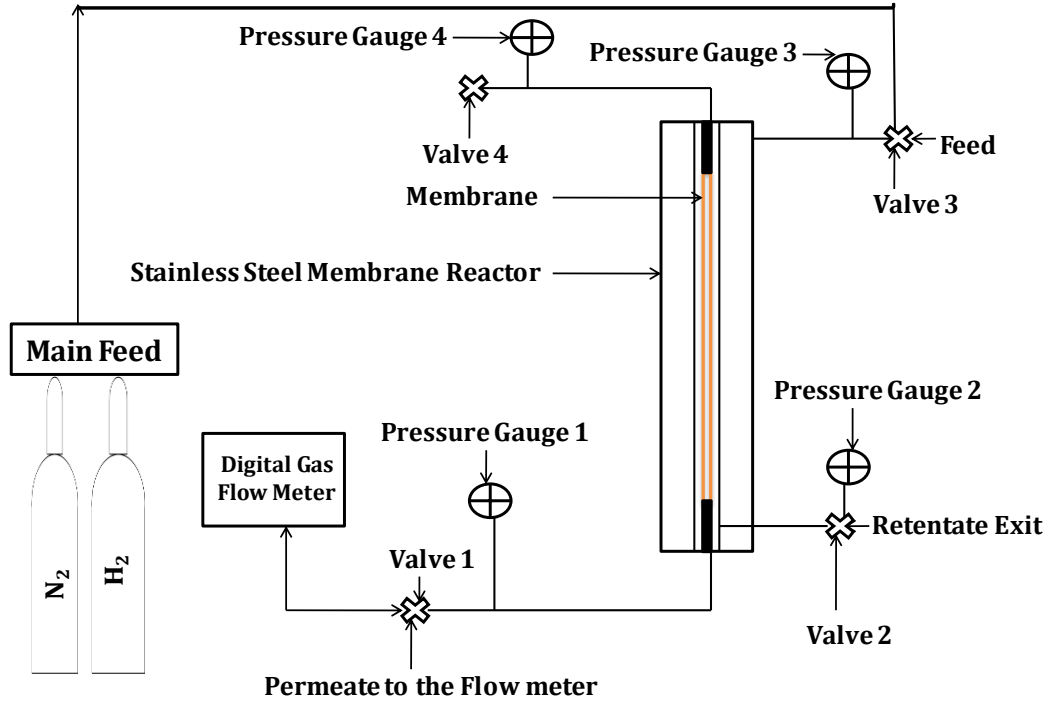


Figure 3.8 - Schematic diagram of the experimental setup.

Permeability is termed as the flux of a specific gas component through the membrane per unit of area at a given pressure gradient taking into account the membrane thickness as expressed in equation 3.5 (Lu *et al.*, 2007; Kentish, Scholes & Stevens, 2008).

$$P_e = \frac{qL}{A\Delta P} \quad (3.5)$$

where P_e is the Permeability ($\text{mol}\cdot\text{m}/\text{m}^2 \text{ s}^{-1} \text{ Pa}^{-1}$), q is the molar flow (mol/sec), A is the surface area of the membrane (m^2), ΔP is the pressure difference (Pa) across the membrane and L the thickness of the membrane (m).

Selectivity is the ability of the membrane to separate (select) the required component from the feed mixture (Kentish, Scholes & Stevens, 2008). Selectivity is defined as the ratio of the pure component permeabilities (P_y and P_z) for single gases as expressed in equation 3.6;

$$\alpha_{y,z} = \frac{P_y}{P_z} \quad (3.6)$$

where P_y is the permeability of y component ($\text{mol}\cdot\text{m}/\text{m}^2 \text{ s}^{-1} \text{ Pa}^{-1}$), and P_z is the permeability of z component ($\text{mol}\cdot\text{m}/\text{m}^2 \text{ s}^{-1} \text{ Pa}^{-1}$).

3.4 Support and Membrane Characterization Methods

3.4.1 Scanning Electron Microscopy (SEM)

The SEM generates a finely focused beam of electrons which is made to scan across the sample under inspection. The beam originates from the heating of a tungsten wire filament (thermionic emission) housed in an electron gun at the top of the microscope column. The beam electrons are accelerated towards the specimen by means of an applied accelerating voltage between the filament assembly and an anode plate. The SEM column and sample chamber are maintained under a high vacuum to allow the electrons forming the beam unhindered path from the filament to the sample surface (Tough, 2014b).

As the beam travels down the column, it undergoes electron optical demagnification as it passes through two electromagnetic lenses (condenser lenses). Just above the specimen the beam comes under the influence of a set of scan coils which deflect the beam in a raster pattern across the sample surface. This scanning section is synchronised with the display monitor where an image of the surface, with high magnification is obtained. Available magnification may exceed 300,000x with resolution of 3-4nm. This compares with a resolution capability of a light microscope of approximately 2550nm. The equipment used was a Leo model S430 SEM (Tough, 2014b).

Scanning electron microscopy (SEM) and energy-dispersive X-ray analysis (EDXA) of the alumina support was taken before silica modification and Pt impregnation. Figures 3.9 and 3.10 depict the SEM micrographs of the inner and outer surface of the alumina support before modification at 2000 magnification. Approximately 10 μm thick alumina layer of highly intergrown alumina crystals was observed. The cross-sectional morphology of the alumina support is also depicted on Figure 3.11 with approximately 20 μm thick. The alumina support was found to be defect-free after permeation experiments.

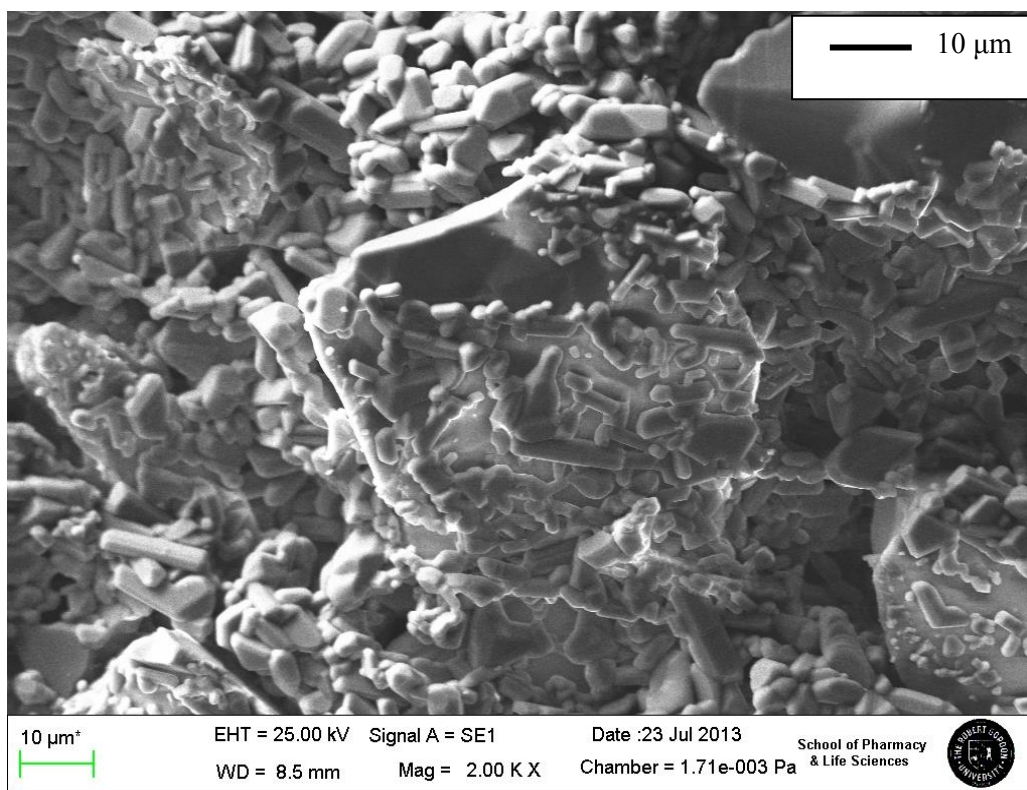


Figure 3.9 - SEM image of the alumina support inner surface.

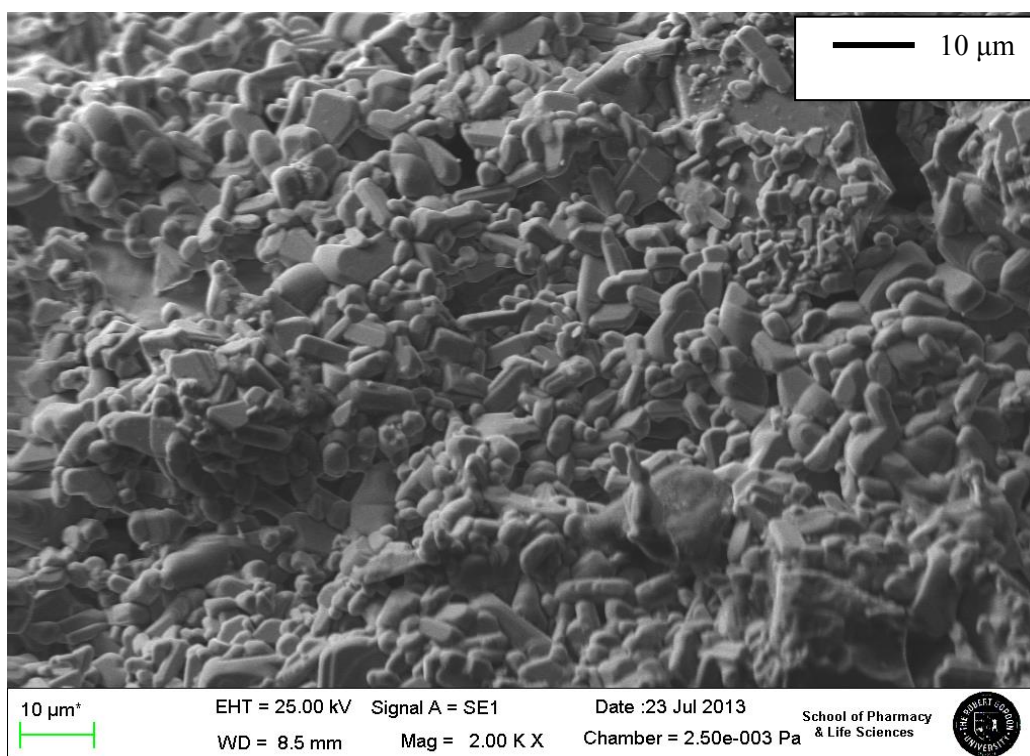


Figure 3.10 - SEM image of the alumina support outer surface.

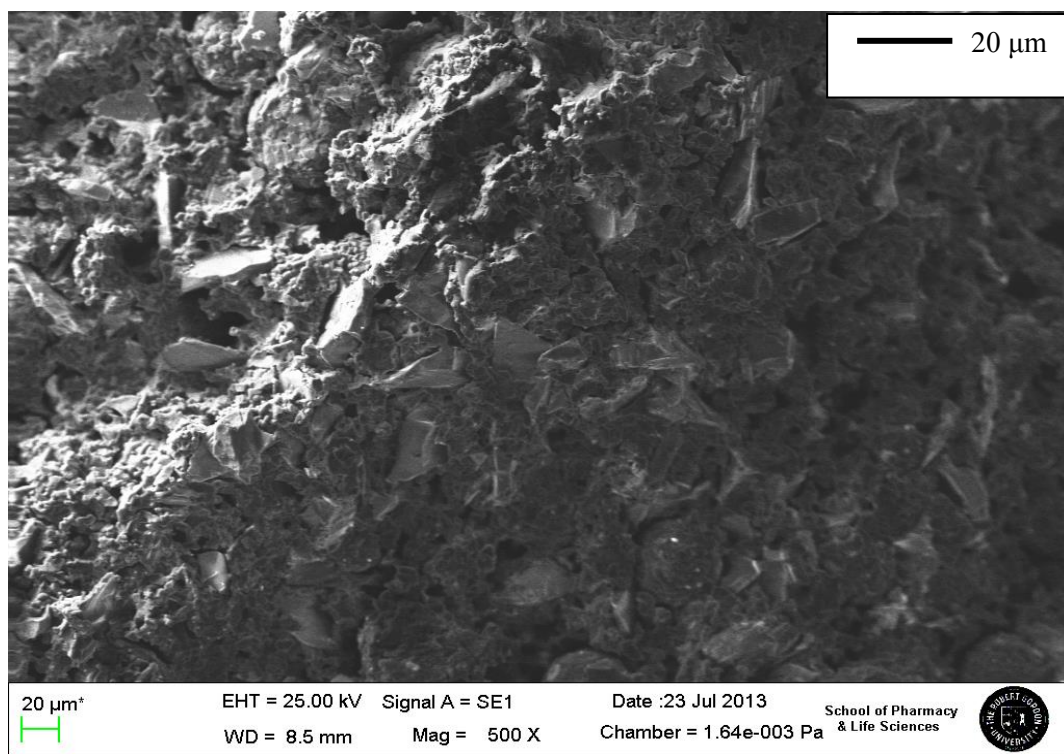


Figure 3.11 - SEM image of the alumina support cross-sectional area.

3.4.2 Energy Dispersive X-ray Analysis (EDXA)

As the scanning electron microscope uses a high energy electron beam to illuminate a specimen, one of the by-products is the generation of x-rays as primary beam electrons interacting with specimen electrons. The production of x-rays occurs in two basic ways. As an electron in the primary beam enters the volume of a specimen atom, it can be scattered elastically or inelastically in various ways (Tough, 2014a).

Primary electrons may slow down by interaction with forces present within the volume of an atom resulting in the electron giving up energy. This energy loss can be accomplished by the emission of x-ray radiation. This type of radiation is known as braking radiation and is observed as a continuous spectrum. This continuous spectrum is regarded as background radiation for EDXA spectrometers (Tough, 2014a).

Inelastic scattering also occurs due to collisions between primary electrons and electrons within specimen atoms. The consequent rearrangement of electrons within electron shells, as atoms strive to reach their lowest energy states, results in the release of energy in the form of x-ray photons. As the energy of these photons is related to the energy between electron shells, the x-ray photons are characteristic of the element present in the specimen. By collecting and

analysing these x-rays, qualitative and quantitative information about the component elements of a specimen may be obtained (Tough, 2014a).

EDXA is a widespread technique regularly employed to biological or chemical as well as physical issues in material science. The samples used for SEM and EDX analysis were obtained by breaking the support into small pieces. The pieces were analysed by SEM followed by EDX analysis.

3.4.3 BET Surface Area and Pore Size Distribution Determination

The N₂ adsorption/desorption isotherm of the alumina support was obtained. The Brunauer-Emmett-Teller (BET) surface area, Barrett-Joyner-Helanda (BJH) pore size distribution methods of the alumina support are depicted in Figures 3.12 and 3.13. It can be seen in Fig. 3.12 that the isotherm exhibits a drop in the desorption branch at $P/P_0 = 0.5$ (dotted line). However, the meniscus curve is not closed, this could be as a result of contaminants in the material. Fig. 3.13 depicts the measurement of the pore-size distribution of the alumina support. An average pore diameter of 4.171 nm is calculated from the pore-size distribution graph.

The adsorption/desorption isotherm exhibits a characteristics of mesopores solids (especially ceramics) resulting in Type IV physisorption isotherm according to the IUPAC recommendations which revealed the presence of mesoporous ($2 < \text{pore size} < 50\text{nm}$) in the membrane undergoing capillary condensation and hysteresis during desorption (Smart *et al.*, 2013; Weidenthaler, 2011).

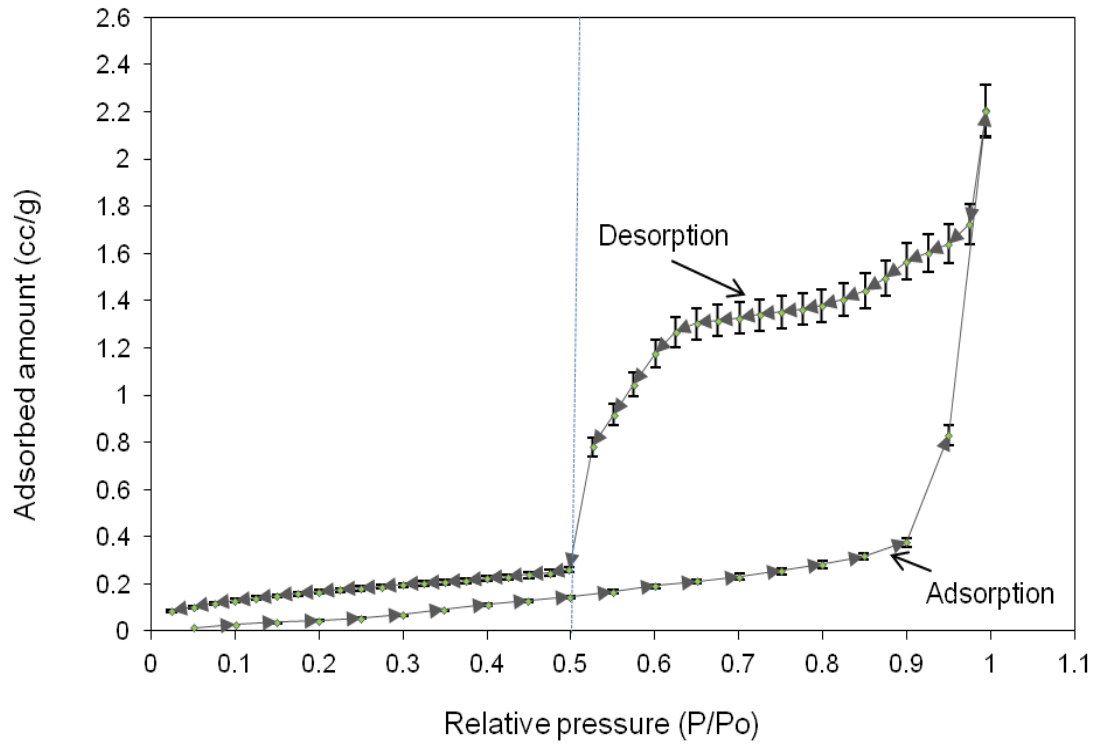


Figure 3.12 - N_2 adsorption/desorption isotherm of the alumina support.

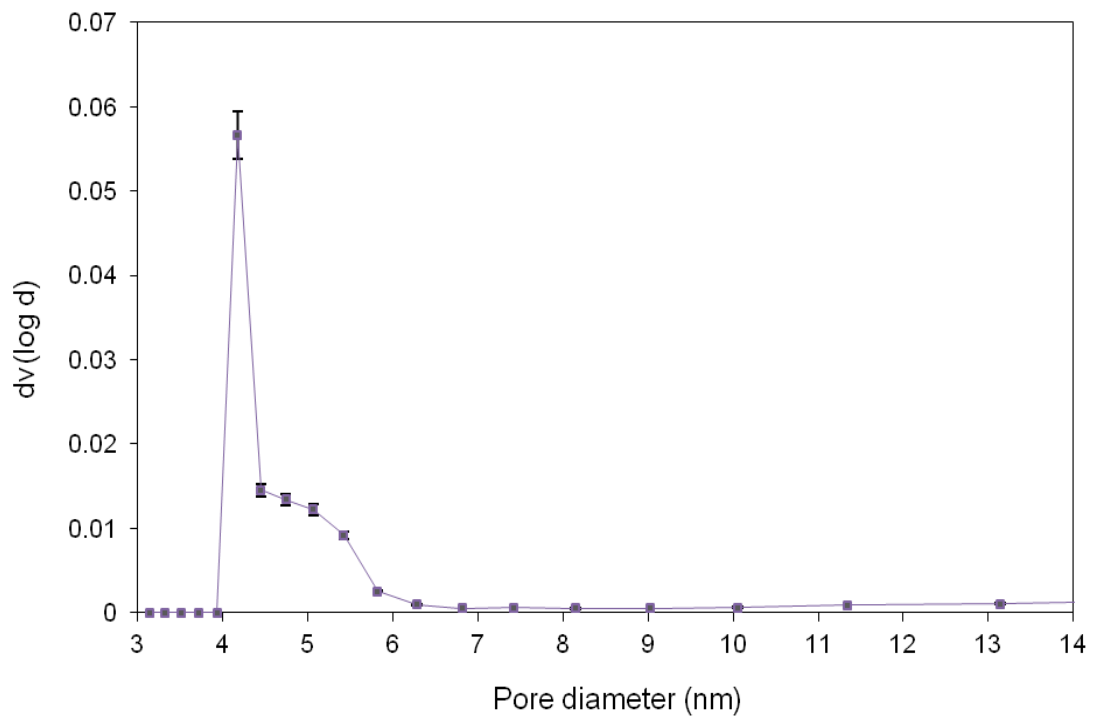


Figure 3.13 - Pore-size distribution of the alumina support measured by N_2 adsorption.

3.4.4 BET Surface Area Determination

The surface areas of both the support and the catalyst samples were determined using Quantachrome instrument version 3.0 surface area analyser, where adsorption was performed at 77 K after degassing at 673 K. The BET surface area, pore volume, and average pore diameter were obtained.

3.5 Safety

3.5.1 Overview of Ethical Issues

This research was supervised under the Robert Gordon University's ethics policy which seeks to make sure that every research is undertaken to the maximum ethical standards and also to all relevant laws for both local and international countries, and appropriate due diligence was undertaken to minimise risk, and adheres to all relevant policies or codes of good practice (www.rgu.ac.uk/file/research-ethics-policy-pdf-146kb 2014).

3.5.2 Minimising Risk

The responsibility for ensuring ethical conduct in this research was extended to everyone engaged in the process. This includes (www.rgu.ac.uk/file/research-ethics-policy-pdf-146kb 2014);

- ❖ Any risk to humans or animals was minimised in this research.
- ❖ The research ensured the protection in respect of confidentiality, the use of data and reporting.
- ❖ We will ensure that this research does not cause unnecessary harm to participants, stakeholders, the environment, the economy and other living beings.
- ❖ Agreements of this kind were made in the name of the University and consequently the University has a responsibility to ensure that they are complied with.

3.5.3 Health and Safety

The research was carried out in accordance with Robert Gordon University's health and safety policy. During this research, we ensured that adequate systems were in place in order to mitigate risk to the appropriate level.

Moreover, a risk assessment was carried out as required for experiments such as handling the gas cylinders, flammable chemicals, and all documents e.g. risk assessment form and control of substances hazardous to health (COSHH) was completed where needed. Personal Protection

Equipment (PPE) was also worn when necessary (www.rgu.ac.uk/file/research-ethics-policy-pdf-146kb 2014).

4 Results

4.1 Membrane Characterization

4.1.1 BET Surface Area, Pore Size and Porosity of Alumina Membrane

The N₂ adsorption-desorption isotherms of the silica membrane is depicted on Figure 4.1. The adsorption-desorption isotherms exhibit the characteristics of mesopores solids (especially ceramics) resulting in type IV and V physisorption isotherm undergoing capillary condensation and hysteresis during desorption (Smart *et al.*, 2013; Weidenthaler, 2011). Different parameters were obtained for the BET and BJH methods. Table 4.1 quantitatively shows the physical properties obtained via nitrogen adsorption for the alumina support and silica membrane. It can be seen in Fig. 4.1 that the isotherm exhibits a drop in the desorption branch at $P/P_0 = 0.5$ (dotted line). However, the meniscus curve is not closed, this could be as a result of contaminants in the material. The BET surface area and BJH pore diameter were 0.364 m²/g and 4.171 nm respectively for the alumina support. The BET surface area increased to about 0.484 m²/g after subsequent dipping the alumina with silica. The BJH average pore diameter also decreased from 4.171 to 3.940 nm (Figure 4.2) which indicates that some amount of silica has penetrated into the alumina support pores which shows a typical mesopore diameter in the range of 2 to 50 nm.

Table 4.1 - BET surface area and average pore diameter measurements of the silica membrane.

Membrane	BET (surface area) m ² /g	BJH (pore diameter) nm
Support	0.364	4.171
Silica Membrane	0.484	3.940

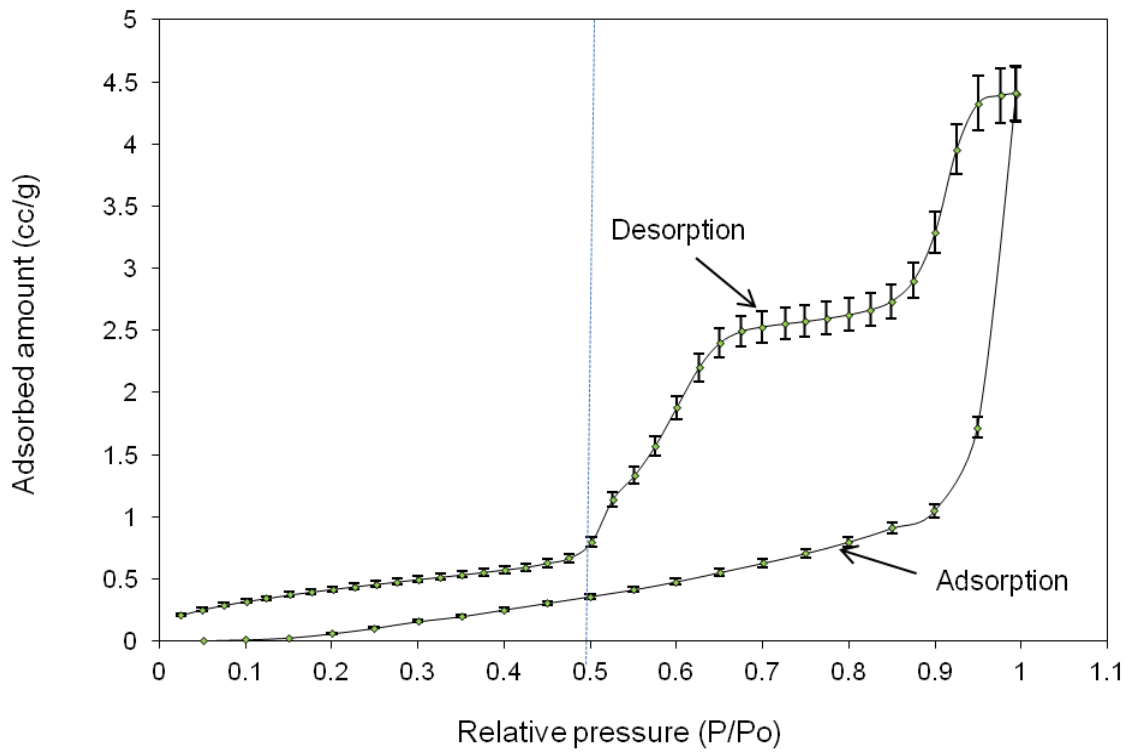


Figure 4.1 - N₂ adsorption/desorption isotherm of silica membrane.

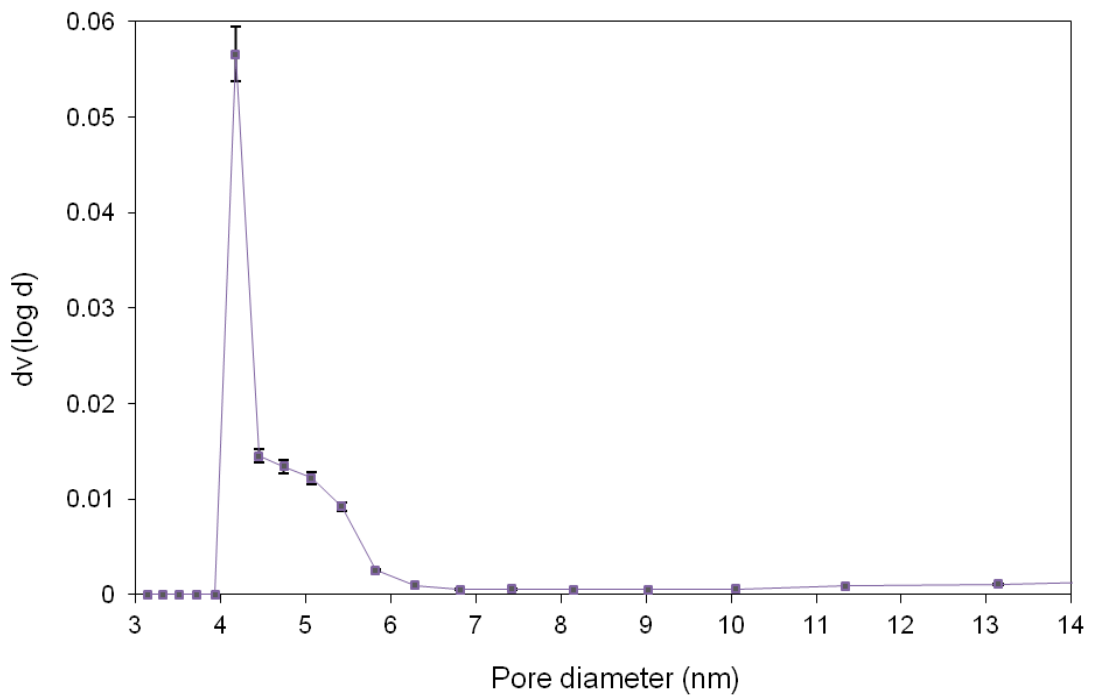


Figure 4.2 - Pore-size distribution of silica membrane measured by N₂ adsorption.

The N₂ adsorption/desorption isotherm of the Pt membrane is shown in Figure 4.3. The isotherm is a Type IV isotherm. Table 4.2 shows the corresponding BET surface area, average pore diameter and pore volume measurements.

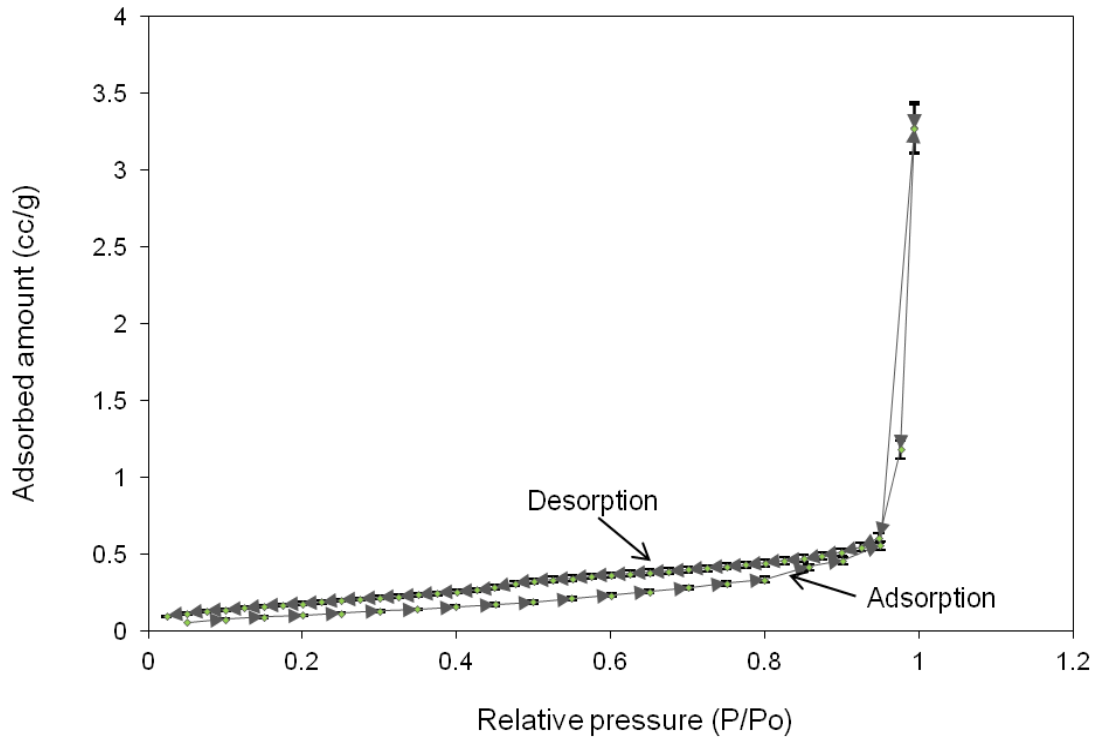


Figure 4.3 - N₂ adsorption/desorption isotherm of Pt membrane.

Figure 4.4 depicts the pore diameter measured by the BJH method of the Pt membrane. The result reveals a somewhat narrow pore size distribution. The average pore diameter was 3.7 nm, and the majority of pore diameters are smaller than 50 nm. This suggests that the material is mesoporous. Lastly, the membrane performance was constant for over 100 hours of operation at roughly 673 K without any degradation, indicating that the membrane was both chemically and thermally stable in the presence of VOC.

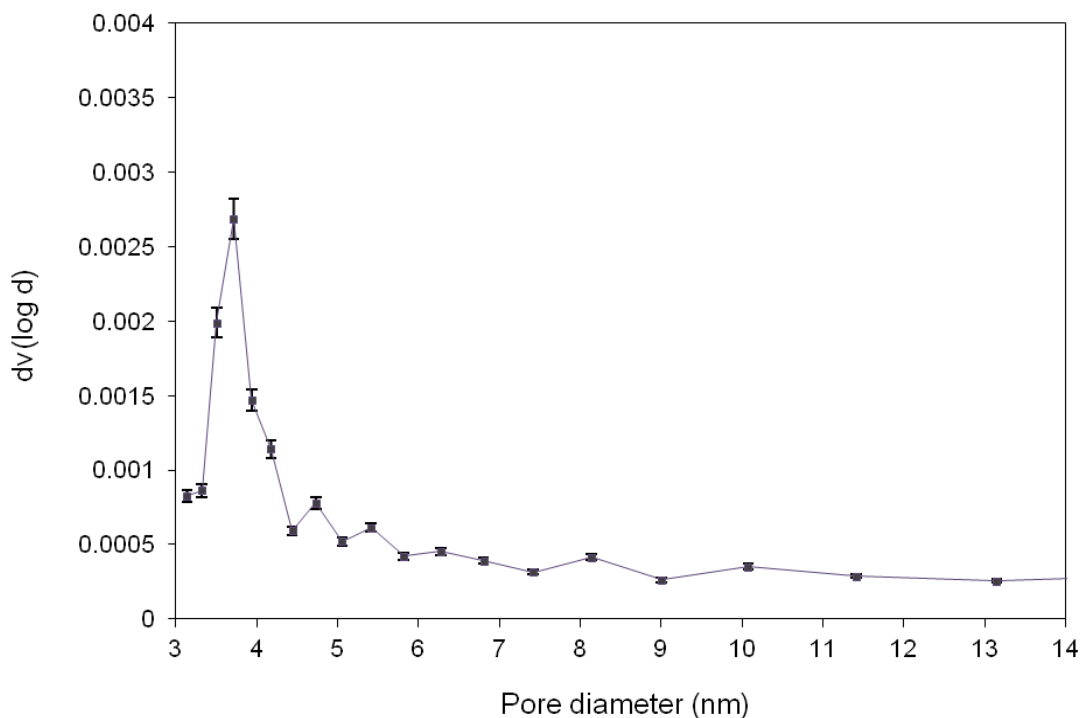


Figure 4.4 - Pore-size distribution of Pt membrane measured by N₂ adsorption.

4.2 Catalyst Characterization

In this study, a platinum metal catalyst was employed due to its relatively high activity in VOC destruction over other noble metals (Benard *et al.*, 2009). Pt/ γ -Al₂O₃ was prepared by depositing H₂PtCl₆ solution on commercial alumina through the simple but effective “reservoir” method.

4.2.1 BET Surface Area

The Pt/ γ -Al₂O₃ membrane sample was subjected to BET surface area and pore volume measurement. The data of specific surface area, average pore diameter and pore volume for the samples are presented in Tables 4.1 and 4.2.

The effect of the Pt weight gain using the reservoir method was studied by measuring the BET surface area. The results clearly show an increase in BET surface area between the alumina support and the Pt-alumina membrane, which may be attributed to the formation of nano-dispersed platinum particles. There was also a reduction in pore diameter which is possibly due to pore blockage caused by the metal platinum particles. Albeit, no changes in the pore volume were observed.

Table 4.2 - BET surface area, average pore diameter and pore volume measurements of the Pt-alumina membrane.

Catalyst	BET surface area (m ² /g)	Average pore diameter (nm)	Pore volume (cm ³ /g)
Support	0.364	4.171	0.005
Pt-alumina	0.426	3.7	0.005

4.2.2 SEM and EDXA of Silica-alumina Membrane

Figures 4.5 and 4.6 depict the SEM images of the inner and outer surface of the silica membrane with 2000 magnification. From Fig. 4.5, intergrown silica crystals are not more visible than shown on Fig. 4.6 owing to the fact that the coating was made from outside surface of the alumina support. This is the reason why only less amount of silica was penetrated to the inner surface of the alumina support compared to the one for outer surface (Fig. 4.6). It can be obviously seen that some amount of silica has been adsorbed by the membrane during the dip-coating process forming a well-intergrown silica crystals after 30 minutes dip-coating, packed densely in the layer on the outside surface (Fig. 4.6) of the alumina support, which seemed to take a significant role in separation rather than the alumina support. The thickness of the inner and outer surface of the silica membrane was obtained as 10 μm .

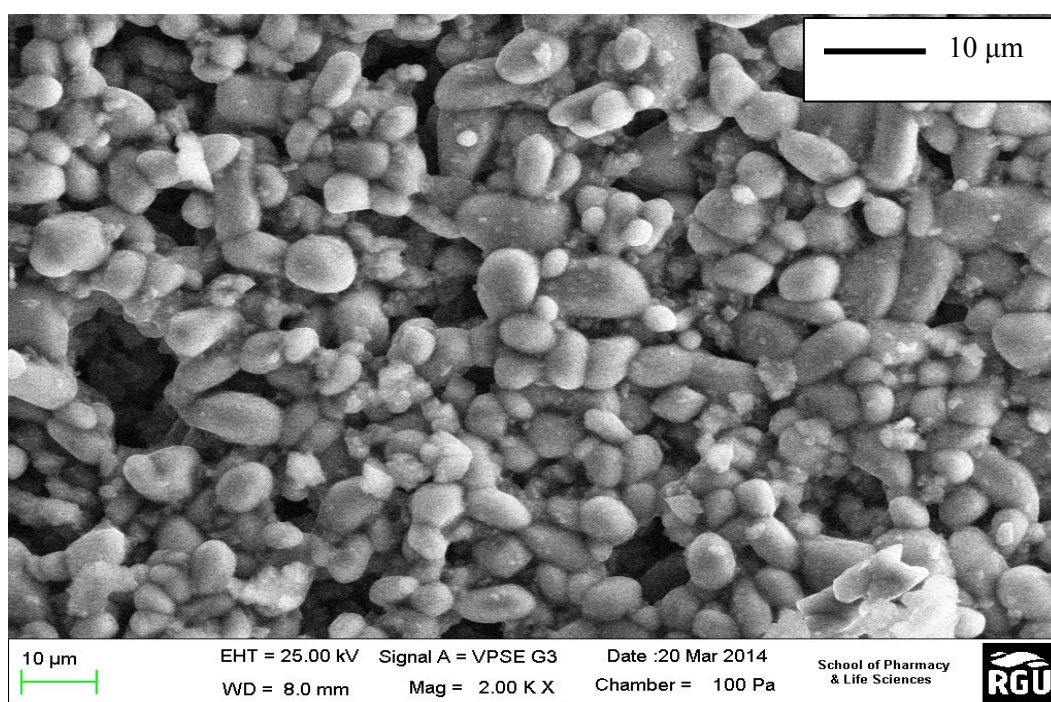


Figure 4.5 - SEM image of the inner surface of the silica membrane.

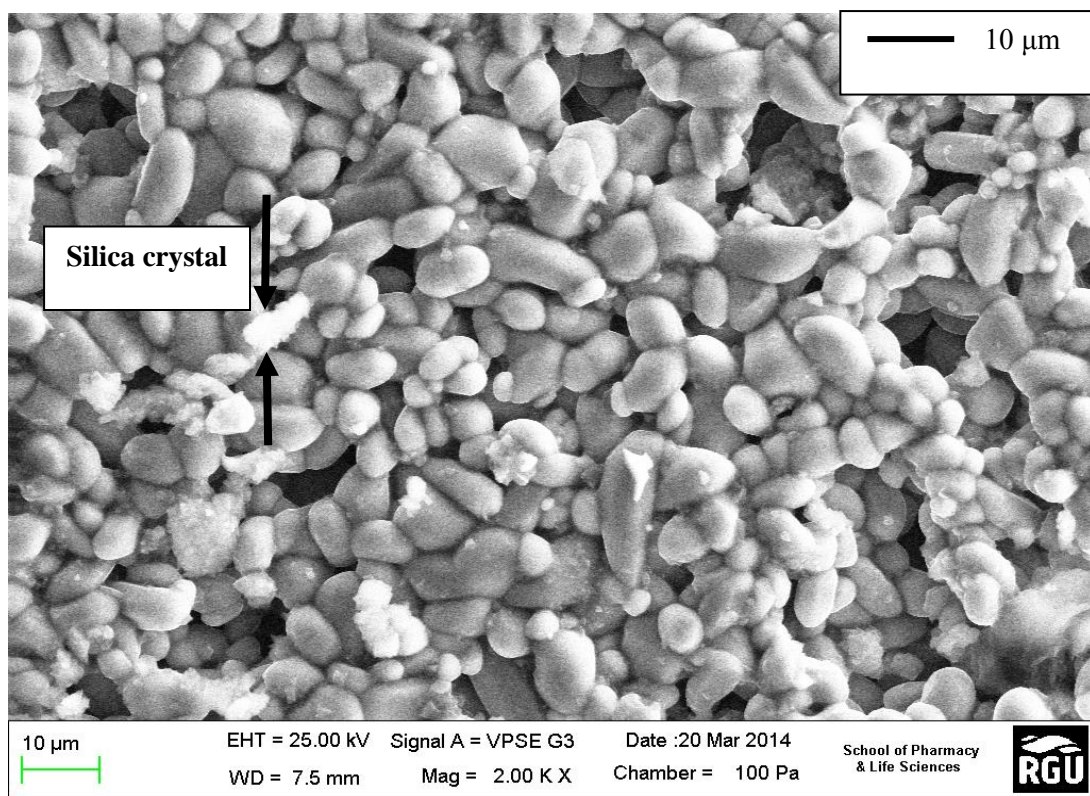


Figure 4.6 - SEM image of the outer surface of the silica membrane.

The EDXA of the outer surface is depicted in Figures 4.7 and the compositional result is shown in Table 4.3, it can be seen that a 32.21 wt% Si is obtained. The EDXA result is in good agreement with the SEM micrographs.

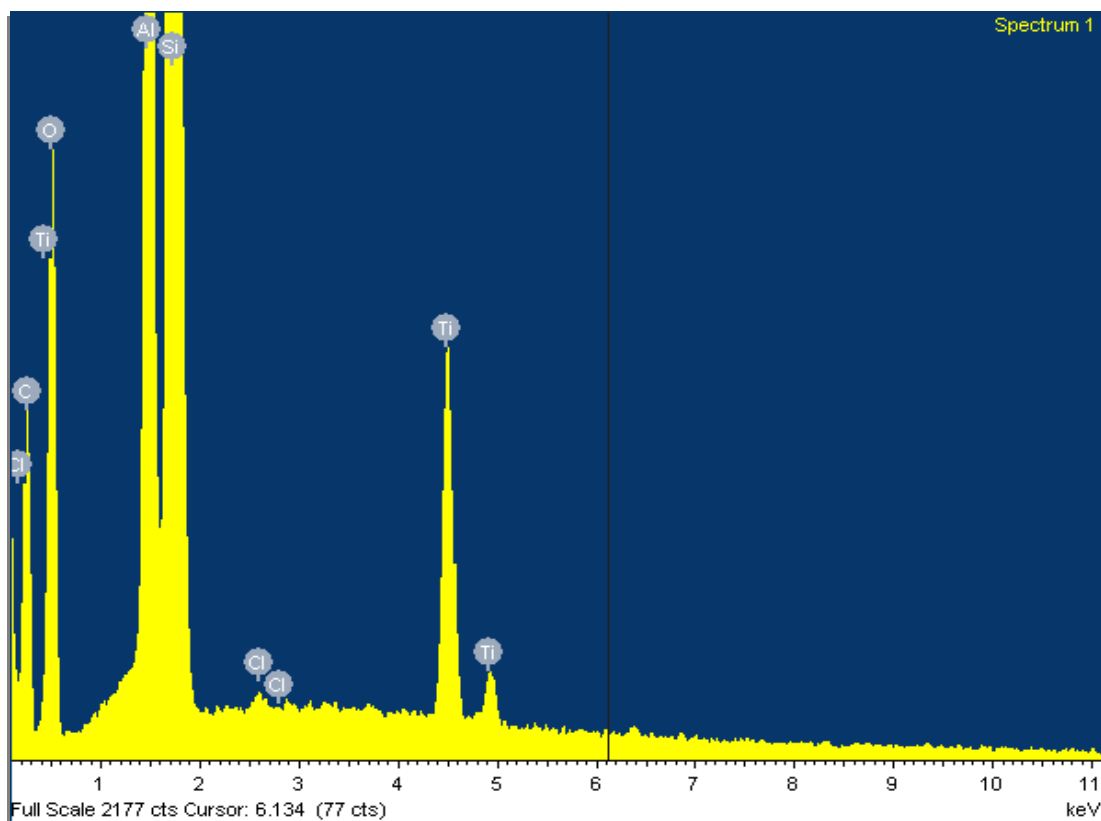


Figure 4.7 - EDXA of the silica membrane outer surface.

Table 4.3 - Outer surface EDX analysis of silica membrane.

Element	Weight (%)	Atomic (%)
SiO ₂ (O K)	26.74	28.99
Al ₂ O ₃ (Al K)	5.81	3.74
Titanium (Ti K)	3.20	1.16
SiO ₂ (Si K)	32.21	19.90
CaCO ₃ (C K)	31.97	46.17
KCl (Cl K)	0.08	0.04
Total	100.01	100

4.2.3 SEM and EDXA of Pt-alumina Membrane

SEM and EDXA of the Pt membrane were taken after Pt impregnation. Figures 4.8, 4.9 and 4.10 depict the SEM micrographs with 5000 magnification of the Pt membranes' inner, outer and the cross-sectional surface respectively. From Fig. 4.8, the intergrown Pt layer is not more visible than shown on Fig. 4.9 owing to the fact that the coating was made from outside surface of the

alumina support. This is the reason why only less amount of Pt was penetrated to the inner surface of the alumina support compared to the one for outer surface (Fig. 4.9). The presence of the well-intergrown Pt packed on the alumina support can be seen on Fig. 4.9. Approximately 2 μm thick Pt layer was observed. Figure 4.10 depicts the SEM micrograph of the Pt membrane cross-sectional area. It can be seen that the Pt content for the cross-section is almost negligible compared to the Pt content on the outer surface. The SEM image of the edge with 2000 magnification of the Pt membrane is also shown on Figure 4.11 with a thickness of between 10 - 12 microns.

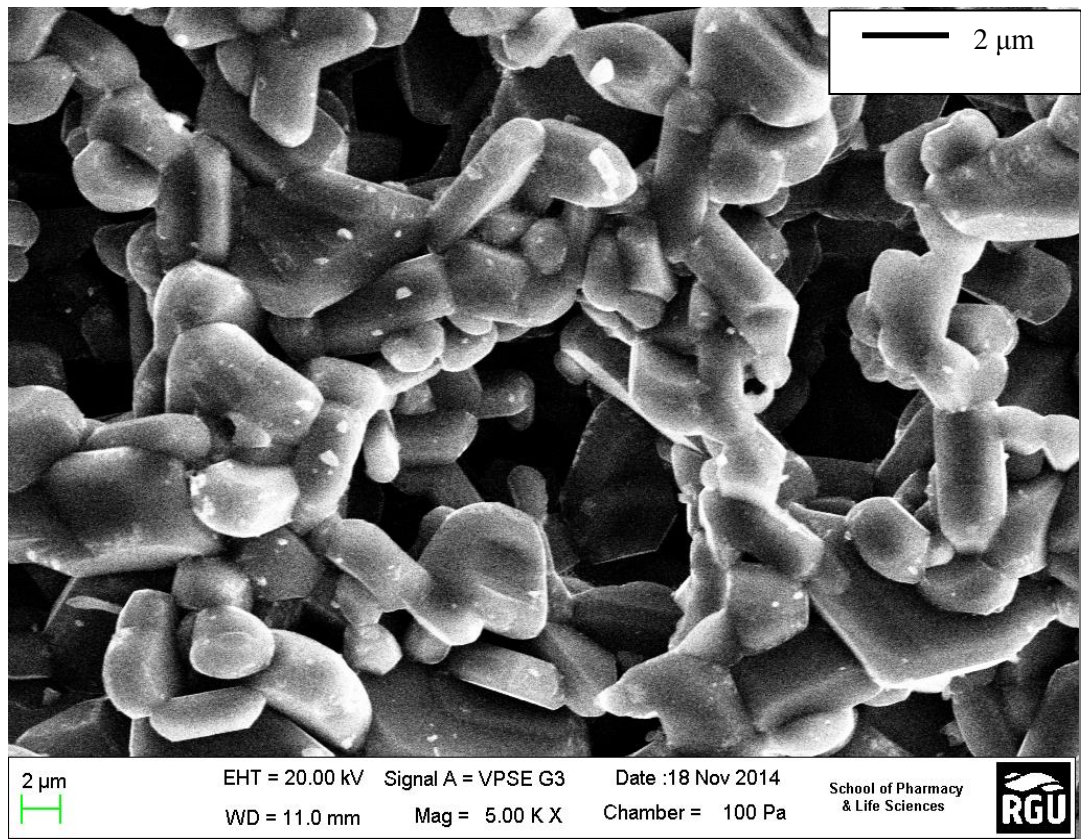


Figure 4.8 - SEM image of the Pt membrane inner surface.

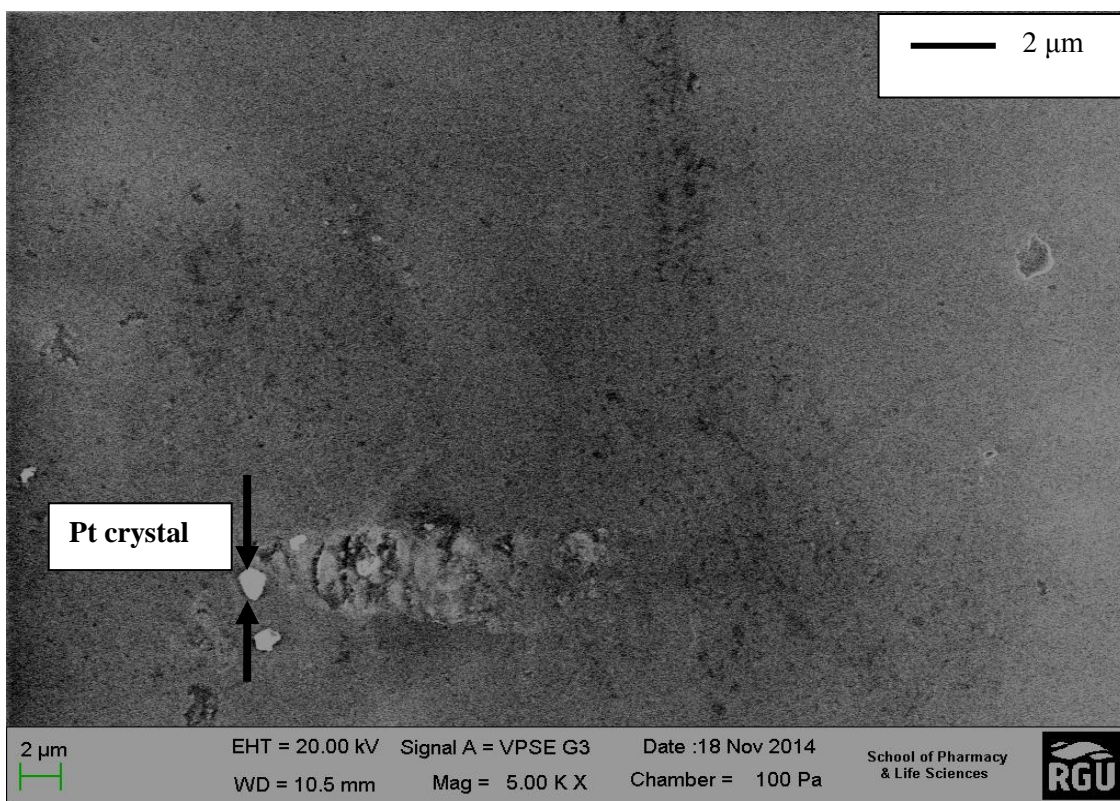


Figure 4.9 - SEM image of the Pt membrane outer surface.

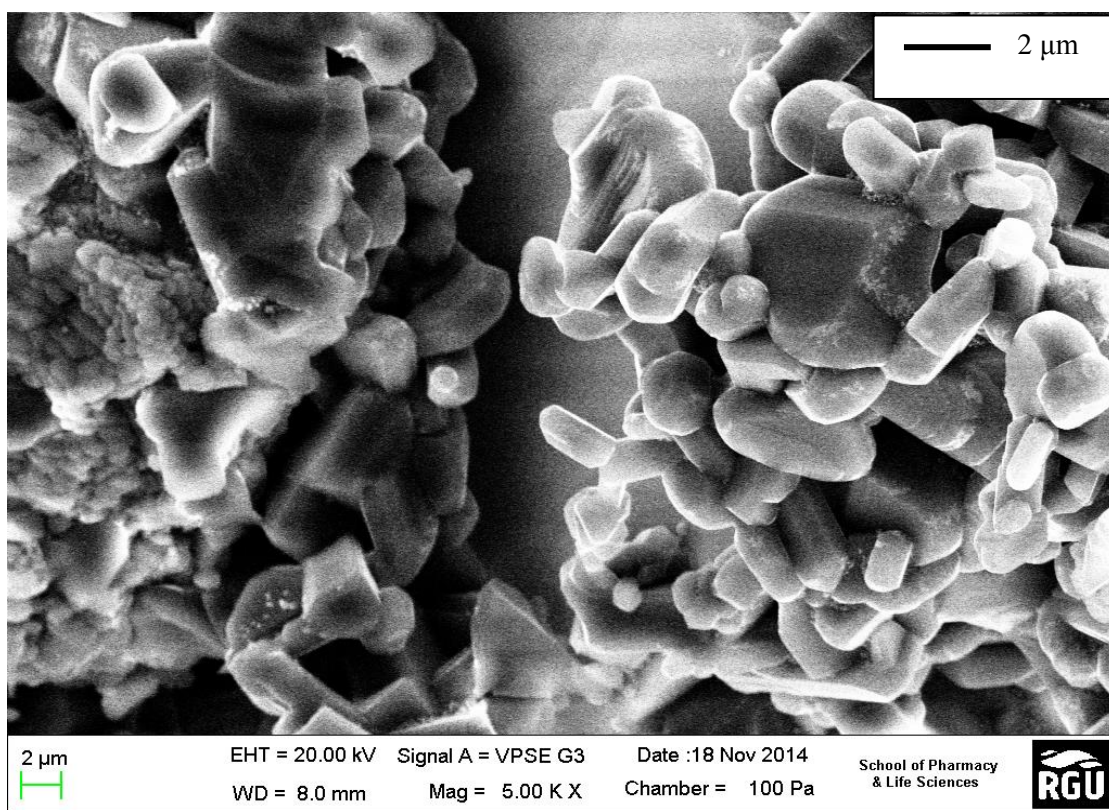


Figure 4.10 - SEM image of the Pt membrane cross-sectional area.

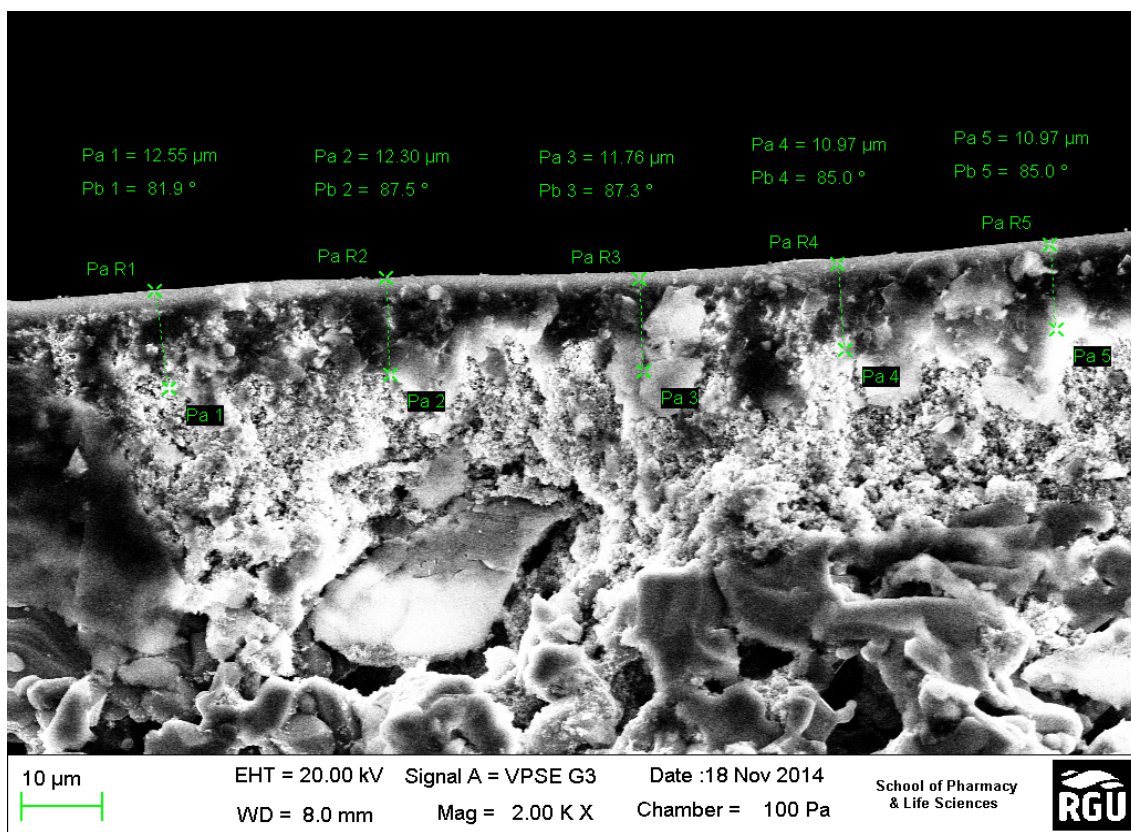


Figure 4.11 - SEM image of the Pt membrane edge surface.

The EDXA composition of the Pt membrane's inner, outer and cross-sectional surface is depicted in Figures 4.12, 4.13 and 4.14 respectively. From Fig. 4.12, almost no amount of Pt was traced by the EDXA. This could be because the alumina support was coated from the outside surface. Contrary to Fig. 4.12, it can be seen that on Fig. 4.13, EDXA confirmed a trace of the Pt metal which corresponds the SEM result for the Pt outer surface. Figure 4.14 depicts the EDXA image of the Pt membrane cross-section. It can be seen that the highest peak shown on Fig. 4.14 was that of Ti with over 50 wt%. These could also be translated that the alumina support was coated from the outside surface. Also, the compositional results are shown in (Tables 4.4, 4.5 and 4.6) respectively. After Pt impregnation, it can be seen in Table 4.5 that a 3.52 wt% Pt is obtained. Pt is the active catalyst for the proposed reaction in order to facilitate the reaction of VOC and oxygen to generate CO₂ and H₂O.

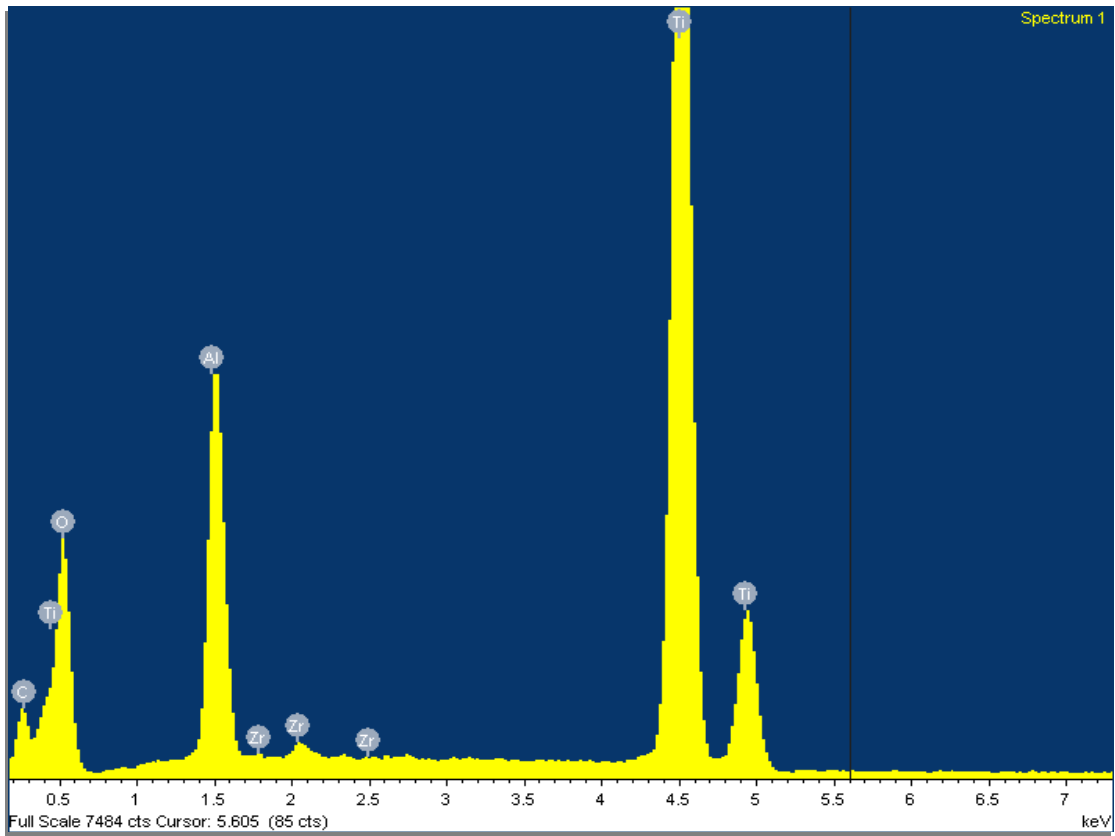


Figure 4.12 - EDXA image of the Pt membrane inner surface.

Table 4.4 - Inner surface EDX analysis of Pt membrane.

Element	Weight (%)	Atomic (%)
SiO ₂ (O K)	42.30	64.95
Al ₂ O ₃ (Al K)	4.00	3.65
Titanium (Ti K)	60.73	31.15
Zirconium (Zr L)	0.94	0.25
Total	107.97	100

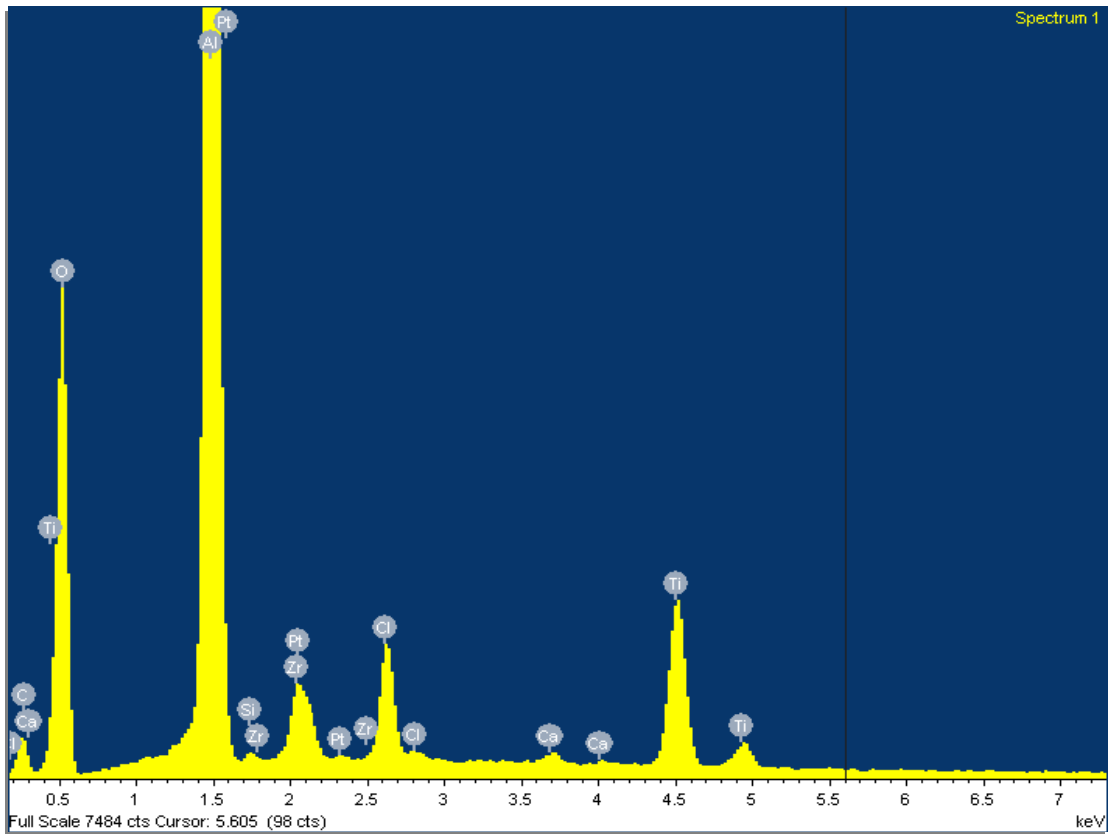


Figure 4.13 - EDXA image of the Pt membrane outer surface.

Table 4.5 - Outer surface EDX analysis of Pt membrane.

Element	Weight (%)	Atomic (%)
CaCO ₃ (C K)	14.41	19.64
SiO ₂ (O K)	50.68	51.88
Al ₂ O ₃ (Al K)	38.52	23.38
SiO ₂ (Si K)	0.28	0.16
KCl (Cl)	3.28	1.51
Wollastonite (Ca K)	0.32	0.13
Titanium (Ti K)	7.94	2.72
Zirconium (Zr L)	1.61	0.29
Platinum (Pt M)	3.52	0.30
Total	120.56	100.02

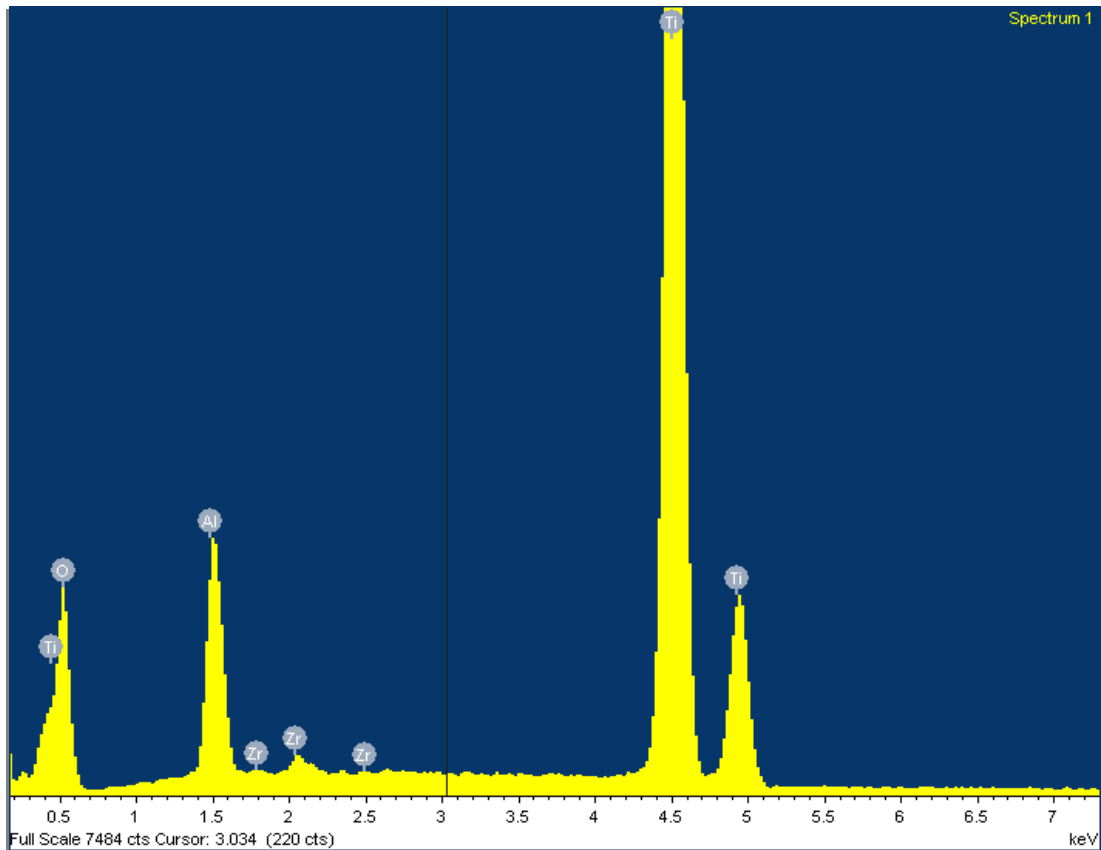


Figure 4.14 - EDXA image of the Pt membrane cross-section.

Table 4.6 - Cross-section EDX analysis of Pt membrane.

Element	Weight (%)	Atomic (%)
CaCO ₃ (C K)	6.73	12.03
SiO ₂ (O K)	43.33	58.14
Al ₂ O ₃ (Al K)	6.68	5.31
Titanium (Ti K)	54.25	24.31
Zirconium (Zr L)	0.89	0.21
Total	111.88	100

4.3 Gas Permeability Study

4.3.1 Defect Repair of Composite Membrane

Membrane defects are formed during the preparation stages. It can be formed either during the dipping, drying, calcination process and sealing (Koutsonikolas *et al.*, 2010) or even during the process of inserting and removing it from the reactor. Any defect on a membrane can be regarded as a crack. For example, a defect is considered in the presence of super-micropores (0.7 nm < pore diameter < 2 nm) instead of ultra-micropores (pore diameter < 0.7 nm (Koutsonikolas

et al., 2010). It is known that any amount of defect on the membrane can significantly lower the membrane selectivity.

There are several methods for porous membrane modification including; dip-coating, chemical vapour deposition (CVD), and pulsed layer deposition (Ahmadian *et al.*, 2011; Benito *et al.*, 2005; Koutsonikolas *et al.*, 2010). Of these modification methods, the dip-coating method has many merits over the other methods including its simplicity, uniform surface and the ability to control the pore structure of the membrane (Ahmadian *et al.*, 2011). However, a lot of research is still needed to examine membrane modification through dip-coating method in order to elucidate the morphological effects of dip-coated membranes.

Lambropoulos *et al.*, (2007) repaired γ -alumina and silica membranes at 573 K by CVD process with a tetraethylorthosilicate (TEOS)/O₃ in a counter reactant configuration. The defect was characterised with a permeability technique and a novel mercury intrusion method. On the other hand, Gopalakrishnan *et al.*, (2007) applied a hybrid processing method for hydrogen-selective membrane preparation. They applied a primary sol-gel silica layer for the CVD zone thickness reduction, and a CVD modification with tetramethoxysilane (TMOS) and O₂ at 873 K. After which they only examined H₂/N₂ selectivity to be 2300 at 873 K. Ahmadian *et al.*, (2011) modified the surface of ceramic supports to facilitate the deposition of defect-free overlying micro and mesoporous membrane. They investigated the effects of dipping time, heating rate, and number of coated layers on microstructure of the modified layers in their study which showed a smoother surface with the crack sizes reduced dramatically after two dip-coating steps.

In this section, a cracked membrane was repaired with boehmite solution (ALOOH), the defected membrane was characterized with permeation technique.

4.3.2 Experimental Procedure

The commercial ceramic support used has 19.8 mm and 25 mm internal and outer diameter respectively, and a permeable length of 318 mm. The feed pressure applied for permeation characterization varied from 0.05 up to 1.00 bar at room temperature. The support's structure was defect-free before the 1st dip. During the removal of the alumina support from the reactor a crack was identified (Figure 4.15) i.e. after gas permeation before boehmite solution modification.

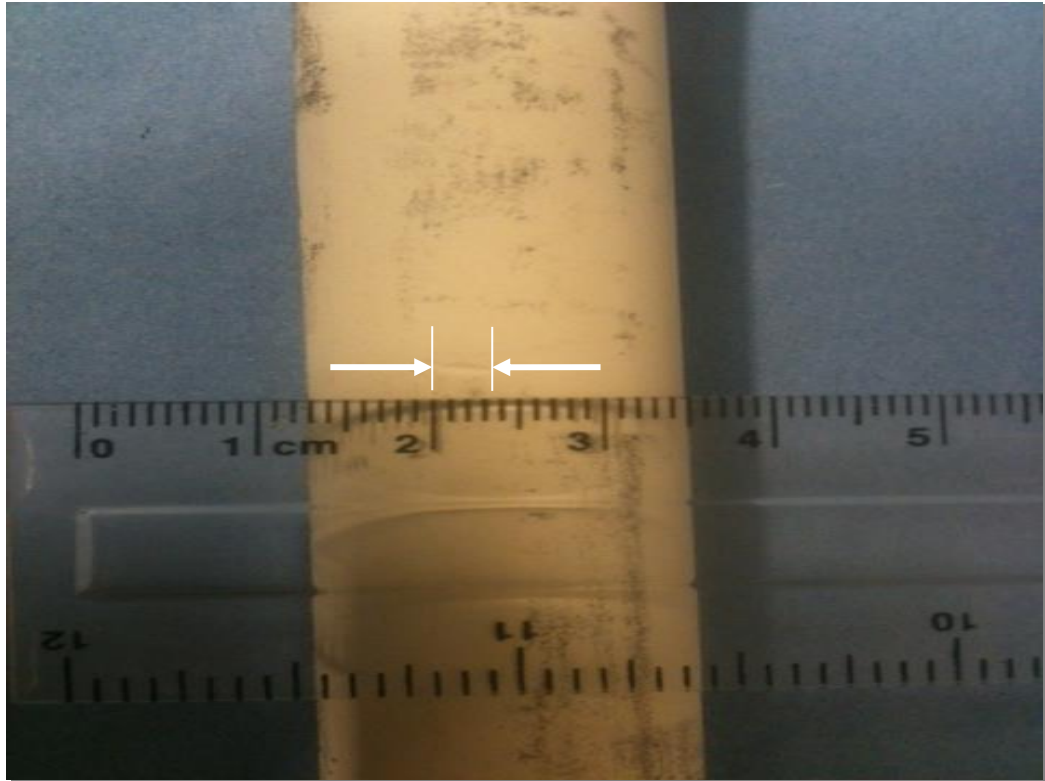


Figure 4.15 - Pictorial view of the cracked membrane.

In order to repair the defected surface of the substrate, a 36g/l boehmite sol was used. A dip-coating method was applied to repair the defected membrane. The internal and external surface of the coarse alumina tube membrane was exposed to boehmite solution for 30 minutes. After this, the membrane was air-dried overnight and then heat-treated using the temperature profile depicted on Figure 4.16. The dipping-drying and firing procedure was repeated in order to achieve the required γ -alumina layer on the coarse support. The prepared membrane was sealed within the stainless steel reactor using graphite seals as shown in Figure 4.17.

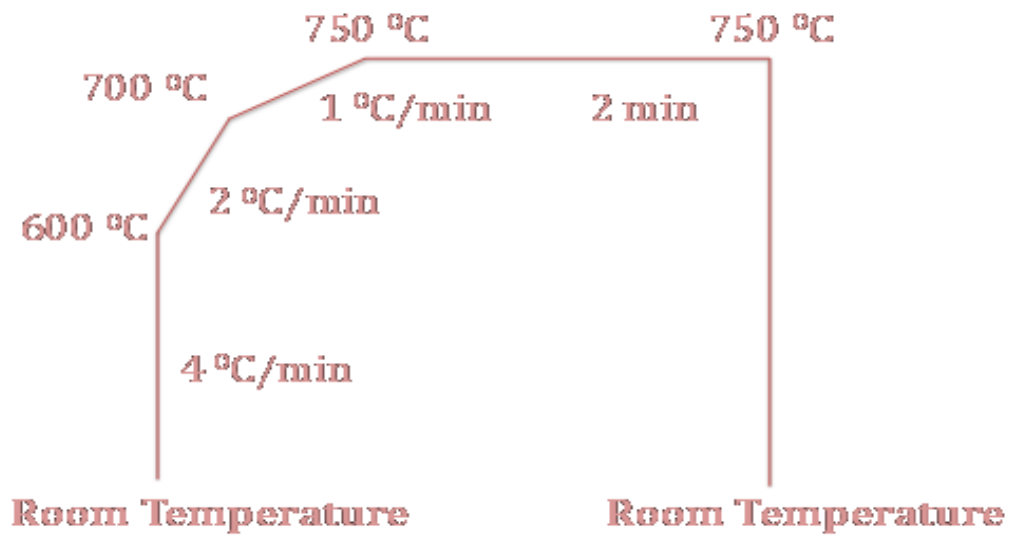


Figure 4.16 - Membrane's heat-treatment profile.



Figure 4.17 - Pictorial view of membrane with the stainless steel reactor showing the graphite ring seals.

Single gas permeation measurements were carried out for gas components H_2 and CO_2 respectively at room temperature with the retentate valve fully open and the permeate connected to the flowmeter to record gas flow rate.

4.3.3 Results and Discussion

Figure 4.18 depicts the results of carbon dioxide permeance against average pressure at room temperature across the alumina support, cracked membrane, first and second dip repaired with boehmite solution stages. It can be seen that the permeance of the alumina support is between 1.50 to $3.04 \times 10^{-7} \text{ mol m}^{-2} \text{ s}^{-1} \text{ Pa}^{-1}$. However, due to the crack which occurred during the removal of the membrane from the reactor, the permeance increased to $2.96 - 5.82 \times 10^{-7} \text{ mol m}^{-2} \text{ s}^{-1} \text{ Pa}^{-1}$. After exposing boehmite solution to the membrane, the surface was repaired with improved performance to some degree, surface cracks are also lowered, and the permeance decreased to between $1.26 - 3.39 \times 10^{-8} \text{ mol m}^{-2} \text{ s}^{-1} \text{ Pa}^{-1}$ after the second dip which is almost parallel to the x-axis indicating that the contribution of viscous flow mechanism was almost negligible and the flow was mainly Knudsen diffusion mechanism. Poshusta, *et al.*, (2000) also reported a CO_2 permeance of $1.5 \times 10^{-7} \text{ mol m}^{-2} \text{ s}^{-1} \text{ Pa}^{-1}$ across silicoaluminophosphate (SAPO)-34 membranes at room temperature. Kusakabe *et al.*, (1996) also reported a CO_2 permeance of $3.0 \times 10^{-7} \text{ mol m}^{-2} \text{ s}^{-1} \text{ Pa}^{-1}$ across the ZSM-5-type zeolite membrane at 30°C . They formed the ZSM-5-type zeolite film for the membrane by mixing a fine silica powder in an aqueous solution of the template and calcining it at 540°C . The template was the mixture of tetrapropylammoniumhydroxide (TPAOH) and tetrapropylammoniumbromide (TPABr). They observed three zones in the film formed on the support tube: a crystalline layer deposited on the support tube, α -alumina macropores partially filled with deposits, and an intermediate layer that was a mixture of deposits and α -alumina particles.

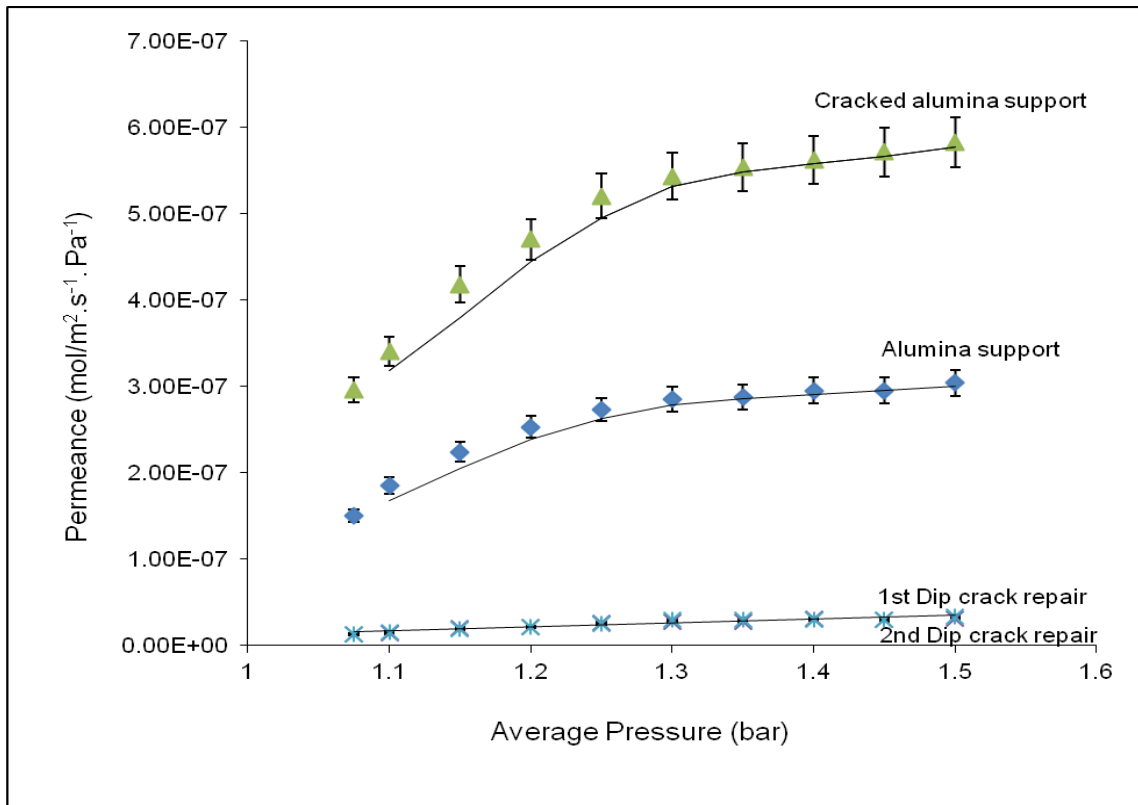


Figure 4.18 - CO₂ permeance against average pressure across tubular membrane at room temperature.

The permselectivities of CO₂ over H₂ across the alumina support, cracked membrane, first and second dip repaired with boehmite solution at room temperature is depicted in Figure 4.19. It can be seen that the selectivities obtained are higher than the ideal Knudsen selectivity (0.21). After exposing the support to boehmite solution, it was observed that a significant increase of CO₂/H₂ selectivity (1.3) was obtained at room temperature for the first dip crack repair as depicted in Fig. 4.19. Subsequent dips however reduced the CO₂ selectivity over H₂. Poshusta, *et al.*, (2000) claimed CO₂/H₂ selectivity of 1.8 at room temperature through silicoaluminophosphate (SAPO)-34 membranes by modifying porous alumina tubular support. Thus, the selectivity obtained in this experiment corroborates the literature Poshusta, *et al.*, (2000). This behaviour is related to the transport regime in the membrane. It is demonstrated experimentally that during the 1st dip repair, surface diffusion of CO₂ in an alumina support with γ -Al₂O₃, can contribute substantially to the transport rate. Moreover, for this system it is of almost the same order of magnitude as the transport caused by ordinary diffusion through the gas phase in the pores. Subsequent dipping results in continuum diffusion and molar flux are therefore independent of pressure. Surface diffusion however is linearly proportional to the pressure provided the fraction of the adsorption sites covered is very low. It is demonstrated that the resulting difference in pressure dependence

of both transport mechanisms can be used to distinguish between diffusion through the gas phase in the pores and surface diffusion.

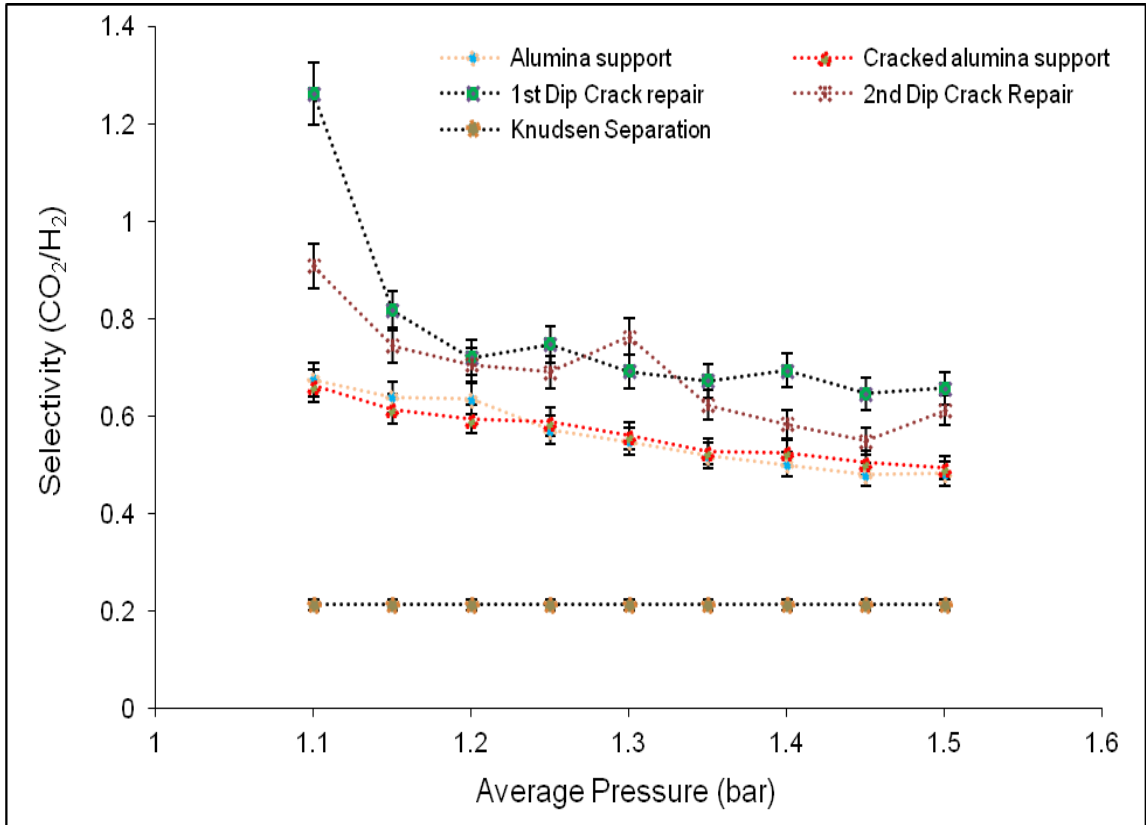


Figure 4.19 - CO₂/H₂ selectivity against average pressure across tubular membrane at room temperature.

A simple but effective technique to modify nanostructure ceramic membranes which involves the dip-coating method was studied and involved the use of boehmite solution to modify alumina support. Several parameters such as dipping time, number of coating, heating rate on the nanostructure were investigated. A high temperature heat-treatment was applied in order to repair defects on the commercial alumina support, and to improve the permselectivity of these membrane above Knudsen regime selectivity. Single gas permeation tests were used to examine the permeance of the membrane. After the first and second modifications with boehmite solution, permeance decreased significantly which indicates a substantial reduction in cracks and pore diameter.

4.4 CO₂ Recovery from Natural Gas by Modifying 30nm Support

4.4.1 Introduction

The prevention of environmental smog from industrial sources which occurs through fossil fuel combustion is now receiving considerable attention worldwide. In the past 20 years, the international community has agreed to cut down greenhouse gases under the Kyoto protocol in 1997 (Yildirim & Hughes, 2003). Also, at the United Nations Climate Change Summit in Doha (2012) a resolution was adopted to extend the reduction in carbon emissions by 2020 under a second commitment period of the Kyoto Protocol (Louise, 2012). Environmentalists have also brought in emergency regulations for the reduction of the flare activities that are responsible for a significant fraction of the emission of greenhouse gases such as carbon dioxide (CO₂) and methane (CH₄) ([www.eia.gov/forecasts/ieo/pdf/0484\(2013\).pdf](http://www.eia.gov/forecasts/ieo/pdf/0484(2013).pdf)). Elimination of gas flaring can be achieved by increasing the amount of recovery through separation and the collection, disposal, capture, and utilization processes (Yildirim & Hughes, 2003).

Therefore, it is imperative to build up new effective technologies to mitigate these emissions. Inorganic membranes applications are technically significant in environmental issues like separation, catalytic reactions among others (Yildirim & Hughes, 2003; Othman, Mukhtar & Ahmad, 2004; Kajama, Nwogu & Gobina, 2014; Mulder, 1996; Nwogu, Gobina & Kajama, 2013). Inorganic membranes for CO₂ removal can be applied *in-situ* without any phase change. Catalytic combustion/oxidation is also being researched as a substitute process for the removal of these pollutants since it is flexible and requires low energy compared to thermal oxidation (Yildirim & Hughes, 2002).

Sol-gel technique is considered one of the most significant technique for the production of meso- and microporous membranes (Smart *et al.*, 2013). It was first used for preparing membranes by Leenaars and Burggraaf, (1985) for ultrafiltration applications. Dip coating is a more general coating technique utilized with sol-gel chemistry (Smart *et al.*, 2013). On the other hand, CVD is a method which allows coating of the membrane by depositing the ceramic layer by chemical reactions at high temperature (Smart *et al.*, 2013).

Surface diffusion has been named as an important mechanism in a number of studies on silica membranes for the selective separation of CO₂. Research, then, has focused primarily on separation of CO₂ from N₂ and CH₄, the surface diffusion mechanism not being considered strong enough for the more difficult separation from H₂. Way and Roberts (1992) used microporous hollow fiber silica membranes for gas separations. They proposed that both the surface diffusion and the molecular sieving mechanism contribute to the permeation properties

of the silica hollow fiber membranes. High permselectivities were observed for CO₂/N₂ of 28 at 40 °C.

In this section, a 30nm commercial ceramic tube was used as a support. A membrane was synthesized via the dip-coating method. The membrane permeability was investigated with single gas permeation experiments at room temperature.

4.4.2 Experimental Procedure

Available commercial porous alumina support of tubular configuration consisted of an average pore diameter of 30nm was employed in this section. The alumina support had an internal and outer diameter of 7 and 10 mm respectively. Pressures of 0.05 up to 5.0 bar at a temperature of 298 K were applied. The support was found to be defect free after characterization. Single gases used in this section consisted of CH₄, CO₂, H₂, He, N₂ and Ar. In a typical experiment, the gas was passed into the shell-side and permeated through the coated membrane at different pressures. The permeate was connected to the flowmeter to measure the flow rates.

4.4.3 Results and Discussion

4.4.3.1 Effect of Gas Permeation and Selectivity at Room Temperature

Figure 4.20 depicts nitrogen permeance across unmodified (alumina support) and silica modified membrane at $1.03 - 1.50 \times 10^5$ (Pa) feed pressure and room temperature. It can be observed that silica modification results in almost 3-fold decrease in the gas permeance which corroborates the literature (Huang *et al.*, 1997) on La₂O₃-modified γ -Al₂O₃ membrane. This result indicates that a considerable amount of silica has penetrated and subsequently modified the surface of the alumina tube.

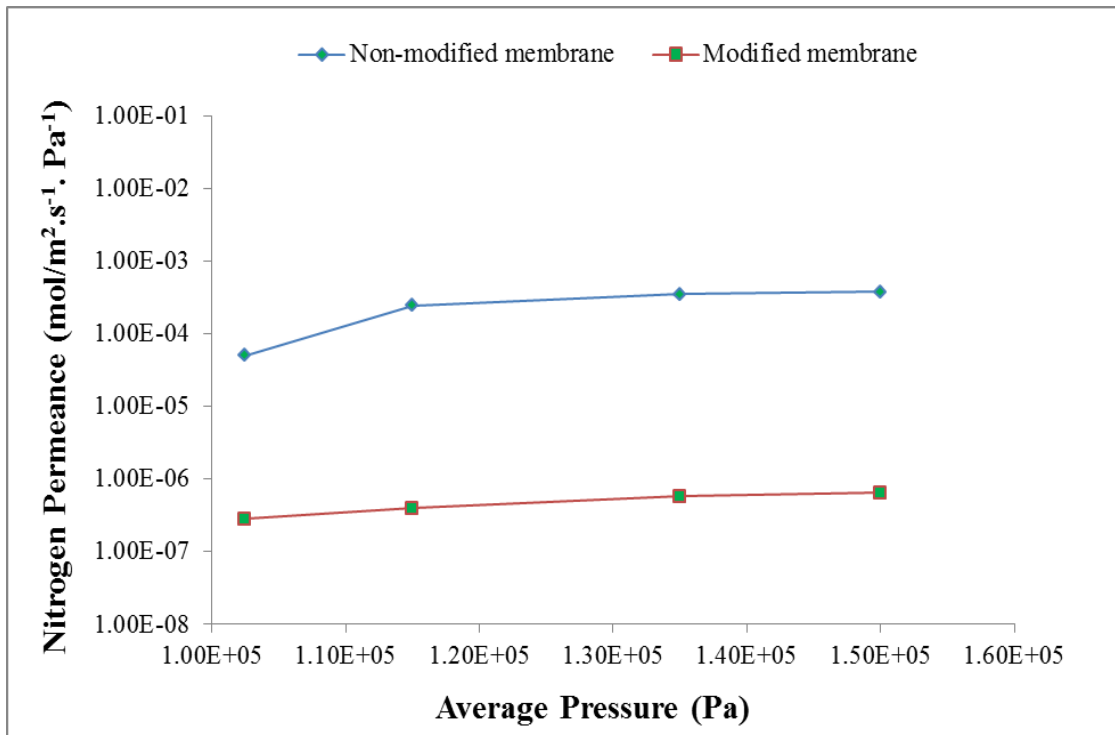


Figure 4.20 – N₂ permeance across non-modified (alumina support) and modified (silica) membrane against average pressure at 298 K.

Figure 4.21 depicts methane permeance across unmodified (alumina support) and silica modified membrane at $1.03 - 1.50 \times 10^5$ (Pa) average pressure and room temperature. It can be seen from Fig. 4.21 that silica modification results in an almost 4-fold reduction in gas permeance. Also, methane permeation could not occur at 1.03 and 1.15×10^5 (Pa) due to the membrane's pore blockage by the silica adhesion on the alumina support which hinders methane transport through the pores at these pressures. Methane permeation started at 1.35×10^5 (Pa). This result corroborates the literature (Huang *et al.*, 1997) on La₂O₃-modified γ -Al₂O₃ membrane. One can conclude that the influence of membrane modification could result in allowing a particular component with the influence surface diffusion mechanism and prevent other gas species to permeate through the membrane.

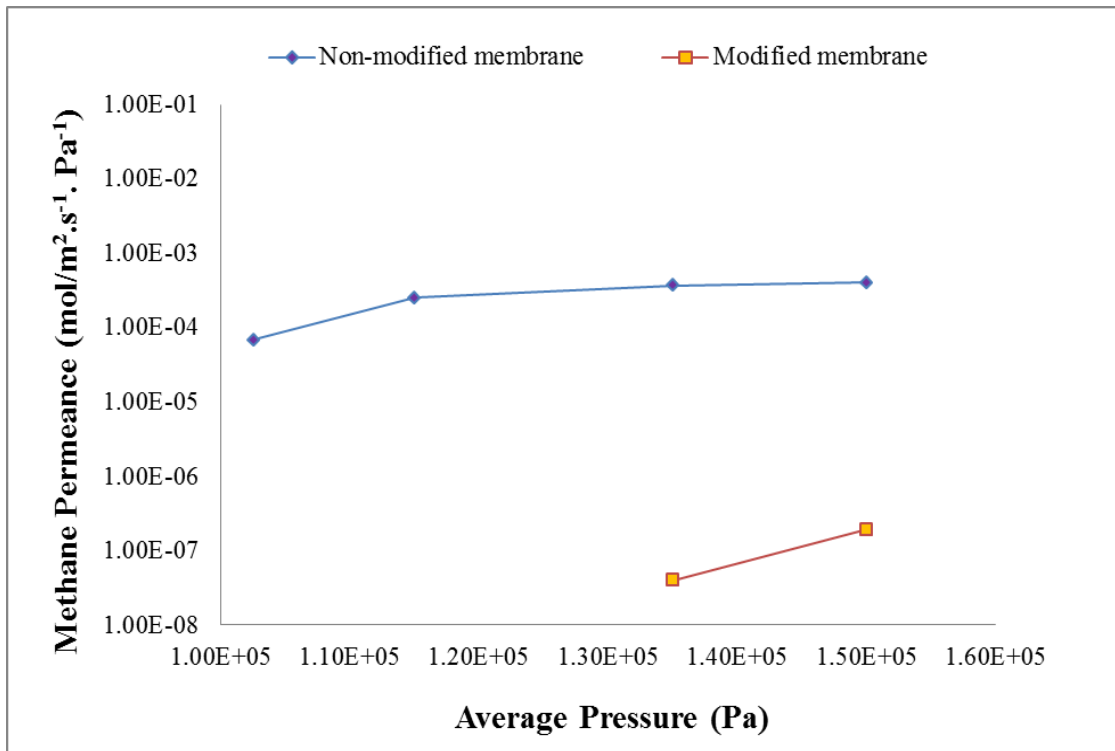


Figure 4.21 - Methane permeance across alumina support and silica membrane against average pressure at 298 K.

Figure 4.22 depicts the influence gas flow rate across silica membrane after fifth dip-coating against feed pressure at 298 K. It can be seen that nitrogen and methane recorded zero flow between 0.05 to 0.7 barg. However, permeation occurred at 1.0 to 5.0 barg but the recorded flow rate was lower than for carbon dioxide and hydrogen. This occurs due to silica modification influencing the membrane's pore which hinders the gases (methane and nitrogen) to pass through the pores but allowing other components (carbon dioxide and hydrogen) to diffuse. Carbon dioxide permeated faster through the pores of the membrane with the influence of the surface diffusion mechanism. The obtained results are in good agreement with the literature (Nwogu, Gobina & Kajama, 2013). Their findings were obtained by modifying macroporous alumina support with silica at pressures between 0.1 up to 6.0 bars and room temperature.

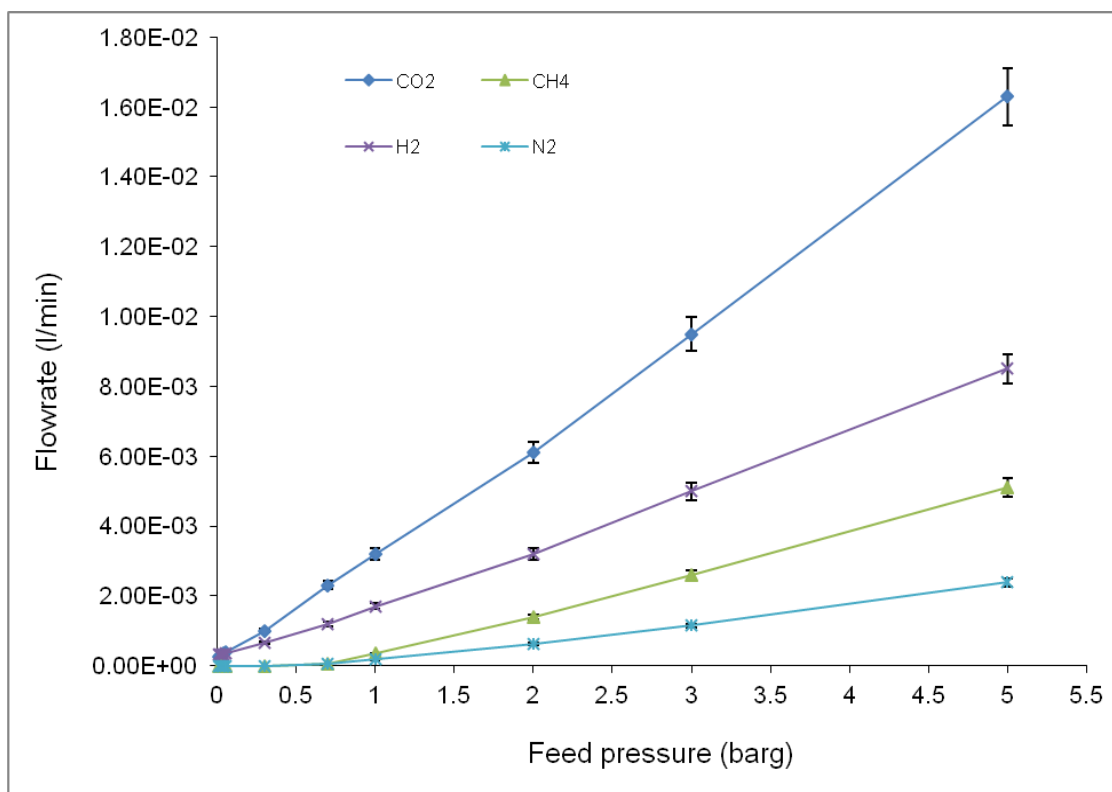


Figure 4.22 - Gas flow rate across silica membrane after fifth dip-coating against feed pressure at 298 K.

Figure 4.23 depicts the selectivities of CO₂ over N₂, H₂, O₂, CH₄ and He against feed pressure across silica membrane at room temperature. CO₂ selectivity was obtained using the ratio of permeability of CO₂ to that of each of the other gases (N₂, H₂, CH₄, O₂ and He) at the same pressures and temperatures. The ideal Knudsen selectivity value was obtained from the inverse square root of the ratio of the respective gas molecular weight. It can be seen that CO₂ selectivity decreased with pressure increase. However, CO₂/CH₄ selectivity of 24.07 was obtained at 0.7 barg and 298 K. Also, the selectivity values obtained for this experiment were higher than the ideal Knudsen separation.

Asaeda *et al.*, (2001) applied the sol-gel techniques to fabricate thin layer silica membranes on porous silica and silica-zirconia supports coated on α -alumina porous cylindrical tubes. The pore size of the silica membrane was around 0.35 nm. They claimed that CO₂ permeance increased through the silica membrane as the temperature decreased, while N₂ and CH₄ permeances increased very slightly, as CO₂ is more adsorptive on the silica surface than N₂ or CH₄. They reported that the porous silica membranes were quite stable when used in dry conditions, while a silica membrane on a silica-zirconia sub-layer was even stable in humid conditions. They achieved a selectivity of 25 for CO₂/CH₄ at 300 °C which is comparable to this experiment.

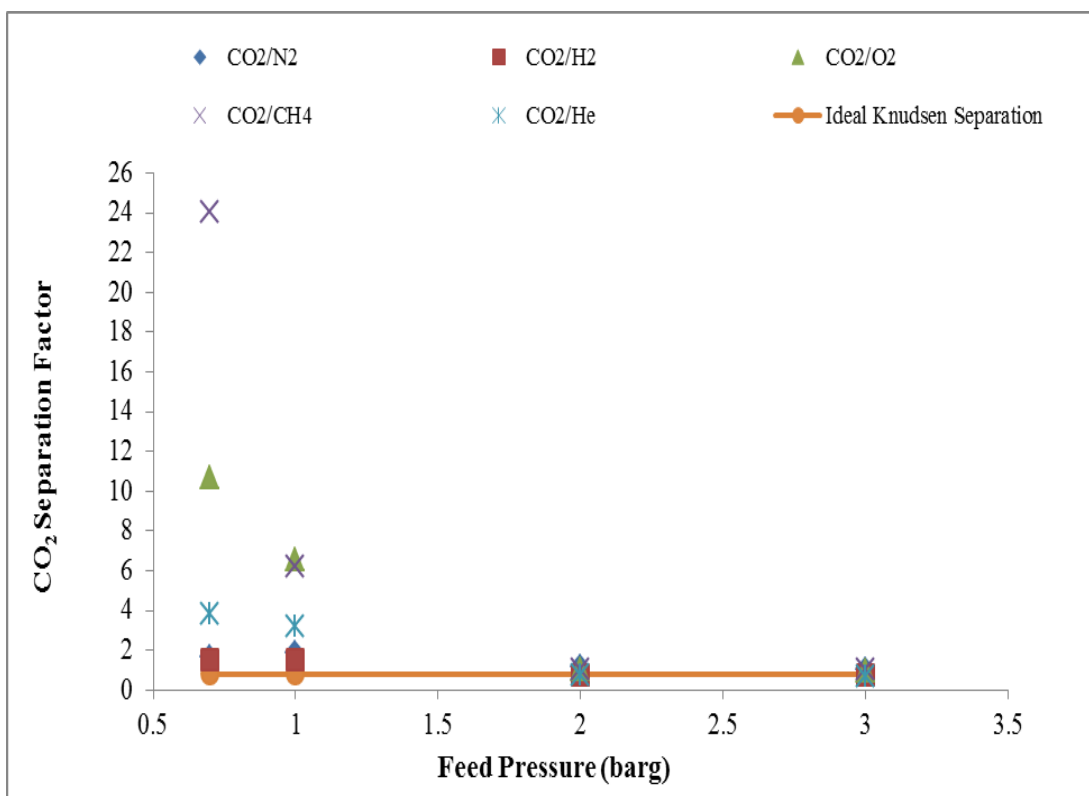


Figure 4.23 - CO₂ selectivity against feed pressure across silica membrane at room temperature.

The dip-coated membrane prepared in this section exhibits higher CO₂ selectivity at pressures of up to 3.0 barg from other gas components. The higher CO₂ permeance rate is attributed to the adhesion of the silica on the alumina support which resulted with surface diffusion mechanism. A CO₂/CH₄ selectivity of 24.07 was also obtained at room temperature and 0.7 barg. The selectivity obtained is comparable to the literature (Asaeda *et al.*, 2001). Such a selectivity value could be useful in a small-scale carbon dioxide removal unit for natural gas treatment processes.

4.5 CO₂ Recovery from Natural Gas by Modifying 15nm Support

4.5.1 Introduction

The world population is expected to increase from 7.16 billion in 2014 (www.worldometers.info/world-population/?utm_expid=4939992-7.scuhn054Q5WX%20vFD9uRG9Xw.2 2014) to 9.2 billion by 2050 (Adewole *et al.*, 2013). Energy consumption is also expected to rise from 15 million megawatts per year in 2014 to 40 million megawatts by 2050 (Adewole *et al.*, 2013). The use of fossil fuels continues to dominate the world's energy demand with about a 23.5% share from natural gas alone which significantly contributes to global climate change due to the related emissions of greenhouse gases such as carbon dioxide, methane, carbon monoxide, nitrous oxide among others (Rui, Ji & Lin, 2011; Brunetti *et al.*, 2010). According to the Trends

in global CO₂ emissions: 2014 Report, China and the United States emitted about 10.3 and 5.3 billion tons respectively of CO₂ in 2013 (http://edgar.jrc.ec.europa.eu/news_docs/jrc-2014-trends-in-global-co2-emissions-2014-report-93171.pdf 2014). In recent years, some carbon reduction policies were introduced in order to mitigate the increase of CO₂ emission globally (Ahmadian *et al.*, 2011). A number of techniques tend to emerge as a substitute for this application such as absorption, adsorption, and membrane processes (Adewole *et al.*, 2013). Sol-gel method or chemical vapour deposition (CVD) technique, or phase separation method is widely applied as the preferred preparation method for inorganic membranes. The porous support provides mechanical strength to the selective top layer of silica. This method is being used to obtain microporous ceramic membranes e.g. by depositing silica layers on ceramic supports. These ceramic supports can either be alumina or porous Vycor glass (Li *et al.*, 1997; Lee & Oyama, 2002). In the sol-gel technique (Kusakabe *et al.*, 1999) polymeric silica sols are deposited on top of a support system consisting of about a micron thick γ -alumina over a macroporous α -alumina of desired thickness. The silica layer is then calcined at 400 to 800 °C, to end up as the separating top layer with thickness of 50 to 100 nm. The silica sols are obtained from the hydrolysis condensation reaction of alkoxysilanes, such as tetramethoxysilane (TMOS), tetraethoxysilane (TEOS), or chlorosilane.

In this section, a defect-free tubular membrane consisting of a thin silica active layer was obtained via the repeat dip-coating method. The effects of temperature and feed pressure on permeate flux have been experimentally studied on single gases for natural gas separation.

4.5.2 Experimental Procedure

The tubular ceramic support used in this section consisted of a nominal pore size of 15nm. The support has a permeable length of 348 mm with I.D and O.D of 7 and 10 mm respectively. Modification of the support was achieved using the repeated dip-coating method using silica. The preparation method is explained in chapter three.

Membrane thickness was calculated using equation 4.1 (Zhu, Fan & Xu, 2011),

$$L = \frac{W_2 - W_1}{A\rho(1 - \varepsilon)} \quad (4.1)$$

where L is the membrane's thickness, W_1 is the weight of the alumina support before coating, W_2 is the total weight of the support and the membrane, A is the membrane's area, ρ is the theoretical density of silica (2.1g/cm³) (Nwogu, Kajama & Gobina, 2015) and ε is the porosity of the membrane (45%).

4.5.3 Results and Discussion

Figure 4.24 depicts the membrane thickness increments as against number of dips. The thickness per dip decreases as the number of dips increases which corroborates with the work of (Nwogu, Kajama & Gobina, 2015) on silica modified membranes. Generally, the total thickness obtained was 5.237×10^{-4} m and the exposure time per dip was 30 min.

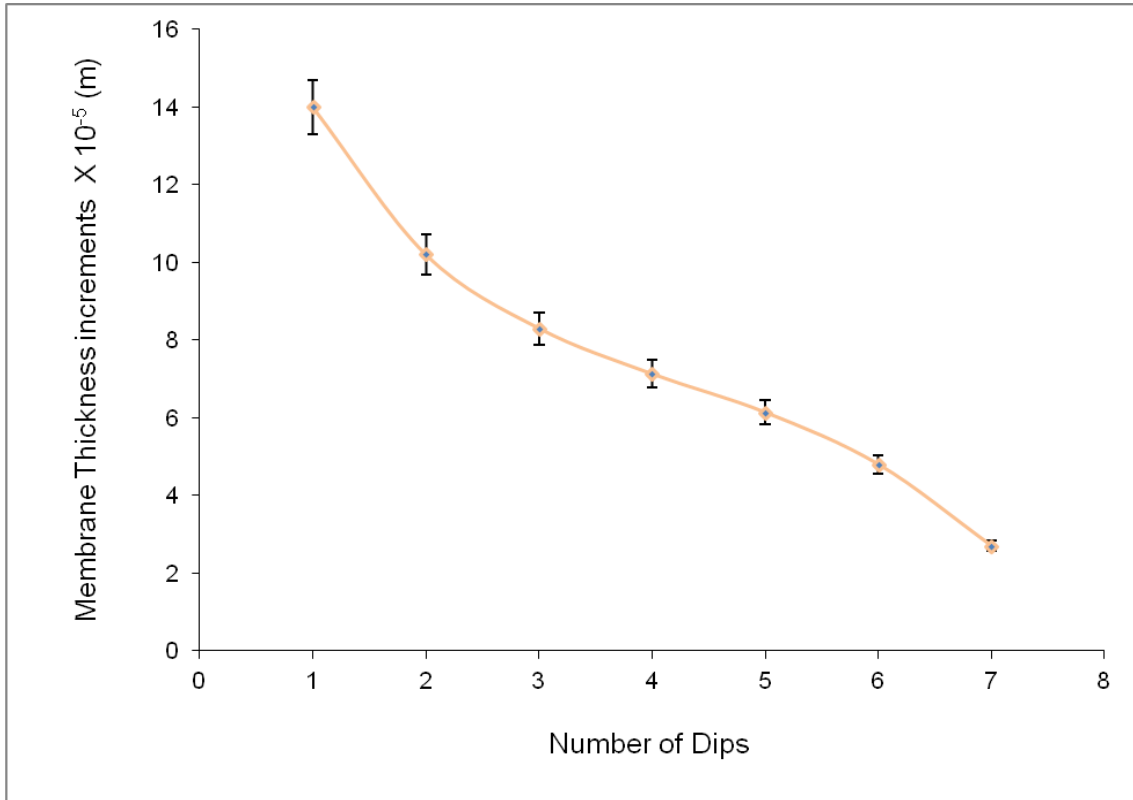


Figure 4.24 - Silica membrane thickness per dip against number of dips.

4.5.3.1 Gas permeation

Gas permeation against feed pressure was obtained across alumina support and silica membrane at temperatures up to 373 K. Figure 4.25 depicts a typical example of single gas permeation behaviour across alumina support with fully opened retentate at 298 K. The feed pressure tested ranged from 0.05 up to 0.40 bar. It was found that the permeate flux increases linearly with increasing feed pressure. It can be seen that He with low molecular weight (4 g/mol) recorded the highest permeate flux while CO_2 with higher molecular weight (44 g/mol) recorded the least permeate flux. In that case, the alumina support does not support CO_2 removal from natural gas process. Ohwoka, Ogbuke & Gobina, (2012a) also obtained the permeation of the gases He, N_2 , CH_4 and CO_2 on alumina support at room temperature and a feed pressure between 0.1 up to 1.0 bar. Their findings also exhibited that He recorded the highest permeation while CO_2 recorded

the least permeation. Therefore, modification of the alumina support is required in order to allow CO₂ separation/transport across the coated membrane.

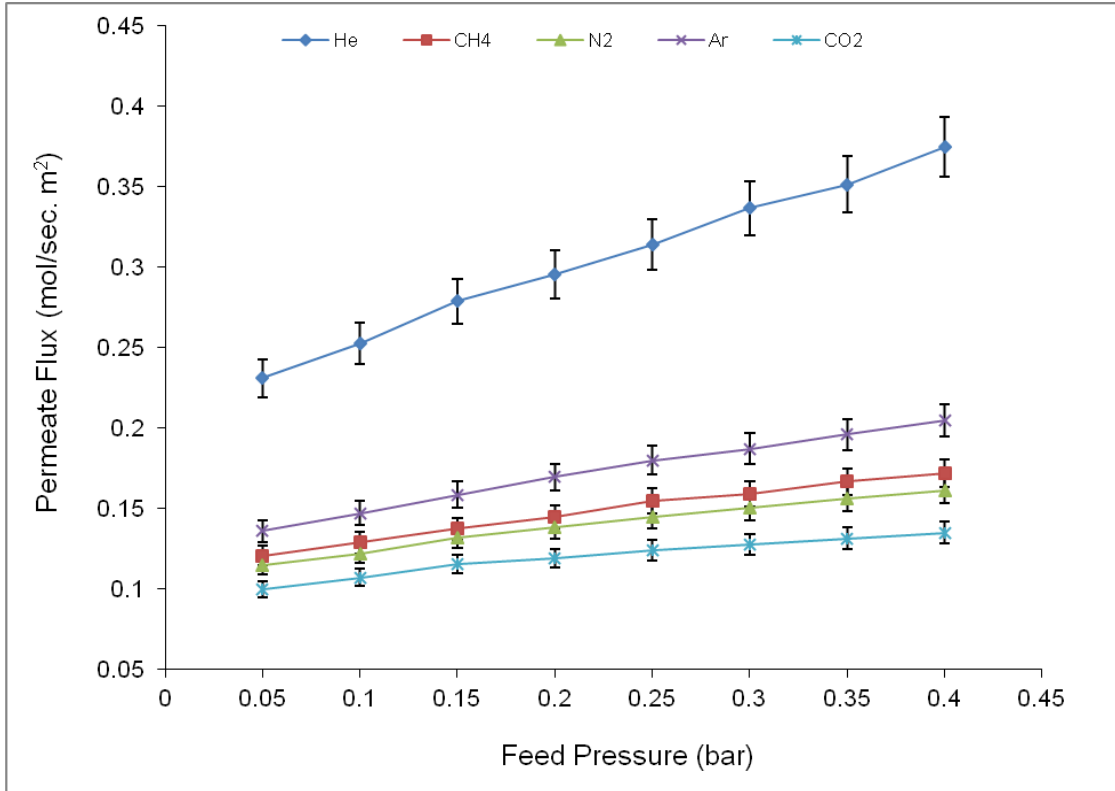


Figure 4.25 - Gas permeates flux across alumina support against feed pressure at 298 K (fully opened retentate).

Figure 4.26 depicts the graph of CH₄ and CO₂ permeation across alumina support and silica membrane against feed pressure at 298 K with fully opened retentate. It is obvious that CO₂ has been positively separated from CH₄ after silica modification. The results corroborate the literature Ohwoka, Ogbuke & Gobina, (2012a) on silica membrane for CH₄ and CO₂ at 0.1 up to 1.0 bar and room temperature. This indicates that silica membranes offer good transport/separation performance for the removal of carbon dioxide from natural gas, mainly methane.

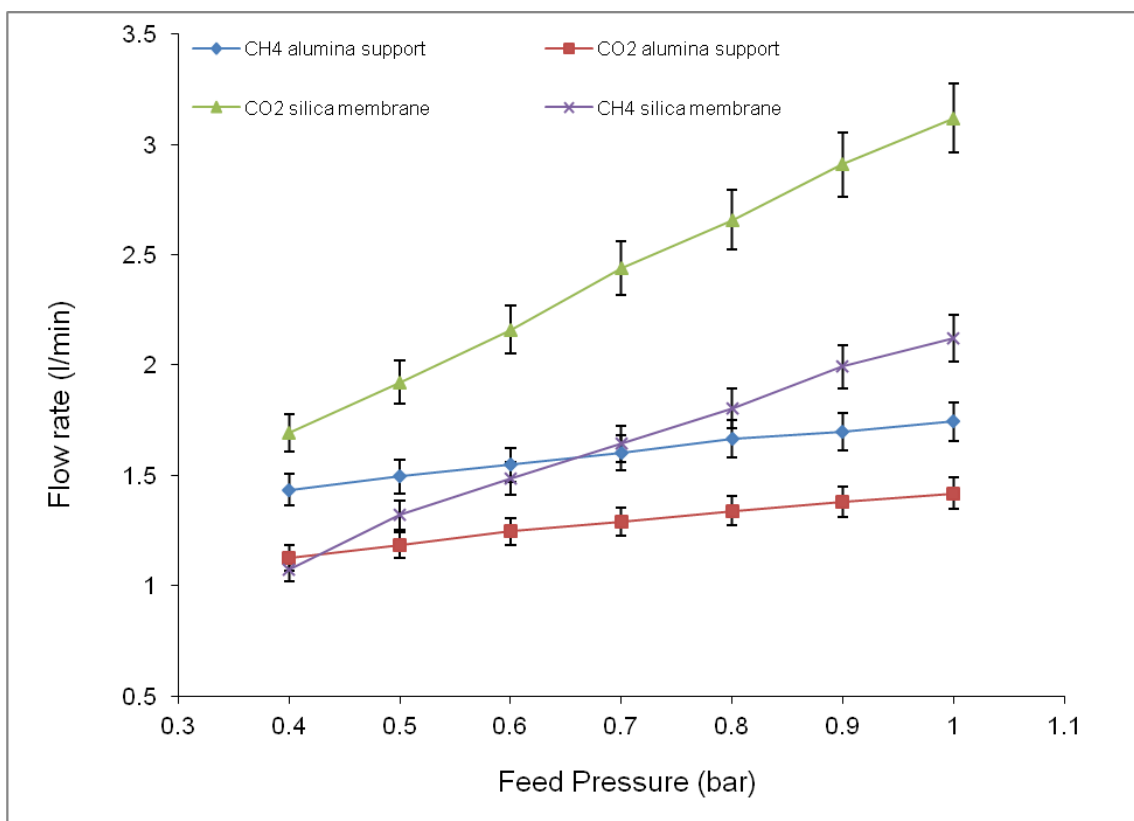


Figure 4.26 - Flow rate of CO₂ and CH₄ across alumina support and silica membrane against feed pressure at 298 K.

Figure 4.27 depicts the graph of CO₂ flow rates against feed pressure across alumina support and silica membrane at 298 K with fully opened retentate. It is obvious that CO₂ permeation increased after silica modification. Ohwoka, Ogbuke & Gobina, (2012a) claimed a successful CO₂ permeation on silica membrane at room temperature and a feed pressure between 0.1 up to 1.0 bar. Their CO₂ permeation increases exponentially with trans-membrane pressure. In this experiment, the higher CO₂ transport achieved through the silica membrane is due to adhesion of silica on the alumina support via the repeat dip-coating method which corroborates the literature (Ohwoka, Ogbuke & Gobina, 2012a).

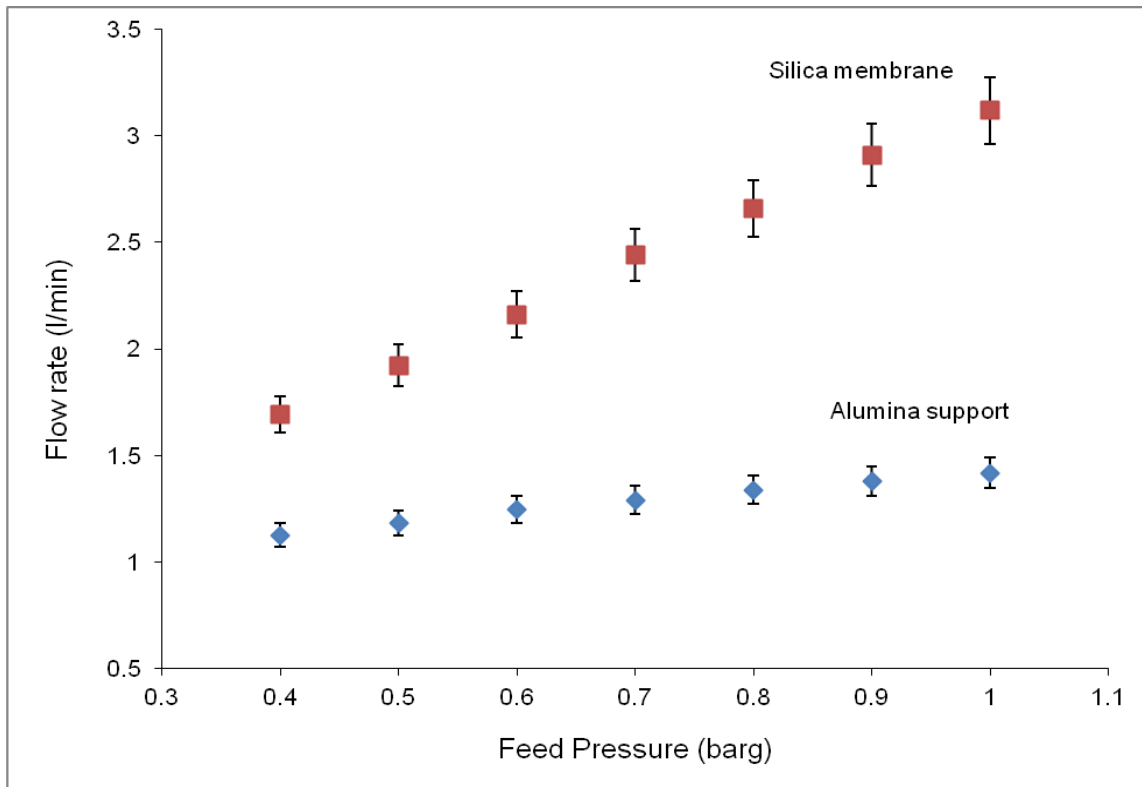


Figure 4.27 - CO₂ flow rate against feed pressure across alumina support & silica membrane at 298 K.

Using equations 2.5 and 2.7 in chapter two, plots of permeance of CO₂ and CH₄ against average pressure is illustrated in Figure 4.28. It can be seen that good linear relationships exist between permeance and average pressure across the silica membrane at room temperature. The values of C_1 and C_2 are obtained by fitting the plots into a straight line shown in Fig. 4.28. It is suggested that an adsorptive transport contribution occurred due to the interaction between gas molecules and the wall of the membrane's pore. CO₂ is known to strongly be adsorbed on the pore walls of silica membrane resulting in surface flow mechanism. It is suggested that interaction between pore wall and CO₂ can be improved by subsequent chemical modification of the pore wall with other materials that can result in an increased adsorptive surface flow as a transport mechanism (Keizer, Uhlhorn & Burggraaf, 1988). Therefore, equations (2.5 and 2.7) becomes;

$$P_t = C_1 P_{av} + C_2 + C_3 \quad (4.2)$$

Where C_3 is constant representing the contribution of adsorptive surface surface flow mechanism.

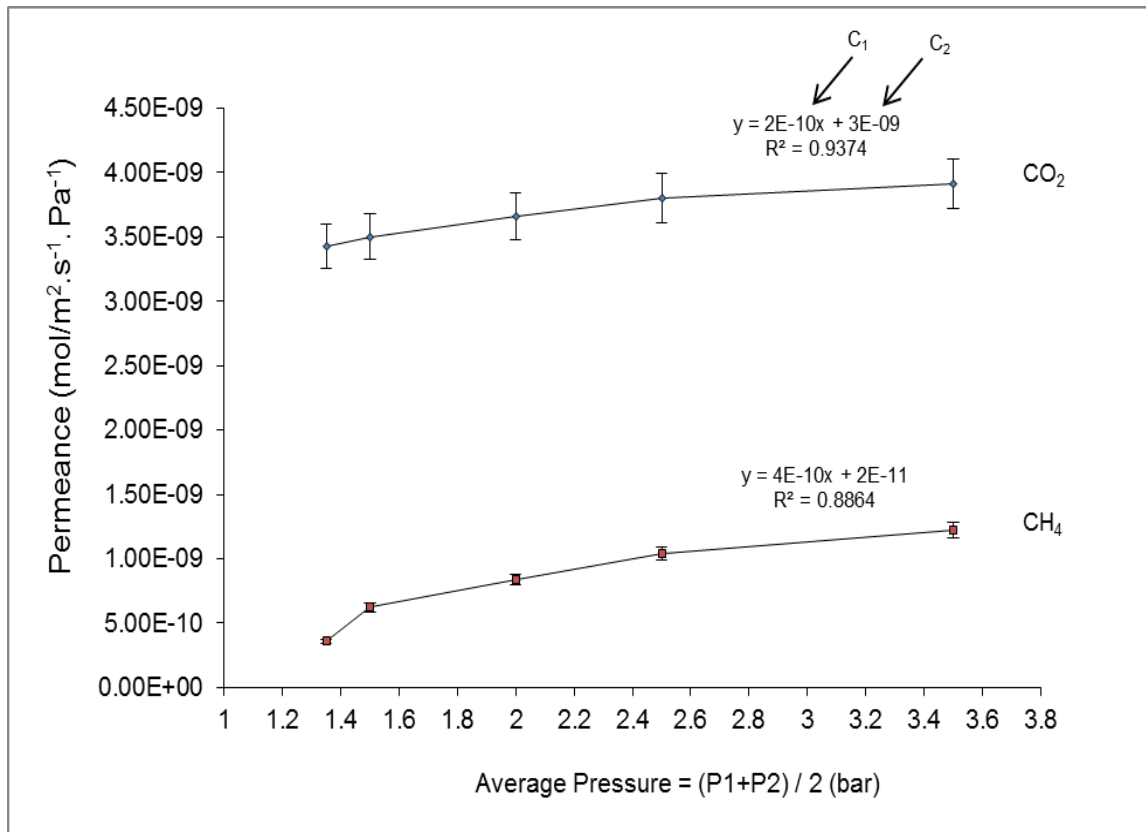


Figure 4.28 - CO₂ and CH₄ permeance across silica membrane against average pressure at 298 K.

Figure 4.29 depicts He permeate flux against permeation temperature at different pressures across silica membrane with fully closed retentate at different trans-membrane pressures. It can be seen that permeate flux decreases as temperature increases. This result corroborates the literature (Cui, *et al.*, 2004). Cui, *et al.*, (2004) also reported temperature dependence of He gas permeance for zeolite membrane at 1 bar. At this condition, Knudsen diffusion mechanism is significant over viscous flow.

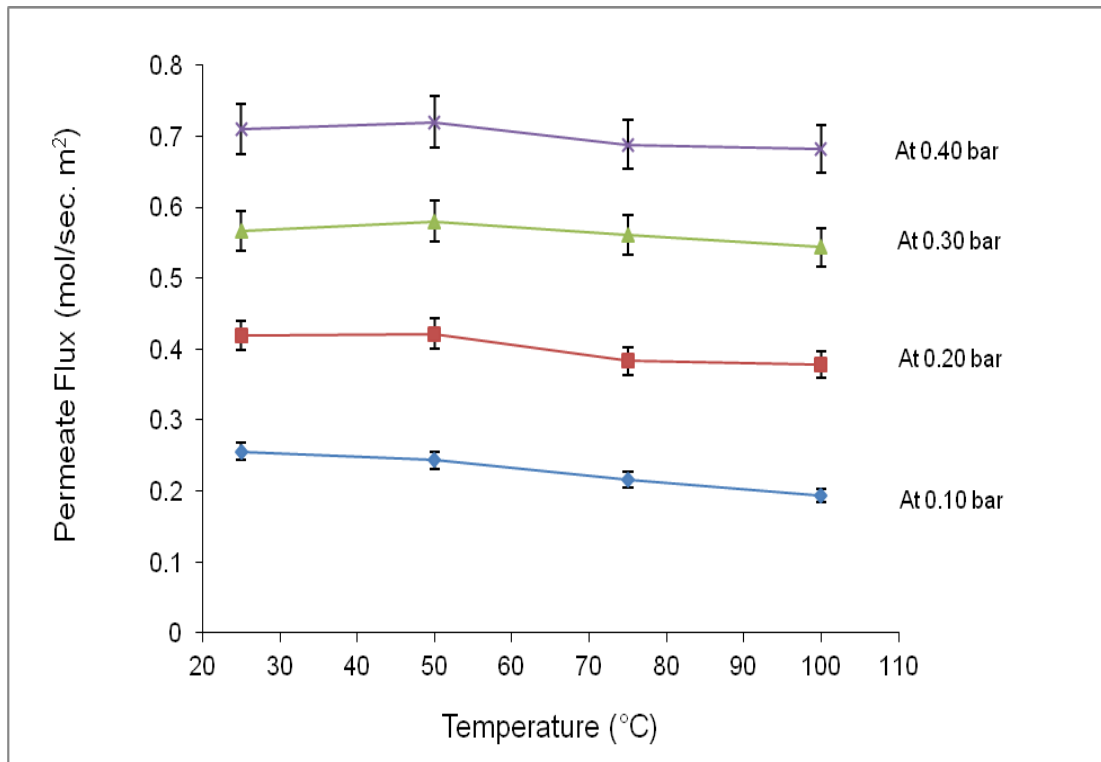


Figure 4.29 - Helium permeation across silica membrane against temperature at different feed pressures.

A laboratory scale tubular silica membrane was used. The influence of permeation temperature and feed gauge pressure of helium, methane, nitrogen, argon and carbon dioxide were examined across the alumina support and silica membrane. The silica membrane offers better carbon dioxide transport/separation from methane with the retentate fully opened at 1.0 barg and 298 K compared to the alumina support. Surface diffusion and viscous flow mechanisms are considered to be negligible for He permeate flux against the tested temperatures (298 up to 373 K) at different feed pressures (0.10 - 0.40 barg). The influence of Knudsen diffusion, viscous flow and surface flow mechanisms were achieved based on the experimental results obtained in this section.

4.6 H₂ Separation Using Inorganic Membranes

4.6.1 Introduction

Hydrogen is extensively used in the chemical, oil refining, petro-chemical and steel industry and is also projected as the clean alternative source of energy (Kanezashi & Asaeda, 2006). Almost 80 percent of the global energy demand comes from fossil fuels such as natural gas, coal among others. Unlike using fossil fuels, hydrogen when combusted produces only water as a byproduct (Adhikari & Fernando, 2006). The world energy consumption is forecast to rise by 56 percent from 2010 to 2040 mainly from coal and natural gas (www.eia.gov/forecasts/ieo/ 2014).

Therefore, it is advantageous to substitute hydrogen with the current fossil fuels because it is widely accepted as a clean energy carrier in, for instance, fuel cell systems. These could help to address the problems linked to energy security which include air pollution and global climate change. The need for hydrogen as a source of renewable energy will be enhanced in the coming years due to its demand for raw material processing in the chemical industry as well as home heating (Meinema *et al.*, 2005).

The literature shows that hydrogen can actually be separated with inorganic membranes (Kanezashi & Asaeda, 2006; Sun & Khang, 1988; Tsotsis *et al.*, 1993; Chai *et al.*, 1994). Inorganic membranes derived from ceramics and metal alloys are candidates for high temperature gas separation. Palladium (Pd) (Kanezashi & Asaeda, 2006; Lewis *et al.*, 2013) and platinum (Pt) (Lewis *et al.*, 2013) alloy metals are the ideal membranes applied for high purity hydrogen production from mixed gas streams even though these metals are expensive. Pd-based membranes are attractive for membrane reactor applications because Pd is highly permeable to hydrogen and offers better thermal stability and selectivity than polymer and microporous membranes (Lewis *et al.*, 2013). Transport of hydrogen through dense Pd membranes follows the solution diffusion mechanism where only hydrogen is transported resulting in high purity (99.9999%), but have been limited in commercialization due to issues which include support quality, surface poisoning due to carbon species, hydride formation, and irreversible damage caused by bulk sulfide formation (Lewis *et al.*, 2013; Bose, 2009; Howard & Morreale, 2008).

The main aim of this section is to report experiments undertaken using a tubular alumina support in order to understand the transport through inorganic membranes (macro- and meso porous) and their corresponding selectivity at different pressures and temperatures for hydrogen separation from natural gas.

4.6.2 Experimental Procedure

Alumina support tubes with 30 and 6000 nm pore diameters were employed in this section. Each alumina support was sealed in a stainless-steel reactor by graphite O-rings which are high temperature resistant. The feed pressure used was between 0.05 up to 2.0 bar and was measured by a pressure transducer. At the permeate, the permeation flux was measured using a flowmeter, and a thermometer to record the required temperature. The permeate side was fully opened to the atmosphere. The permeate pressure was always the atmospheric one.

4.6.3 Results and Discussion

Figure 4.30 depicts the single gas permeation of hydrogen, helium and nitrogen across mesoporous membrane. The permeation of molecules with the smaller molecular weight such as $H_2 = 2 \text{ g/mol}$ and $He = 4 \text{ g/mol}$ diffuses faster with pressure whilst the larger molecular weight $N_2 = 28 \text{ g/mol}$ had low permeation. These results are indicative of the Knudsen diffusion transport mechanism which states that the permeation flux is directly proportional to the inverse square root and the molecular weight of gases.

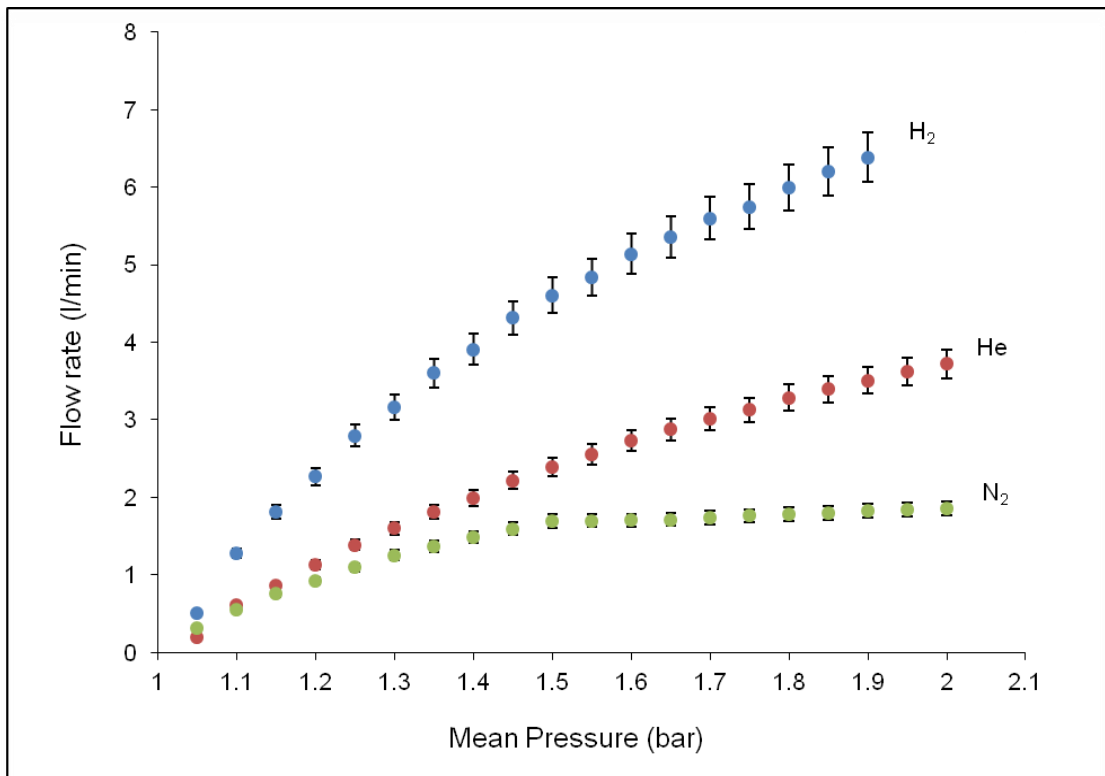


Figure 4.30 - Gas permeation across mesoporous membrane against mean pressure at 298 K.

Figure 4.31 depicts hydrogen permeation across macro- and meso porous membranes against feed pressure (0.1 to 1.0 barg) at 298 K. The results show a higher hydrogen permeation with respect to the macro porous membrane, this indicates that the higher the pore size, the higher the permeation rate.

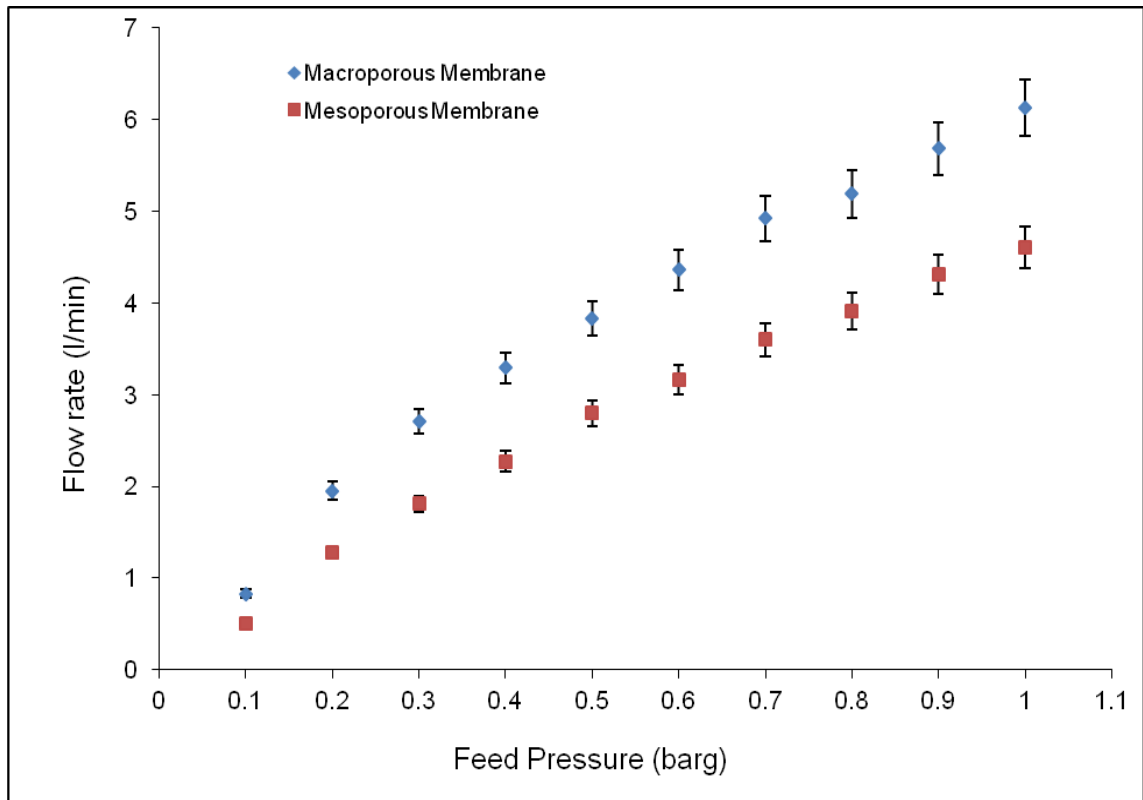


Figure 4.31 - Hydrogen permeation across macro- and meso porous membranes against feed pressure at 298 K.

Figure 4.32 depicts hydrogen, helium and nitrogen permeation against temperatures across mesoporous membrane at 1.5 barg feed pressure. The permeation of molecules with the smaller molecular weight such as hydrogen and helium increased with temperature whilst the larger molecules like nitrogen is independent of temperature. The results obtained corroborate the literature Gopalakrishnan & da Costa, (2008). Gopalakrishnan & da Costa, (2008) also observed a higher permeation rate for helium and hydrogen at temperatures between 100 °C up to 400 °C on silica membrane.

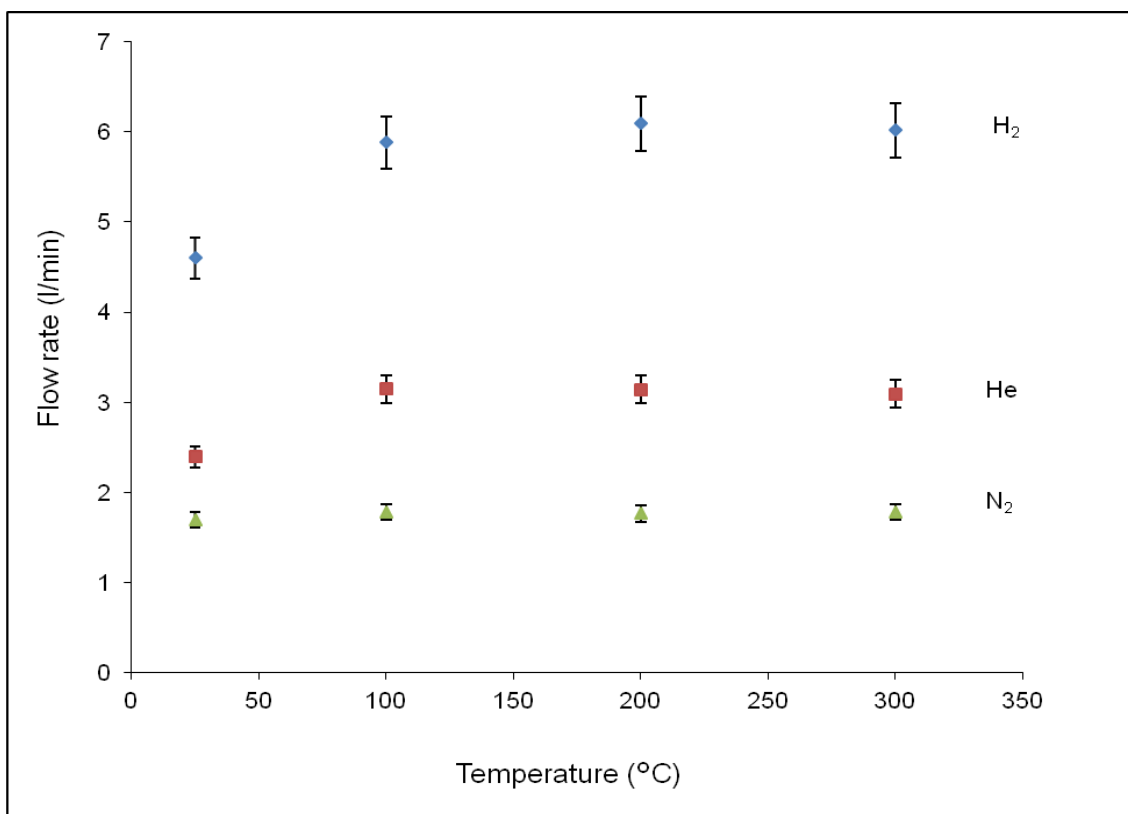


Figure 4.32 - Gas permeation against temperature across mesoporous membrane at 1.5 barg.

The effect of temperature on H₂/He gas selectivity across mesoporous membrane at 1.6 barg feed pressure is depicted in Figure 4.33. Hydrogen selectivity of 1.96 over helium was obtained at 300 °C which is almost 2 fold of the Knudsen ideal selectivity. Also, an improvement of H₂ selectivity is achieved as the temperature increased from 25 °C to 300 °C. Figure 4.34 depicts H₂/N₂ selectivity against feed pressure across macro- and meso porous membranes at 25 °C. It can be seen clearly that a selectivity of 1.36 and 2.72 at 1 bar were obtained from macro- and meso porous membranes. Snape *et al.*, (2012) reported H₂/N₂ selectivity of 3.7 using γ -alumina membrane at 573 K and 0.35 bar. Their value is higher than this experimental value (2.72) at 298 K and 1 bar. The decrease of the selectivity of these mesoporous membrane might be based partly on the experimental temperature difference (298 K) compared to the literature (573 K). It is for this reason that the mesoporous membrane was modified with silica in order to reduce the membrane's pore diameter and enhance selectivity, and the experimental temperature was increased to 573 K which also renders the selectivity increased to 3.07 reported in section 4.7.3.1, which is close to the literature Snape *et al.*, (2012). This is a clear indication that the smaller the pore diameter, the higher the selectivity one can achieve.

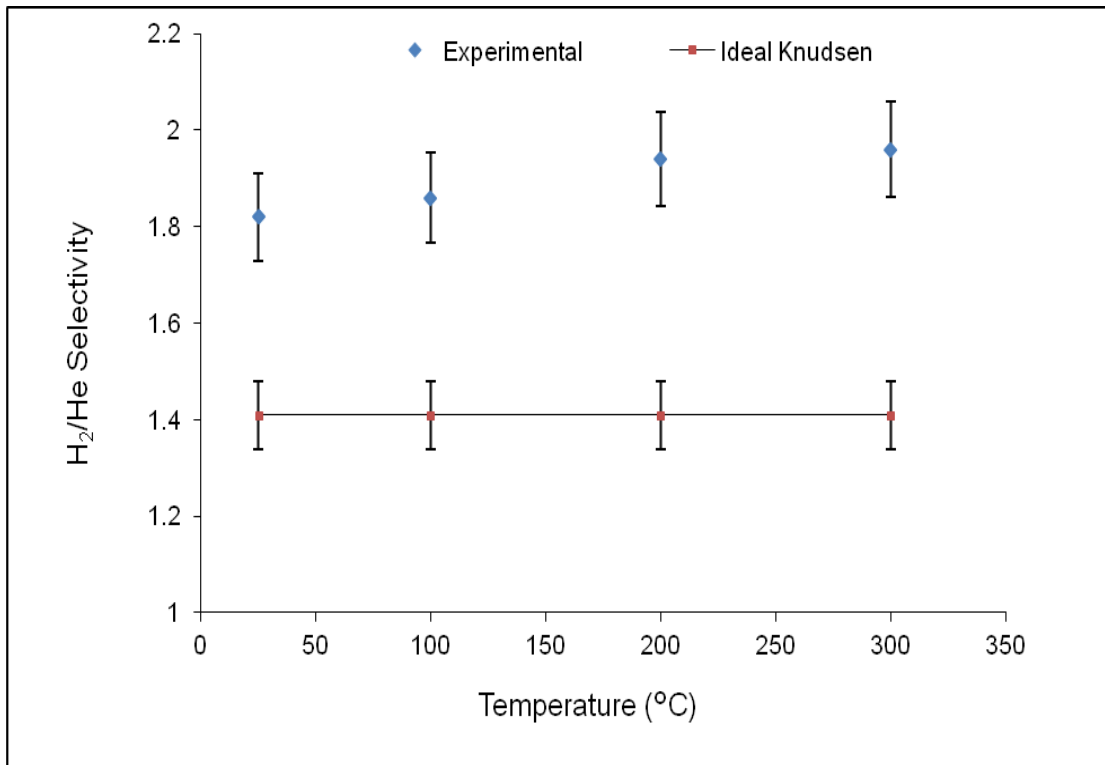


Figure 4.33 - H₂/He Selectivity across mesoporous membrane against temperature at 1.6 barg.

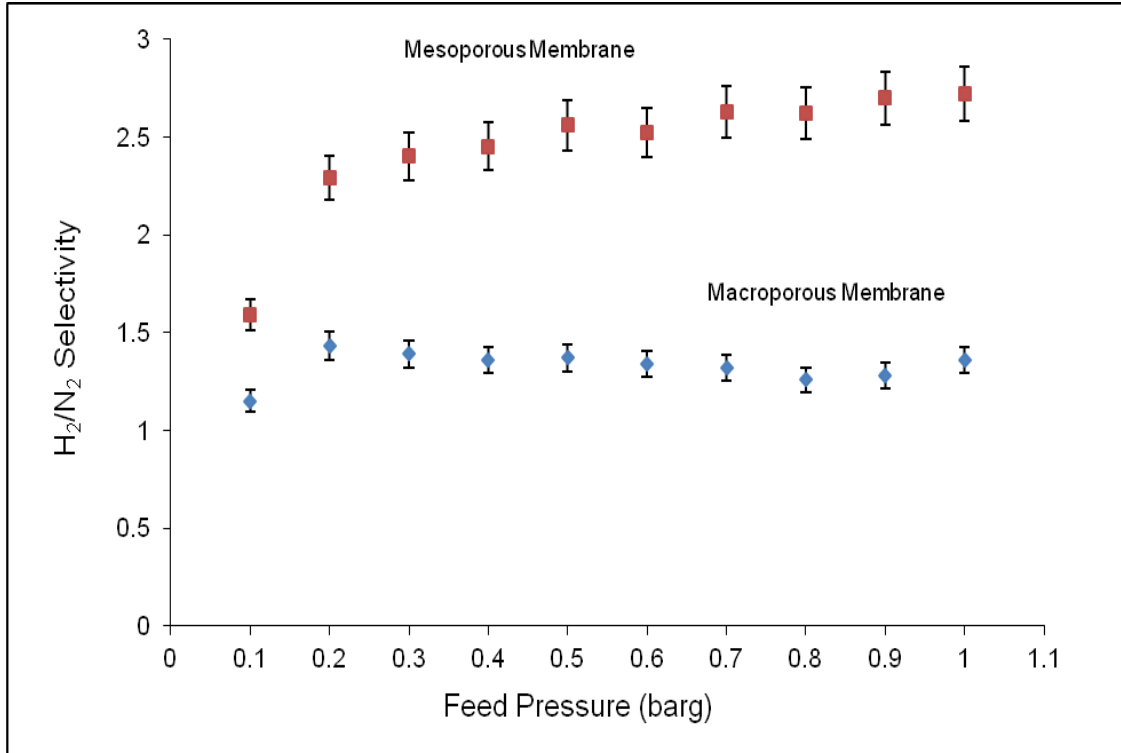


Figure 4.34 - H₂/N₂ Selectivity against feed pressure across macro- and meso porous membranes at 298 K.

It is demonstrated that, H₂ gas permeation increased from 4.6 to 6.0 l/min at temperature range between 25 up to 300 °C. Also, H₂/He and H₂/N₂ selectivities attained values of 1.96 and 2.72 at 300 °C respectively. High temperature also favoured H₂ diffusion as the H₂ selectivity over He on the mesoporous membrane increased with almost 2 fold compared to the ideal Knudsen selectivity (1.4).

4.7 H₂ Recovery Using Silica-Based Membrane

4.7.1 Introduction

Hydrogen separation was initiated by Permea (which is now a section of Air Products) in the past three decades through the application of Prism membrane (Baker, 2001). From that time, a considerable increment worth about US\$ 150 million annually was injected into membrane-based gas separation (Baker, 2001). Research into the application of membrane-based gas separation as well as catalytic processes plays a vital role in the petrochemical industry particularly for the state-of-the-art membrane science and technology. State-of-the-art membrane technology can effectively compete with the conventional ones in the areas of energy-saving, using simple and non-harmful materials, recovery of minor but valuable compounds from the main stream, easy to operate, low maintenance process (Bessarabov, 1999) to mention a few examples.

Porous ceramic membranes have been used for light gas molecules separation e.g. hydrogen and helium from gas mixtures (Gopalakrishnan and da Costa, 2008; Yoshino *et al.*, 2005). Microporous and dense membranes are suitable for high temperature gas separation (Meinema *et al.*, 2005). Microporous membranes are membranes with less than 2 nm pore sizes. The system generally has a macroporous support with some ceramic intermediate layers and a highly selective top layer (Meinema *et al.*, 2005). The top layer possesses the separating capacities. Dense inorganic membranes are made of either polycrystalline ceramic materials or metals which select specific gas specie to pass through the dense material (Meinema *et al.*, 2005). Silica based membranes have been considered in high-purity hydrogen separation (Gopalakrishnan and da Costa, 2008; Yoshino *et al.*, 2005). These can be achieved by either sol-gel or chemical vapour deposition (CVD) processes as reported in most literature (Gopalakrishnan and da Costa, 2008; Yoshino *et al.*, 2005; Ahmad, Othman & Mukhtar, 2004).

The objective of this section is to modify alumina support with silica for the selective separation of hydrogen via the proposed dip-coating method using a 15nm nominal pore diameter.

4.7.2 Experimental Procedure

The experimental set-up used in this section is shown earlier in chapter three. It consists of a stainless steel tubular membrane reactor cell. Graphite rings seals which are high temperature resistant consisting of an I.D and O.D of 10.2 and 24 mm used as a seal to firmly hold the membrane within the stainless steel reactor. A digital flowmeter to measure the permeation rates across the membrane was also used. The surface morphology of the silica membrane was prepared using the repeated dip-coating method (Gobina, 2006; Nwogu *et al.*, 2013) described in detail in chapter three.

4.7.3 Results and Discussion

4.7.3.1 H₂ Permeation and Selectivity

Figure 4.35 depicts gas permeation results across the dip-coated silica membrane. The permeation of molecules with smaller molecular weight such as H₂ was higher than those of the larger molecules like N₂ and CO₂. These results are indicative of molecular weight dependant (Knudsen diffusion) transport mechanism H₂ > CH₄ > N₂ > CO₂ with molecular weight 2 > 16 > 28 > 44 (g/mol). Nwogu, Kajama & Gobina, (2015) claimed the same on silica modified membrane, where CO₂ recorded the least permeation.

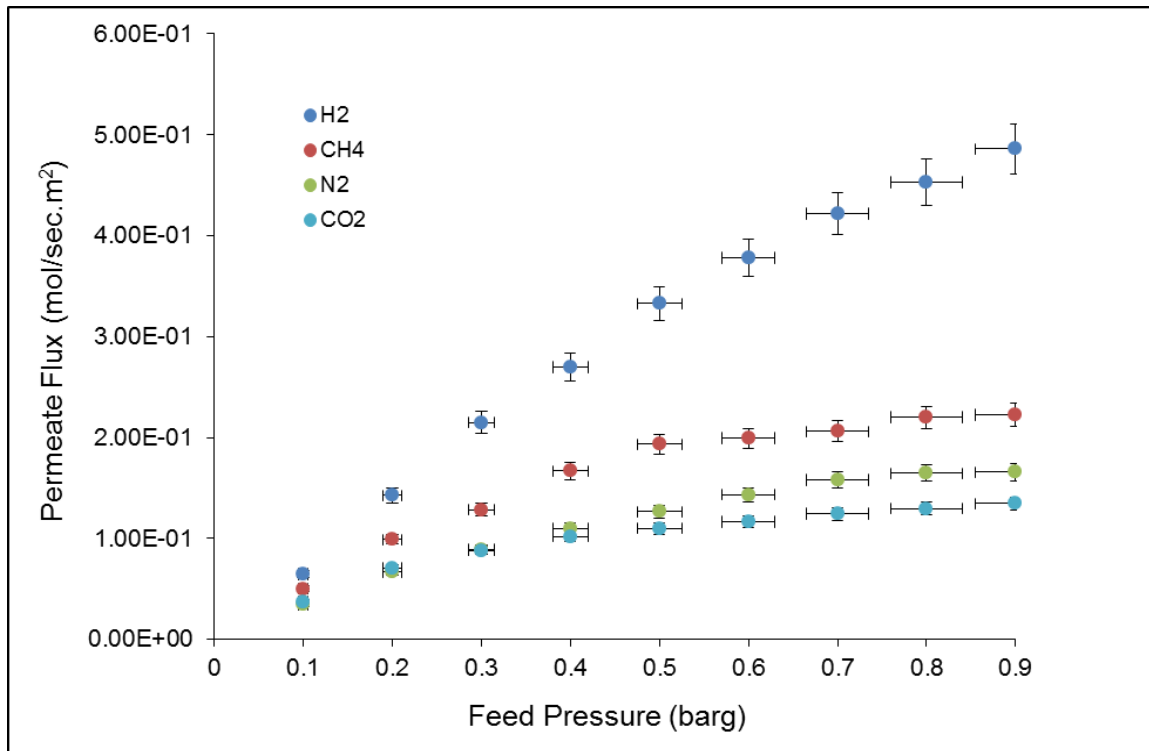


Figure 4.35 - Gas permeate flux across silica membrane against feed pressure at 298 K.

Figure 4.36 depicts hydrogen permeation against feed pressure across alumina support and silica membrane at 298 K. It can be seen that after silica deposition, H₂ permeation rose from 3.3 to about 6.4 l/min at 0.9 bar. H₂ selectivity and a viscosity ratio over N₂, CH₄, Ar and CO₂ across the coated silica membrane at 298 K and 0.9 bar was obtained as 2.93, 2.18, 3.51 and 3.61 and 0.50, 0.80, 0.39 and 0.60 (Table 4.7). This shows a clear indicative that H₂ selectivity over these gases are close to that of the ideal Knudsen selectivity when compared to viscous flow mechanism.

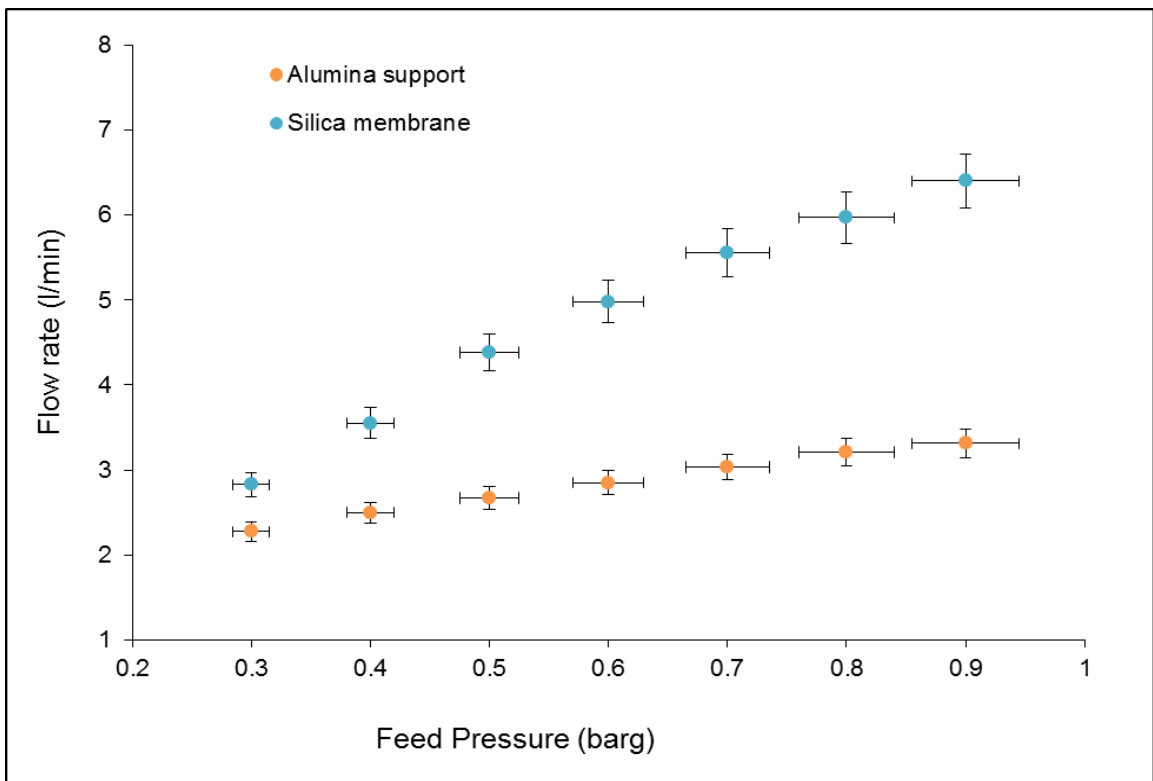


Figure 4.36 - H₂ permeation across alumina support and silica membrane against feed pressure at 298 K.

Table 4.7 - H₂ selectivity at room temperature and 0.9 bar.

Hydrogen selectivity at 298 K and 0.9 bar			
Gas	Experimental H ₂ selectivity	Viscosity ratio (μ Pa s)	Ideal Knudsen selectivity
H ₂ /N ₂	2.93	0.50	3.74
H ₂ /CH ₄	2.18	0.80	2.83
H ₂ /Ar	3.51	0.39	4.47
H ₂ /CO ₂	3.61	0.60	4.69

Figure 4.37 depicts hydrogen selectivity over nitrogen across silica membrane against temperature at 0.9 barg. It can be seen that higher selectivity of 3.07 was obtained at the peak temperature (300 °C) even though the selectivity diminishes to 2.72 at 50 °C and 2.89 at 200 °C.

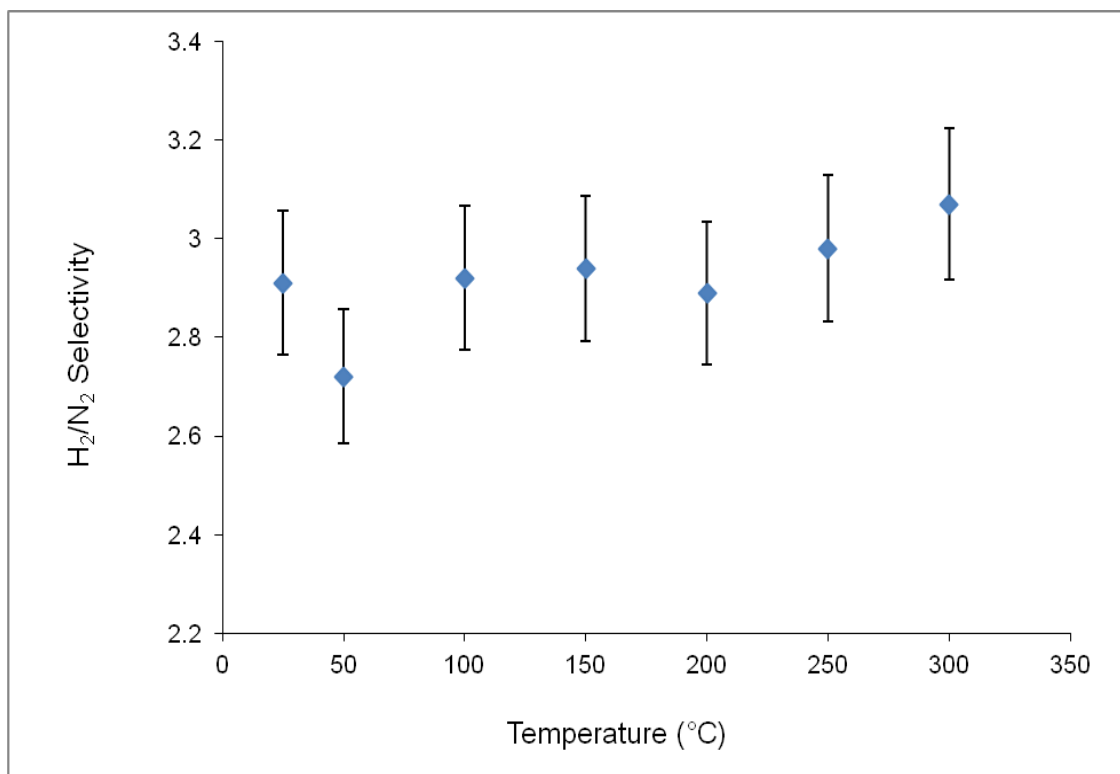


Figure 4.37 - H₂/N₂ selectivity across silica membrane against temperature at 0.9 barg.

Figure 4.38 depicts H_2/CH_4 selectivity against temperature across silica membrane at 0.9 barg. It can be observed that hydrogen selectivity over methane was 2.20 at 25 °C before diminishing to 2.16 at 50 °C. Higher hydrogen selectivity over methane was obtained at 200 °C before diminishing at the final temperature of 300 °C. From this result, one can conclude that hydrogen separation from methane could also be possible. As the temperature increases, residence time on the surface of the membrane is suspected to decrease, and thus activated mechanism could dominate.

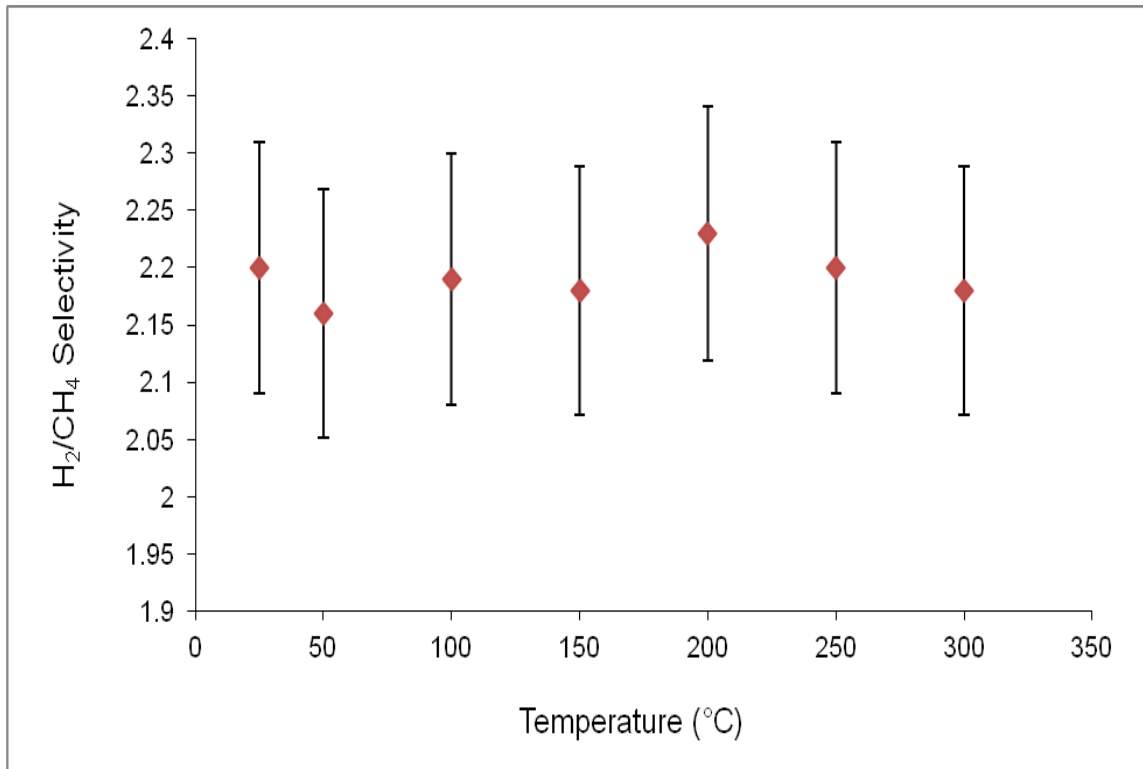


Figure 4.38 - H_2/CH_4 selectivity against temperature across silica membrane at 0.9 barg.

Figure 4.39 depicts H_2/Ar selectivity against temperature across silica membrane at 0.9 barg. It can be observed that hydrogen selectivity over argon was almost linear. The selectivity diminished to 3.40 at 50 °C and rose to its peak of 3.75 at the final temperature of 300 °C. Simultaneous rises in both permeate flux and selectivity for lighter molecules indicate that rapid transport across the membrane which is probably through activated mechanism.

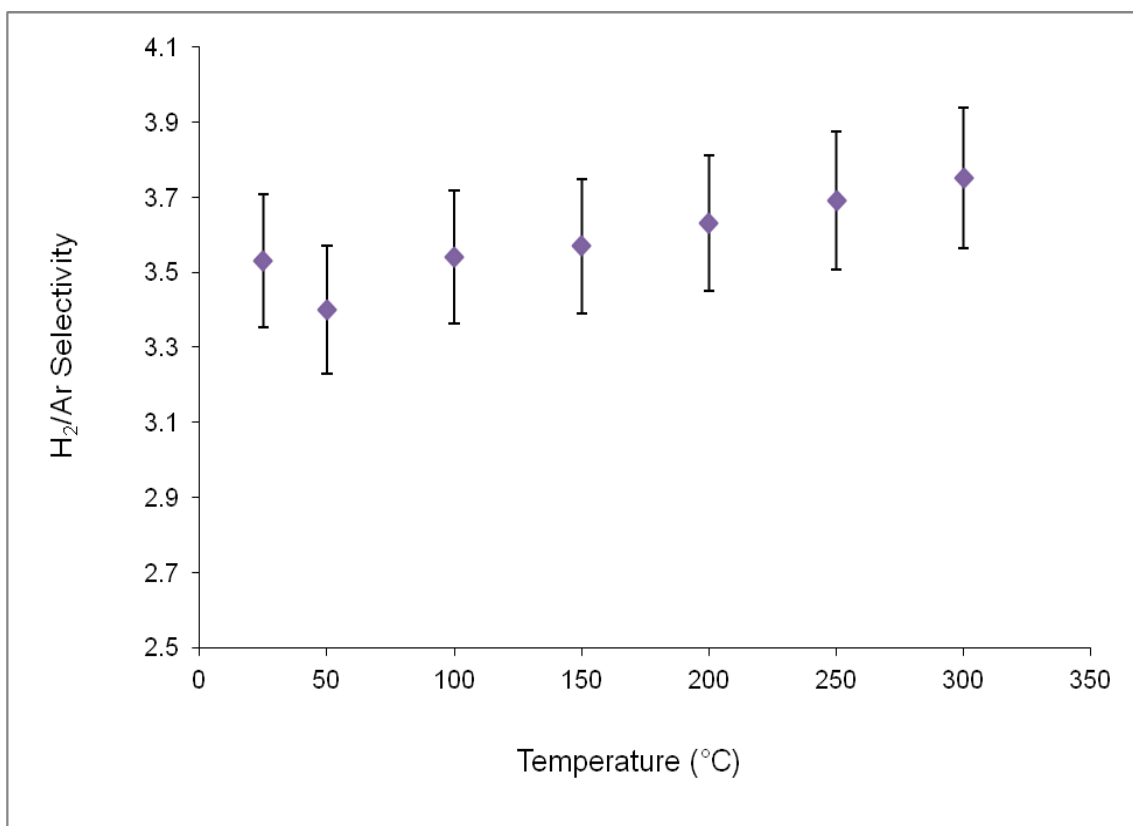


Figure 4.39 - H₂/Ar selectivity against temperature across silica membrane at 0.9 barg.

Modification of inorganic membrane support with silica was demonstrated via the dip-coating method. The permselectivities of H₂/N₂, H₂/CH₄, H₂/Ar and H₂/CO₂ obtained in this experiment were lower than the ideal Knudsen selectivity. The decrease of selectivity of the silica membrane could be attributed to partly on the poor adhesion of the alumina support. Although, it could also be as a result of low hydrogen adsorption on the pore wall of the silica membrane. Replacing the silica membrane for hydrogen adsorption by other materials such as palladium is recommended for further studies.

4.8 VOC Recovery Using Silica-Based Membrane

4.8.1 Introduction

Hydrocarbons are among the most common air pollutants vented from many industrial processes e.g. chemical (Khan & Ghoshal, 2000), metal cleaning (Huang *et al.*, 1997) among others. The venting of these hydrocarbons into the atmosphere contributes enormously to poor air quality. From an environmental point of view, it is imperative to separate and recover these hydrocarbons from the waste gas stream. A number of emerging techniques are being developed as a substitute to more established processes such as absorption, adsorption and condensation (Khan & Ghoshal, 2000; Huang *et al.*, 1997).

Membrane processes have recently emerged as the state-of-the-art technology for such application. This technique was earlier applied in the last five decades for desalination purposes (Khan & Ghoshal, 2000), volatile organic compounds (VOC) removal (Khan & Ghoshal, 2000; Huang *et al.*, 1997; Tahir & Koh, 1999; Saracco & Specchia, 2000) and natural gas processing. Polymeric membranes such as a hollow fibre composite membrane of silicone rubber have been used. Polymeric membranes have very low permeabilities for solvents but their selectivities are quite high (Huang *et al.*, 1997). Indeed, polymeric membranes cannot resist harsh chemical environments and cannot withstand high temperatures. Therefore, ceramic membranes can substitute polymeric membranes since these are chemically resistant and thermally stable. (Uhlhorn *et al.*, 1990; Uhlhorn, Keizer & Burggraaf, 1992) used gamma alumina ($\gamma\text{-Al}_2\text{O}_3$) membranes with a pore diameter of 2.5 nm and magnesium oxide (MgO) modified membranes with a lower pore size in order to separate propene from nitrogen ($\text{C}_3\text{H}_6/\text{N}_2$) mixtures. The membranes recorded both permeabilities and separation factors higher than those for Knudsen diffusion.

In this section, propylene and nitrogen permeation through silica membrane were carried out at various pressures as the driving force and ambient temperature.

4.8.2 Experimental Procedure

The alumina support employed consisted of internal and outer diameter of 7 and 10 mm respectively. The support has a permeable length of 348 mm and a porosity of 45%. Pressures of 0.05 to 0.45 barg and temperatures of 22 °C (295 K) were applied. Samples of the unmodified (alumina support) and modified (silica) membrane (Figure 4.40) were used for nitrogen adsorption and scanning electron microscopy respectively. Permeation behaviour of pure gases nitrogen (N_2) and propylene (C_3H_6) were measured at different feed pressures ranging from 0.05 to 0.45 bar. Permeate readings were recorded as l/min at ambient temperature.

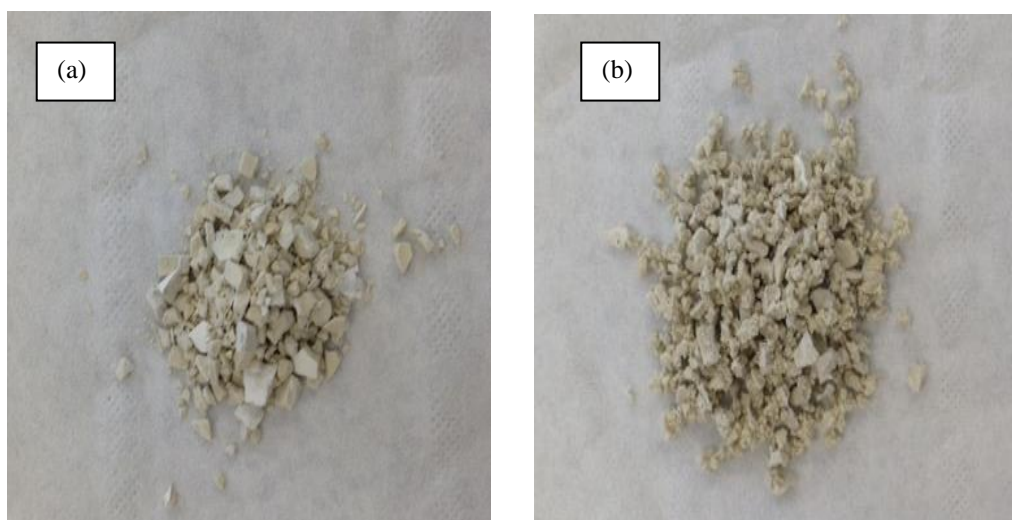


Figure 4.40 - (a): Crushed sample of the alumina support, (b): Crushed sample of silica membrane.

4.8.3 Results and Discussion

4.8.3.1 Propylene and nitrogen permeation and selectivity

Figure 4.41 depicts nitrogen and propylene gas flow rates against feed pressure across silica membrane at 298 K. Permeation rate increases with the feed pressure. It can be observed that propylene has a slightly higher flow rate compared to nitrogen despite its higher molecular weight ($N_2 = 28 \text{ g/mol}$; $C_3H_6 = 42 \text{ g/mol}$). This result is consistent with the contribution of surface flow mechanism. Figure 4.42 depicts the selectivity of C_3H_6 over N_2 . A highest selectivity of 1.79 at 0.05 barg was obtained. This selectivity increased by a factor of 2 compared to the ideal Knudsen selectivity (0.82). From the obtained gas permeation and selectivity, one can conclude that hydrocarbon could be separated from nitrogen.

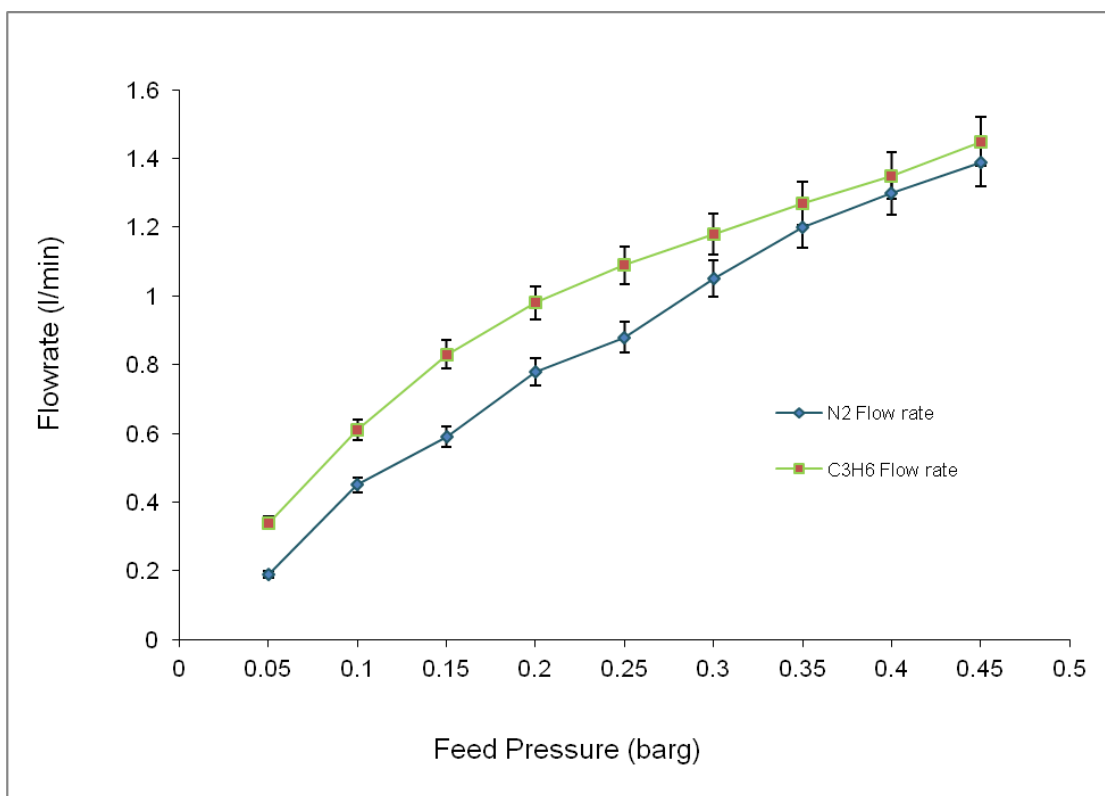


Figure 4.41 - Nitrogen and propylene gas flow rates against feed pressure across silica membrane at 298 K.

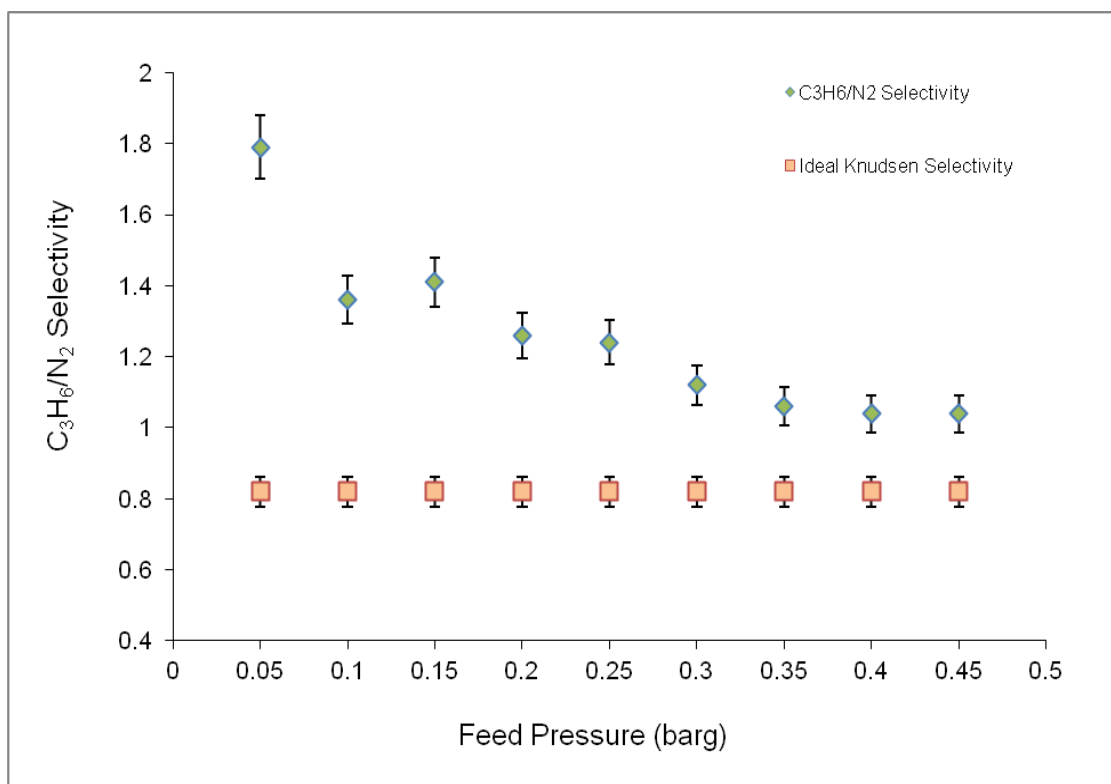


Figure 4.42 - C₃H₆/N₂ selectivity across silica membrane against feed pressure at 298 K.

Defect-free mesoporous silica membrane has been developed on the alumina substrate by the dip-coating technique. The prepared membrane was defect free as confirmed by the propylene and nitrogen permeation data. The high propylene selectivity obtained at low pressure drop is indicative of selective surface diffusion transport mechanism.

5 VOC Destruction in a Flow-Through Membrane Reactor

5.1 Introduction

VOC destruction to carbon dioxide and water using Pt/ γ -Al₂O₃ catalysts has been claimed by several authors (Tahir & Koh, 1999; Benard *et al.*, 2009; Radic, Grbic & Terlecki-Baricevic, 2004; Gluhoi, Bogdanchikova & Nieuwenhuys, 2006; Kim *et al.*, 2004). Additionally, Pt catalysts are superior in comparison to Au-containing systems and Co₃O₄-CeO₂ mixed oxides (Gluhoi, Bogdanchikova & Nieuwenhuys, 2006; Liotta *et al.*, 2009). Pina, Menéndez & Santamaria, (1996) have suggested the concept of employing the Knudsen-diffusion catalytic membrane reactor for the combustion of VOCs. They have highlighted that a flow-through configuration of a membrane reactor, operating in the Knudsen diffusion regime, will provide an intimate contact between VOC and O₂ molecules as well as the active sites. Saracco & Specchia, (2000) have succeeded in experimentally improving catalytic filters through tailored techniques. These catalytic filters were tested for their performance towards the catalytic combustion of selected VOC compounds. Their experimental data is in good agreement with those predicted by an isothermal model based on a pseudo-homogeneous approach and solved numerically by the finite-difference method. Benard *et al.*, (2010) studied the chemical reaction of the catalytic oxidation of VOCs in order to compare performances of a conventional reactor and a flow-through membrane reactor. Their findings exhibited that the catalytic membrane reactor performed better than the conventional reactor in terms of efficiency. They have suggested that the flow-through membrane reactor may lead to decreased light-off and total VOC combustion temperature in addition to a lower overall Pt loading.

In this section, the performance of the membrane reactor was studied. The main focus of this study is to investigate the possibility of improving VOC conversion with the use of a commercially available alumina support impregnated with a platinum (Pt) catalyst incorporated into a flow-through membrane shell tube. The effects of the main operating variables such as the feed molar flow rates, reaction temperatures, and partial pressures were examined. The performances of the membrane reactor under different selected VOCs were also studied. The permeability performance of the membrane reactor was also studied.

5.2 Experimental Procedure

VOC conversion in equation 2.1 (chapter two) was carried out in a tubular porous alumina membrane reactor. The membrane module employed was a flow-through membrane reactor.

Figure 5.1 depicts the schematic cross-section of the experimental flow-through membrane reactor. VOC destruction experiments were carried out under different reaction temperatures starting from 447 to 700 K. The feed pressures used were from 0.01 up to 6.56 bar. The flow rates were typically from 13 up to 452ml/min, and different VOC/O₂ feed gas composition were fed into the feed side of the membrane reactor. The products (permeate) were analyzed by a CO₂ analyzer (CT2100-Emissions Laser Sensor).

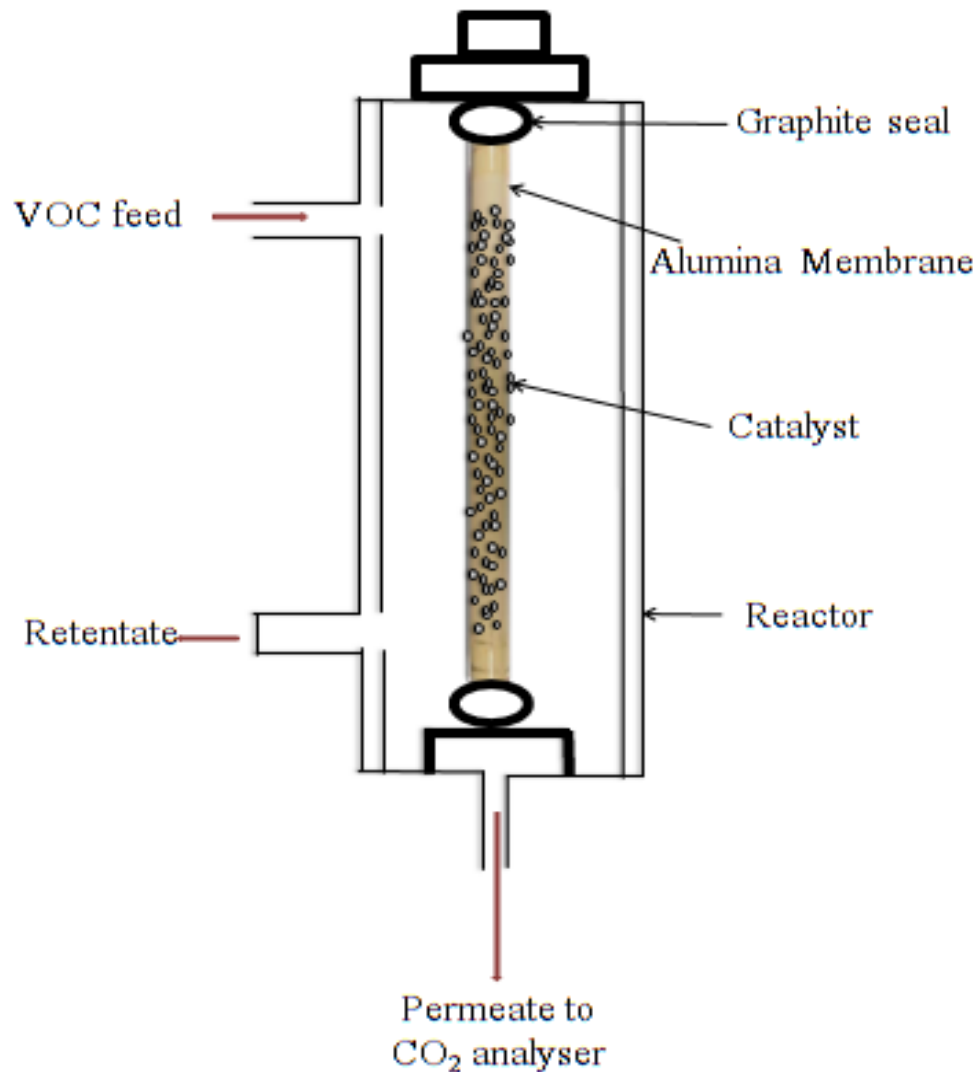


Figure 5.1 - Schematic cross-section of flow-through tubular membrane reactor.

5.2.1 Performance/Characteristics of the Membrane Reactor

The conversion of VOC obtained using the membrane reactor quantifies its performance. This was defined in terms of the molar flow rate of the VOC that occurred in the reaction as well as the molar flow rate (products) of CO₂ leaving the membrane reactor in the permeate stream.

The advantage of the membrane reactor for VOC destruction was based on the catalytic reaction. The influence of the product on conversion enhancement has been acknowledged throughout the literature (Gluhoi, Bogdanchikova & Nieuwenhuys, 2006; Julbe, Farrusseng & Guizard, 2001; Benard *et al.*, 2009; Rusu & Dumitriu, 2003; Saracco & Specchia, 2000). As the VOC conversion enhances, the CO₂ yield approaches close to one hundred percent. The experimental measurements were straightforward. The contributions of the reactant flow rates, transmembrane pressure, reaction temperature and membrane permeability among others influences the extent of conversion enhancement. The relationships between different parameters such as reaction temperature were quantified. These will help in selecting the methods in order to improve the process in future.

5.3 Results and Discussion

The experimental results of the selected VOCs (propane, propylene and n-butane) destruction and gas permeation in the Pt/Al₂O₃ membrane reactor are discussed below.

5.3.1 Gas Permeation

Permeation experiments were carried out at 25 °C using propylene as the permeating gas in order to quantify the viscous and Knudsen flow contributions. Figure 5.2 depicts the permeate flux of the untreated and Pt/Al₂O₃ membranes. Eqn. (5.1) was used to relate the permeation flux and average pressure (Pina, Menéndez & Santamaria 1996).

$$F = \beta P_{av} + K \quad (5.1)$$

where β and K equals;

$$\beta = 0.125 \frac{\varepsilon r^2}{L \tau \mu RT}, K = 1.06 \frac{\varepsilon r}{L \tau \sqrt{MRT}} \quad (5.2)$$

where, F is the permeation flux per unit of time and area, ε is the porosity of the membrane, r is the mean pore radius (m), $P_{av} = (P_1+P_2)/2$ is the average pressure (Pa), μ is the viscosity (Pa-s) and L is the thickness of the membrane (m), τ is the tortuosity, M is the molecular weight of the diffusing gas (g/mol), R gas constant (8.314 J.K⁻¹.mol⁻¹) and T the permeation temperature (K). β and K can be regarded as viscous and Knudsen contributions to the permeation flux.

From Figure 5.2, it can be seen that the slope of the line corresponding to the untreated (virgin) membrane is high indicating a large viscous flow contribution. On the other hand, after 3.52 wt% Pt impregnation, a lower slope is obtained which indicates a reduction in the viscous flow

contribution. The obtained results almost corroborate the literature (Pina, Menéndez & Santamaria, 1996). Pina, Menéndez & Santamaria, (1996) claimed the same using untreated membrane (α -Al₂O₃). After depositing 4.9 wt.% of γ -Al₂O₃ at 1 bar, they have achieved almost a horizontal line indicating predominantly Knudsen diffusion contribution.

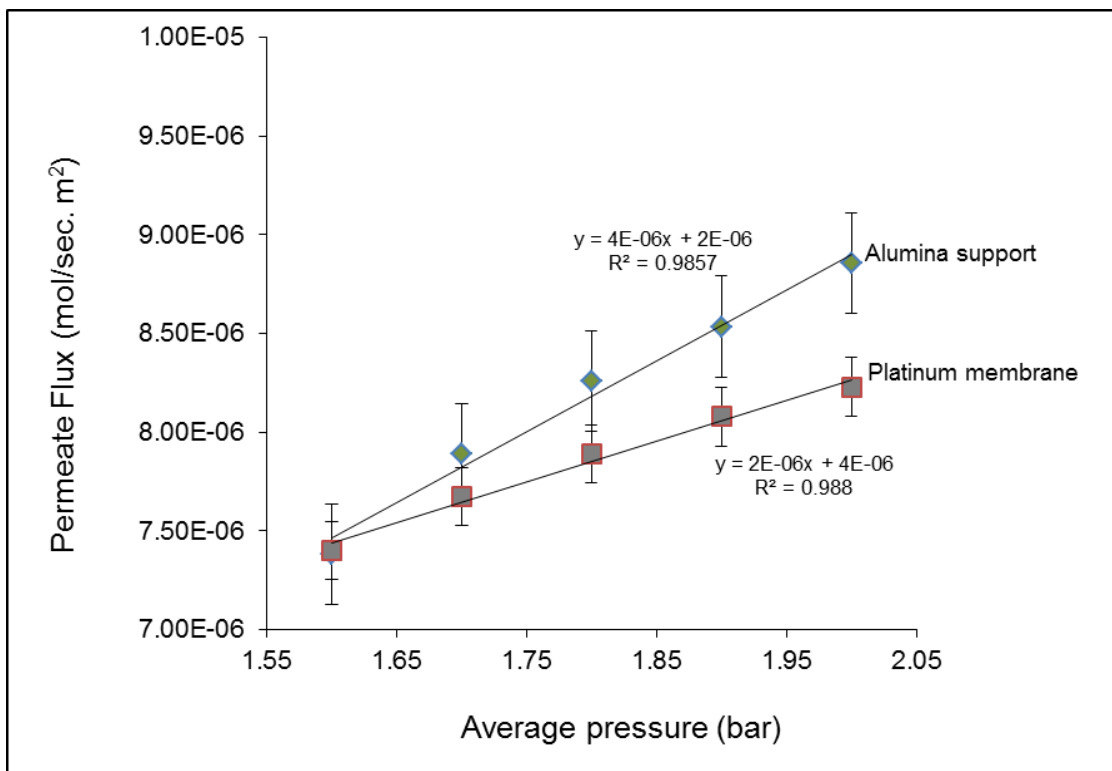


Figure 5.2 - Permeation flux across alumina support and platinum membrane against average pressure at 298 K.

5.3.2 Propane Conversion

Pt catalyst to be deposited on the alumina membrane is the key subject to be addressed in order to achieve a higher conversion of VOC (at minimum precious metal content) to less harmful products inside the catalytic membrane. The application of higher Pt contents would possibly result in a further activity increase (Saracco & Specchia, 2000). In addition, Pt concentrations higher than 5 wt% are only employed in industrial practice (Jackson *et al.*, 1993; Saracco & Specchia, 2000).

Figure 5.3 depicts propane conversion curve in the tubular membrane reactor against reaction temperature (194 to 232 °C) on 3.52 wt% Pt catalyst at different total flow rates ranging from 180 to 286ml/min. It can be seen that 72% propane conversion is achieved at a temperature of 232 °C. Gluhoi, Bogdanchikova & Nieuwenhuys, (2006) obtained 72% propane conversion at nearly 275 °C on 1-wt% Pt/Al₂O₃. Saracco & Specchia, (2000) also obtained 72% propane

conversion at nearly 365 °C on 5-wt% Pt/ γ -Al₂O₃. Therefore, the temperature at which the catalytic combustion takes place for this VOC in this study is lower than those obtained in the literature (Saracco & Specchia, 2000; Gluhoi, Bogdanchikova & Nieuwenhuys, 2006) for the same organic compounds on Pt/ γ -Al₂O₃ catalysts. The low conversion temperature (232°C) obtained in this experiment could be as a result of Pt dispersion on the alumina which enhances the conversion at lower temperature compared to the literature.

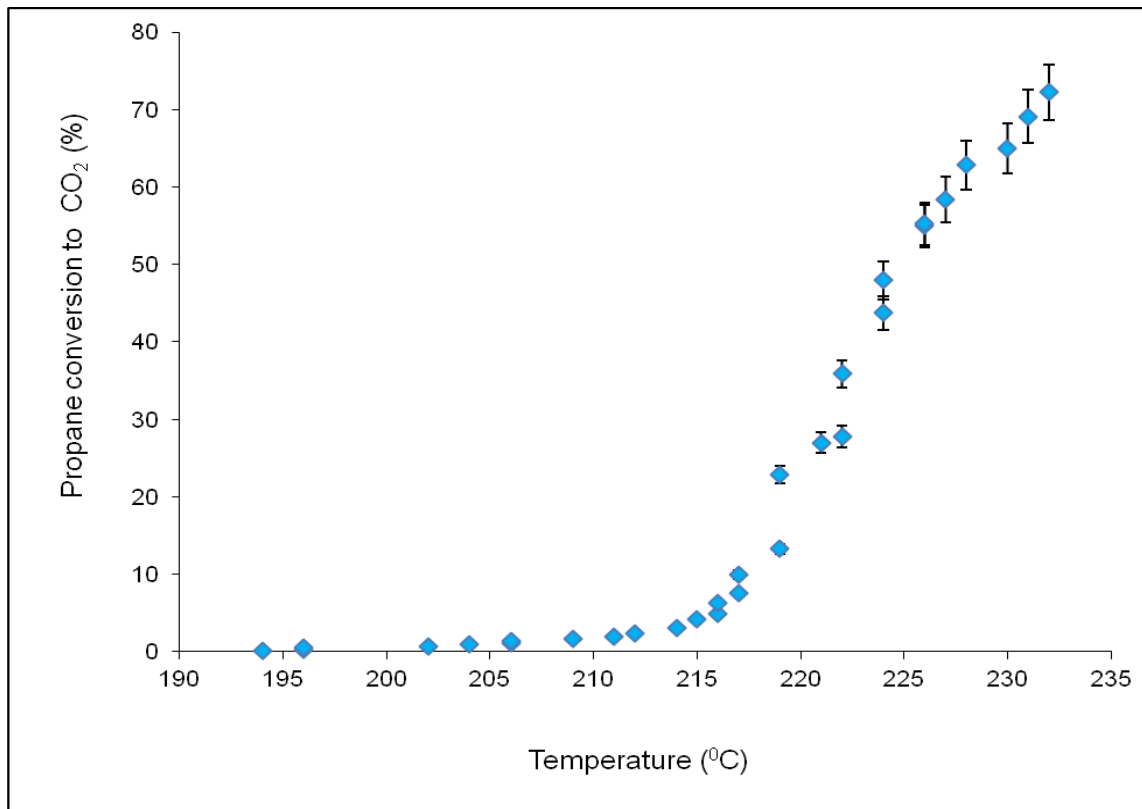


Figure 5.3 - Propane conversion against reaction temperature (194 to 232 °C).

Figure 5.4 depicts propane conversion curve in the tubular membrane reactor against reaction temperature (235 to 427 °C) on 3.52 wt% Pt catalyst at different total flow rates ranging from 185 to 222ml/min. The general behaviour of the Pt/Al₂O₃ based catalysts is in good agreement with that reported in the literature (chapter 2). Propane conversion of 93% is achieved at a reaction temperature of 427 °C, this result corroborates the literature (Saracco & Specchia, 2000) on 5-wt% Pt/ γ -Al₂O₃. It should be noted that our conversion was attained at only a fraction of the catalyst loading compared to the literature (Saracco & Specchia, 2000).

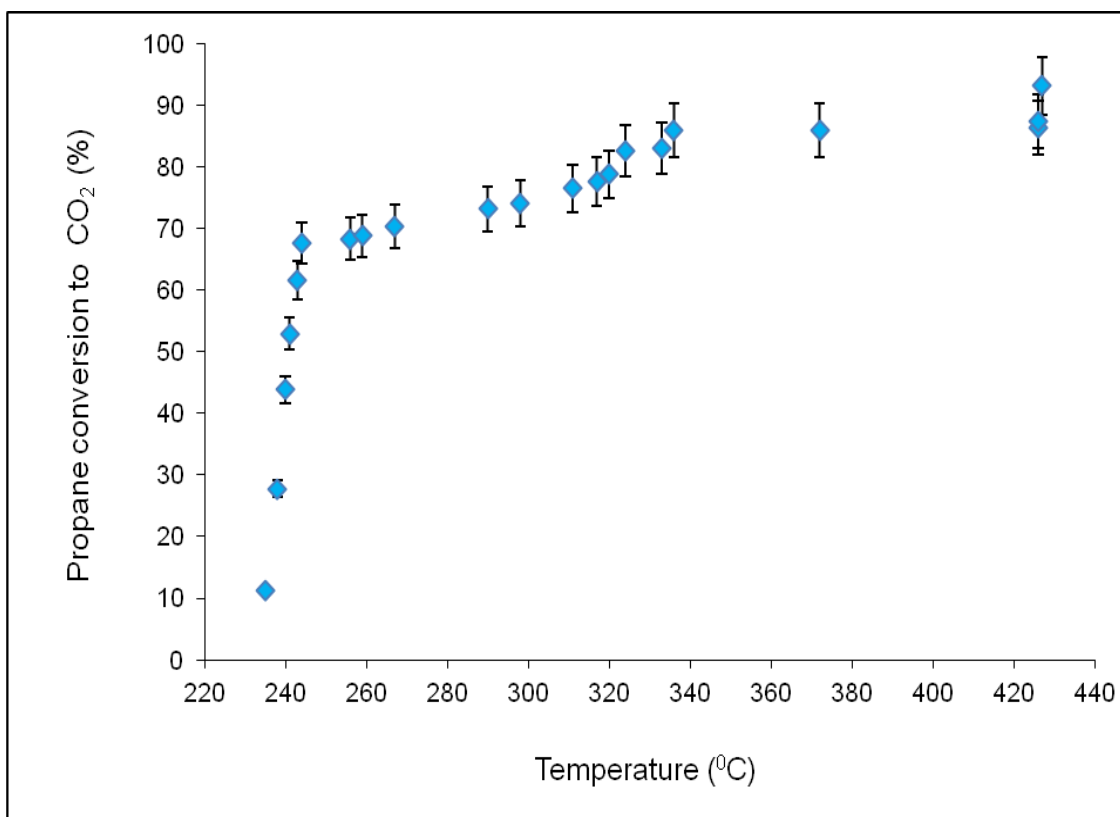


Figure 5.4 - Propane conversion against reaction temperature (235 to 427 °C).

Figure 5.5 depicts the relationship between propane conversion curve in the tubular membrane reactor against reaction temperature (225 to 333 °C) on 3.52 wt% Pt catalyst at different total flow rates ranging from 219 to 358ml/min. It can be seen that 86% propane conversion is achieved at a reaction temperature of 333 °C. Saracco & Specchia, (2000) claimed 86% propane conversion at a reaction temperature of over 350 °C. Therefore, the temperature at which the catalytic combustion takes place corroborates the literature (Saracco & Specchia, 2000) for the same VOC on 5-wt.% Pt/ γ -Al₂O₃ catalysts.

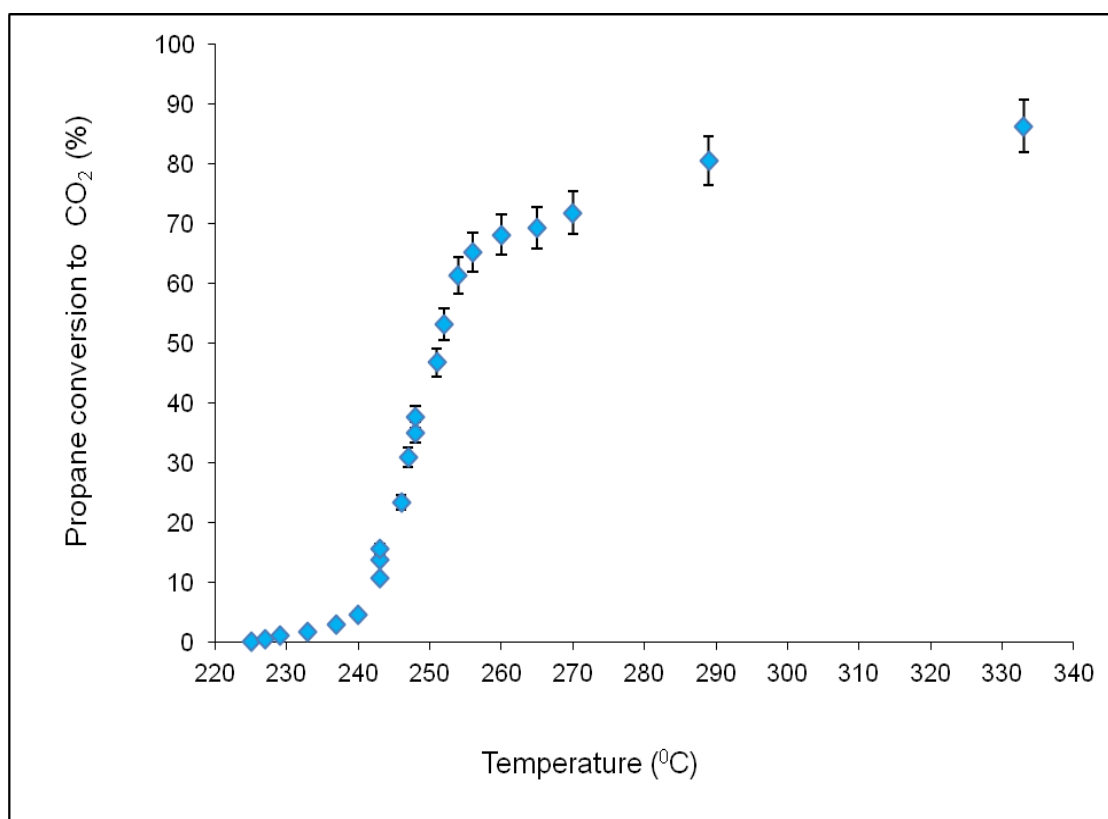


Figure 5.5 - Propane conversion against reaction temperature (225 to 333 °C).

Figure 5.6 depicts propane conversion curve in the tubular membrane reactor against reaction temperature (226 to 378 °C) on 3.52 wt% Pt catalyst at different total flow rates ranging from 166 to 270ml/min. It can be seen that a 95.47% propane conversion is achieved at a reaction temperature of 378 °C. Saracco & Specchia, (2000); Gluhoi, Bogdanchikova & Nieuwenhuys, (2006) also obtained complete oxidation (100%) of propane at almost 450 °C with 5-wt% Pt content. In their work, they have achieved 95% propane conversion at a reaction temperature of almost 430 °C. Therefore, in this study, the temperature at which the catalytic combustion takes place for propane is lower than the one obtained from the literature (Saracco & Specchia, 2000) for the same VOC on 5-wt% Pt/ γ -Al₂O₃ catalysts.

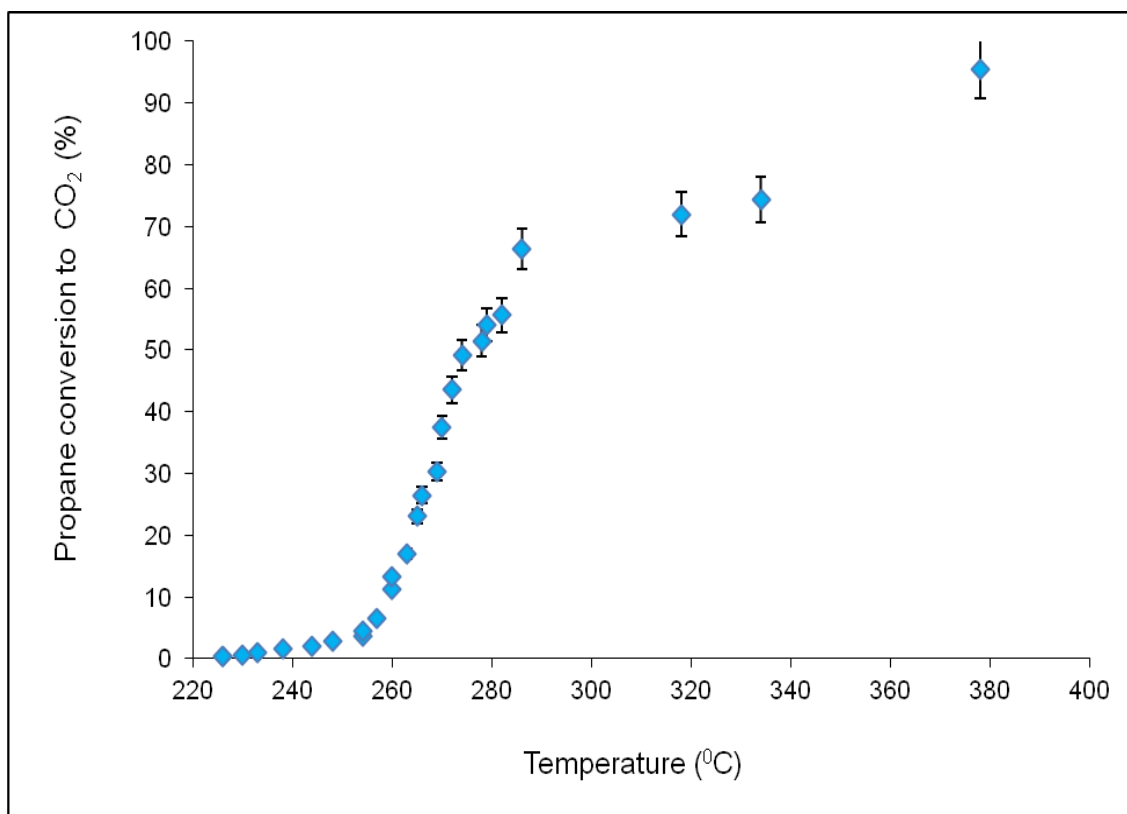


Figure 5.6 - Propane conversion against reaction temperature (226 to 378 °C).

5.3.3 N-butane Conversion

Figure 5.7 depicts the relationship between (20% n-butane and 80% nitrogen) conversion curve in the tubular membrane reactor against reaction temperature (242 to 273 °C) on the 3.52 wt% Pt catalyst at different total flow rates ranging from 271 to 319ml/min. It can be observed that a 46% n-butane conversion is achieved at a reaction temperature of 273 °C on 3.52 wt.% Pt/ γ -Al₂O₃ catalysts. Okal & Zawadzki, (2009) obtained 46% n-butane conversion at 295 °C using 4.6% Ru/ γ -Al₂O₃ catalyst. From their findings, it can be translated that Pt catalyst is superior to other noble metals for VOC abatement.

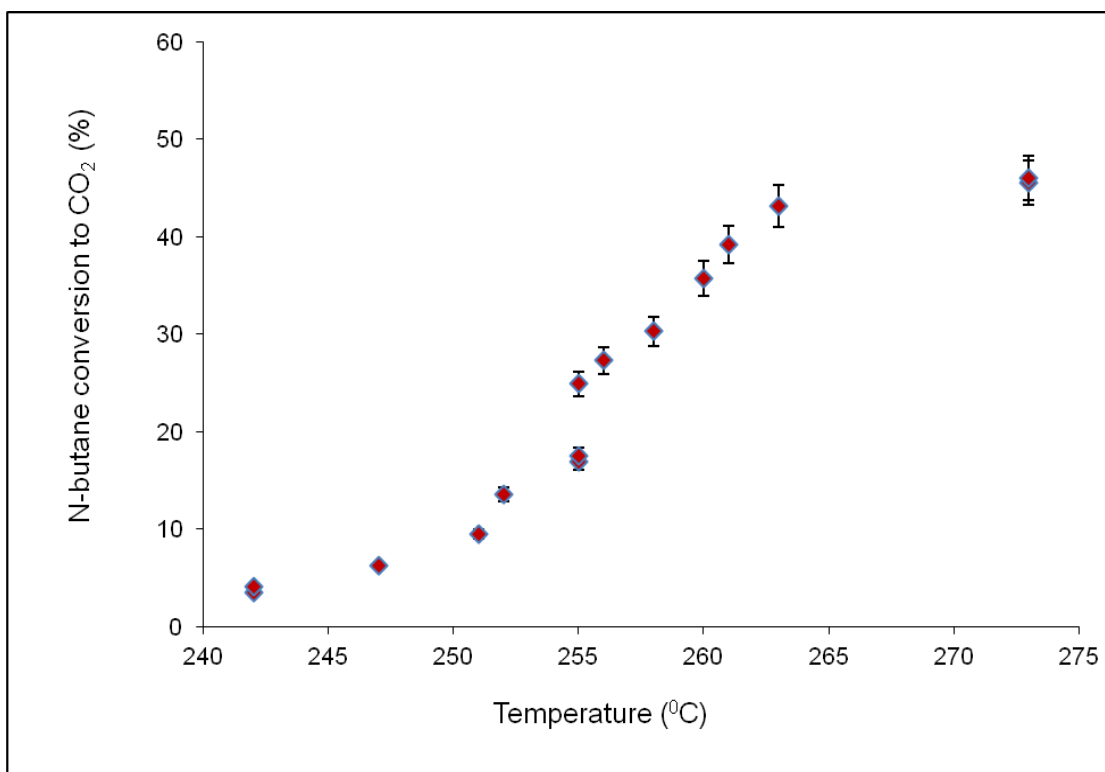


Figure 5.7 - N-butane conversion against reaction temperature (242 to 273 °C).

Figure 5.8 depicts the relationship between (20% n-butane and 80% nitrogen) conversion curve in the tubular membrane reactor against reaction temperature (195 to 259 °C) on 3.52 wt% Pt catalyst at different total flow rates ranging from 295 to 379ml/min. It can be seen that a 48% n-butane conversion is achieved at a reaction temperature of 259 °C on 3.52 wt.% Pt/ γ -Al₂O₃ catalysts. A slight conversion increment is obtained compared to run 1 as well as a reduction in the reaction temperature.

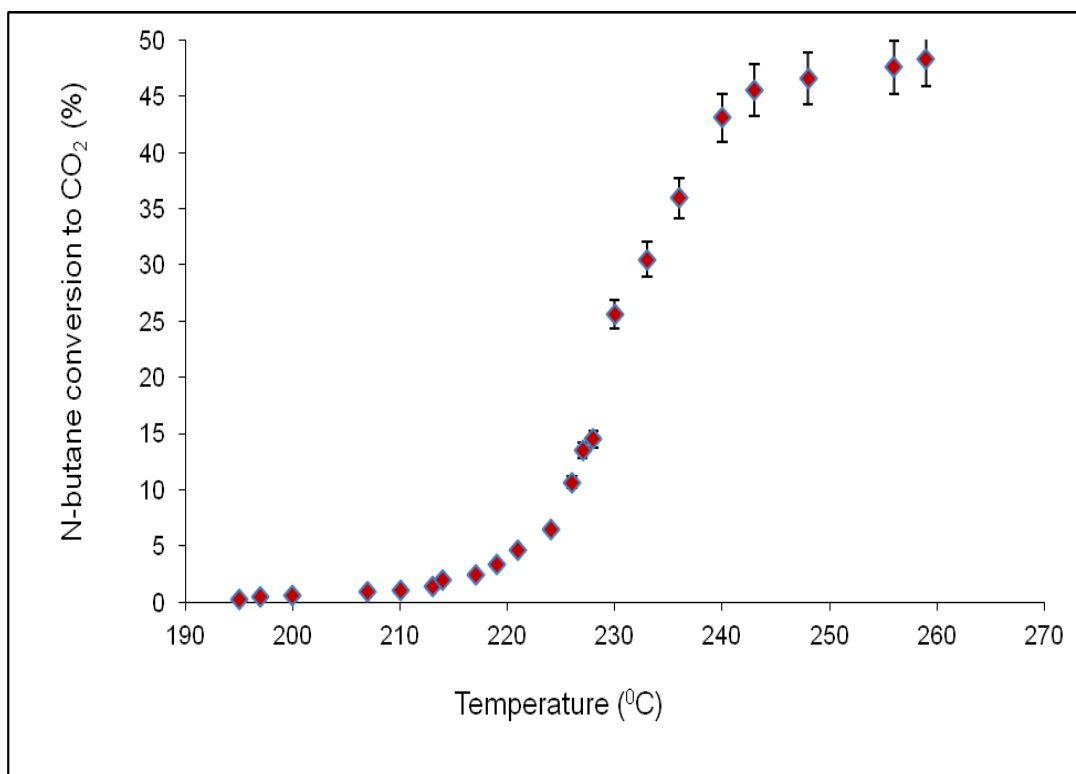


Figure 5.8 - N-butane conversion against reaction temperature (195 to 259 °C).

Figure 5.9 depicts the relationship between (20% n-butane and 80% nitrogen) conversion curve in the tubular membrane reactor against reaction temperature (200 to 244 °C) on 3.52 wt% Pt catalyst at different total flow rates ranging from 329 to 424ml/min. It can be seen that, a 51% n-butane conversion is achieved at a reaction temperature of 244 °C on 3.52 wt.% Pt/ γ -Al₂O₃ catalysts. From this result, it can be observed that an increment of 5% conversion is obtained compared to run 1 (Fig. 5.7) and a reduction of 30 °C in the reaction temperature.

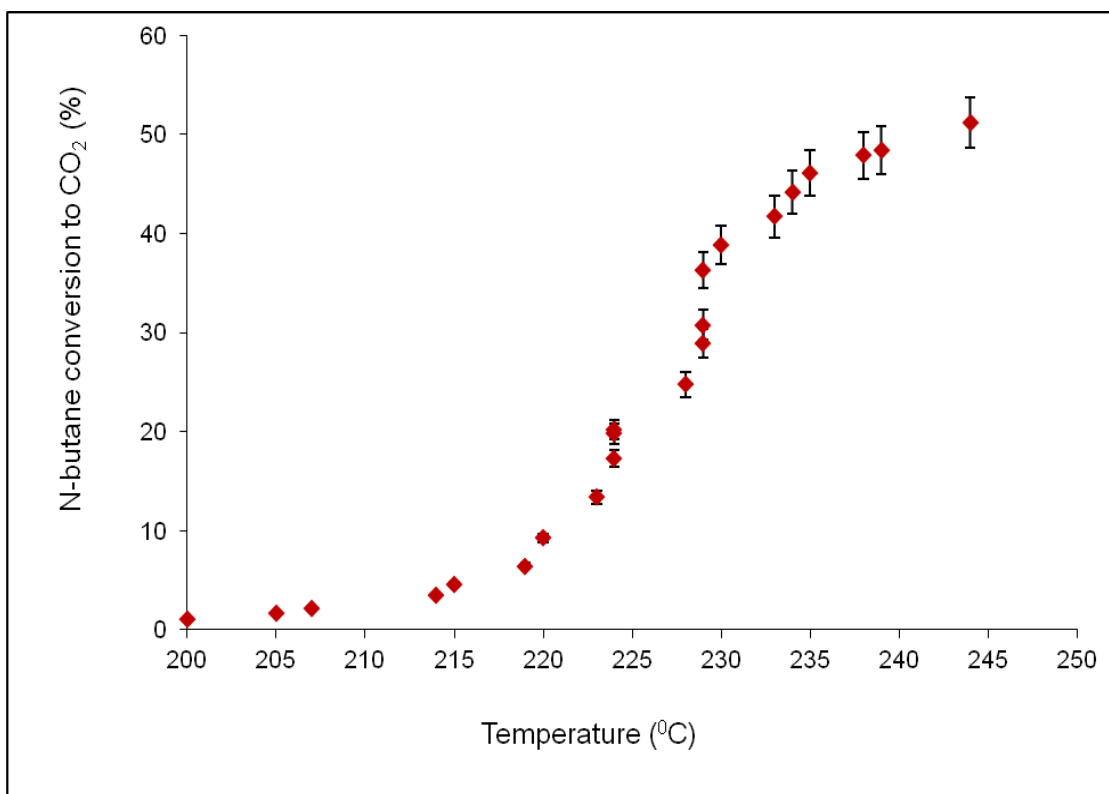


Figure 5.9 - N-butane conversion against reaction temperature (200 to 244 °C).

Figure 5.10 depicts the relationship between (20% n-butane and 80% nitrogen) conversion curve in the tubular membrane reactor against reaction temperature (183 to 245 °C) on 3.52 wt% Pt catalyst at different total flow rates ranging from 310 to 445ml/min. As can be seen from Fig. 5.10, a 52% n-butane conversion is achieved at a reaction temperature of 245 °C on Pt/ γ -Al₂O₃ catalyst. This result corroborates the literature (Okal & Zawadzki, (2009) using 4.6% Ru/ γ -Al₂O₃ catalyst where they achieved a 52% n-butane conversion at almost 320 °C where a 75 °C temperature difference was observed between Pt and Ru catalysts.

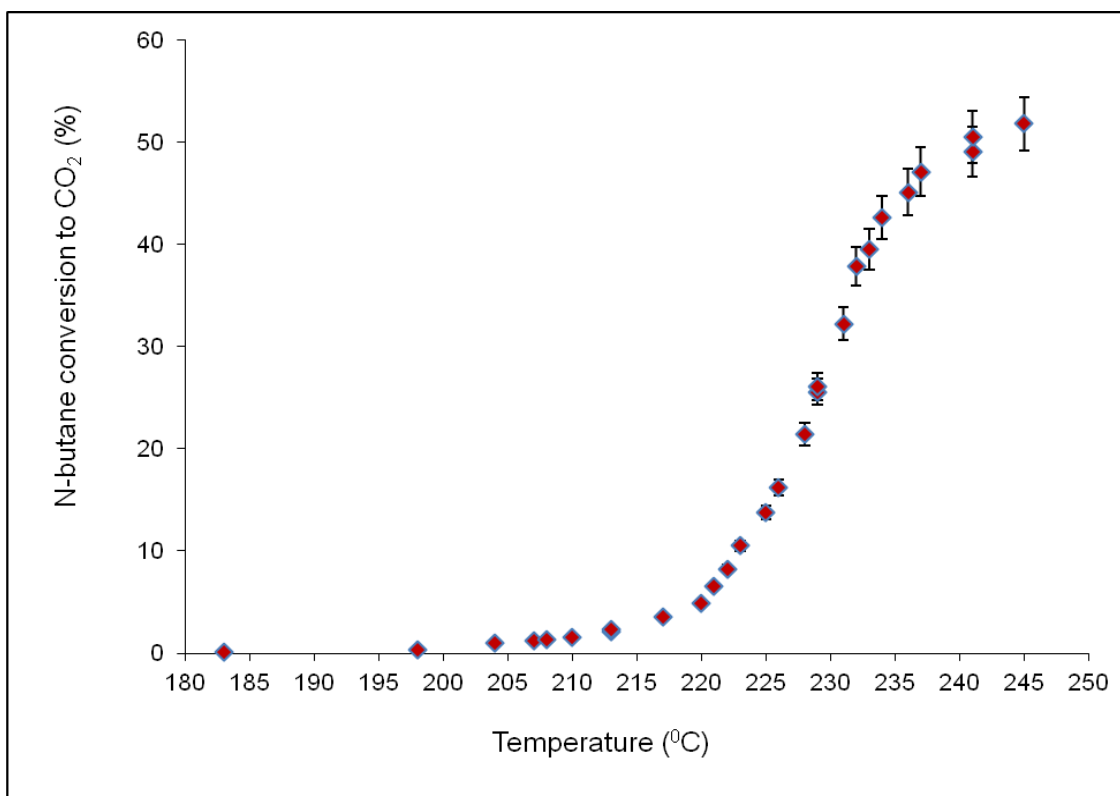


Figure 5.10 - N-butane conversion against reaction temperature (183 to 245 °C).

5.3.4 Propylene Conversion

Figure 5.11 depicts the relationship between propylene conversion curve in the tubular membrane reactor against reaction temperature (174 to 220 °C) on 3.52 wt% Pt catalyst at different total flow rates ranging from 148 to 452ml/min. From Fig. 5.11, a 68% propylene conversion is achieved at a reaction temperature of 220 °C on Pt/ γ -Al₂O₃ catalyst. Saracco & Specchia, (2000) obtained a similar conversion at almost 260 °C with 5-wt% Pt content. It can be seen that, in this study, the temperature at which the catalytic combustion takes place for propylene is lower than the one obtained from the literature (Saracco & Specchia, 2000) on 5-wt% Pt/ γ -Al₂O₃ catalysts.

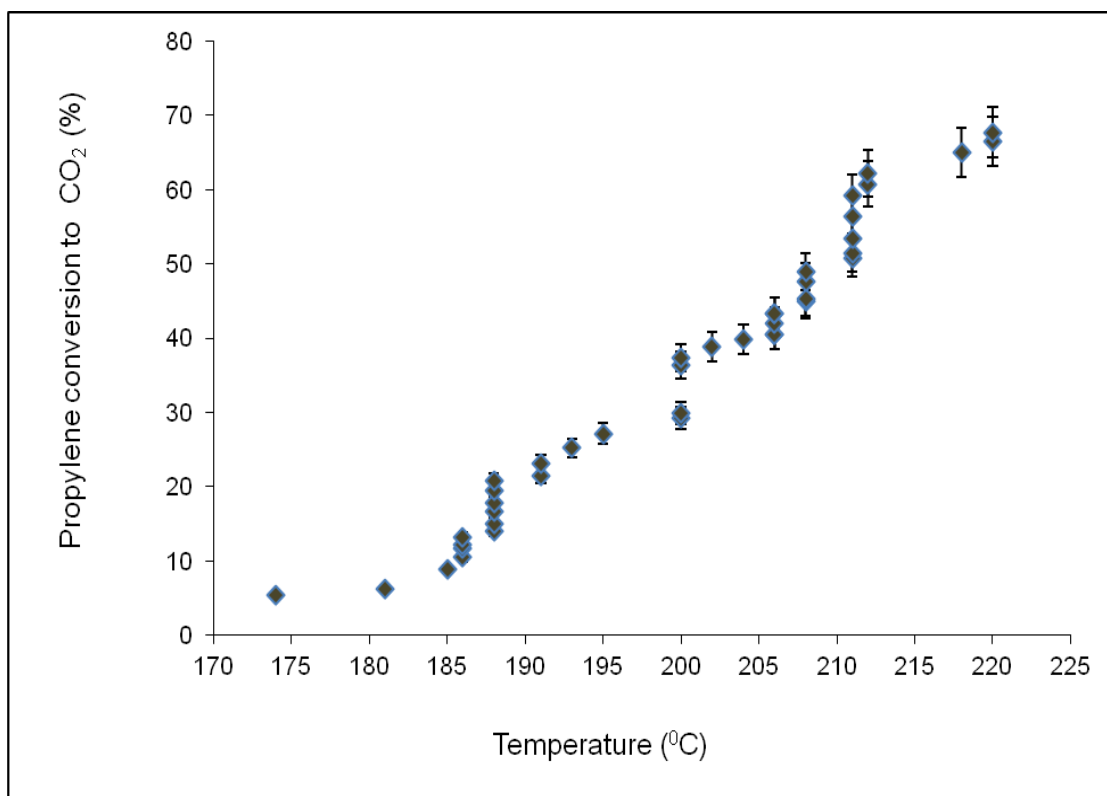


Figure 5.11 - Propylene conversion against reaction temperature (174 to 220 °C).

Figure 5.12 depicts the relationship between propylene conversion curve in the tubular membrane reactor against reaction temperature (187 to 331 °C) on 3.52 wt% Pt catalyst at different total flow rates ranging from 175 to 312ml/min. From Figure 5.12, an 80% propylene conversion is achieved at a reaction temperature of 331 °C on Pt/ γ -Al₂O₃ catalyst. This result corroborates the work of (Saracco & Specchia, 2000) where they achieved 80% propylene conversion at nearly 300 °C with 5-wt% Pt content.

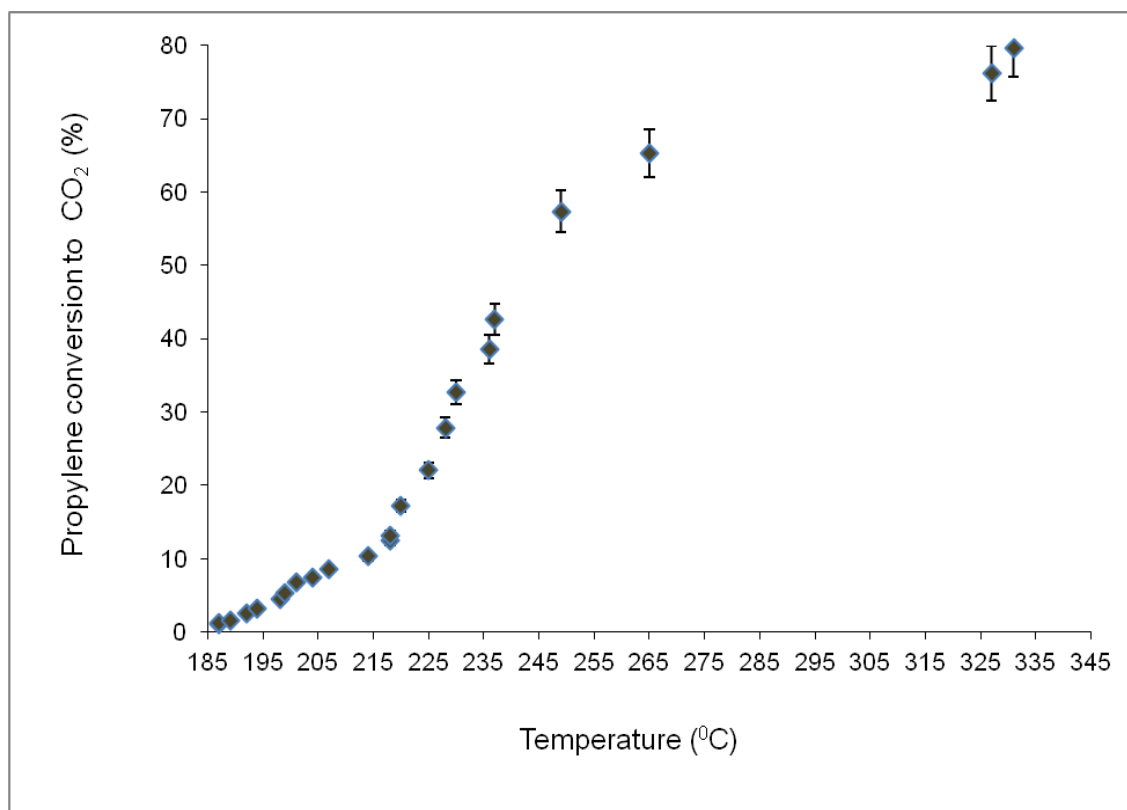


Figure 5.12 - Propylene conversion against reaction temperature (187 to 331 °C).

Figure 5.13 depicts the relationship between propylene conversion curve in the tubular membrane reactor against reaction temperature (190 to 420 °C) for the 3.52 wt% Pt catalyst at different total flow rates ranging from 187 to 297ml/min. From Fig. 5.13, 82% propylene conversion is achieved at a reaction temperature of 420 °C on Pt/ γ -Al₂O₃ catalyst. Saracco & Specchia, (2000) obtained a similar conversion at nearly 300 °C with 5-wt% Pt content. From Fig. 5.13, it can be seen that 75% conversion is obtained at 262 °C were it takes up to 372 °C before the next conversion occurred. Therefore, the residence time before the next conversion occurred was longer. This could be as a result of exothermic reaction which takes longer to release energy for the next conversion to occur.

The above results indicates that the temperature at which the oxidation was performed depend on the nature of the organic compounds present in the waste gas stream. The catalyst was exposed to several activity runs. The same catalyst was then cooled down and the temperature was lowered to ambient temperature before starting each experiment.

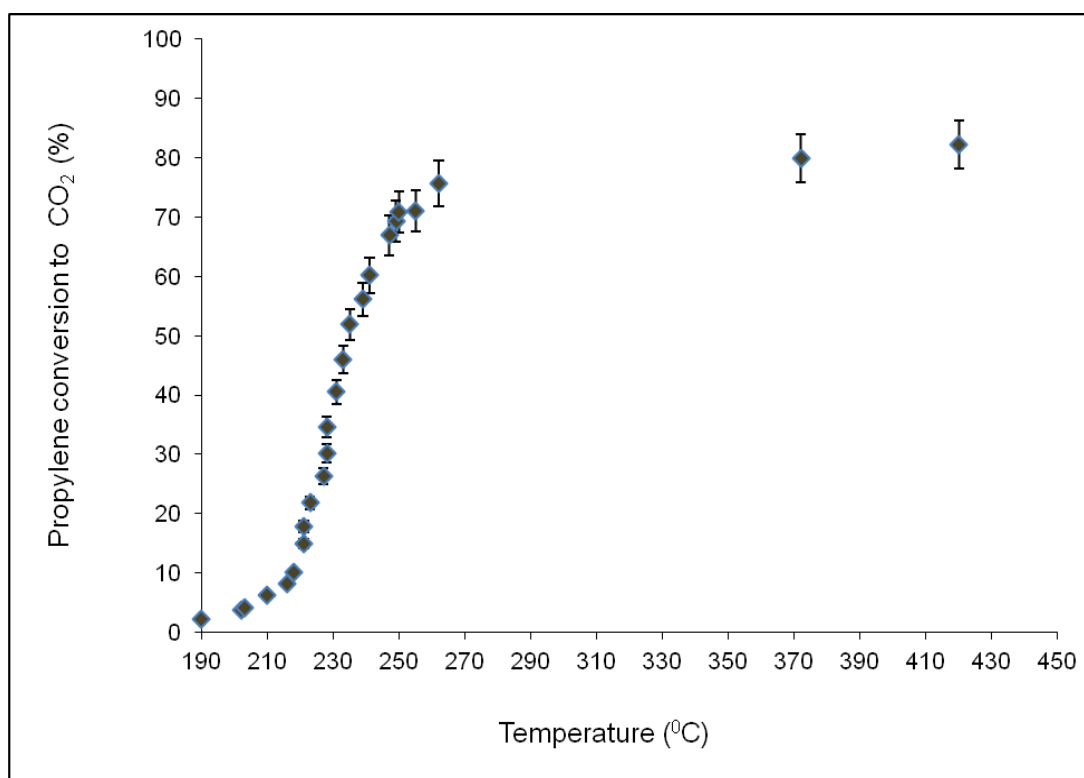


Figure 5.13 - Propylene conversion against reaction temperature (190 to 420 °C).

In general, the experimental VOCs conversion occurred because in the Knudsen diffusion regime, the probability of collisions between the molecules and the membranes pore wall is maximised which renders the optimum use of the catalyst deposited on the pores of the membrane (Pina, Menéndez & Santamaria, 1996). The fact that a high conversion is achieved at moderate temperature is also an indication that the impregnation of the catalyst is uniformly distributed and well dispersed over the surface of the membrane. Otherwise, if there was any crack on the membrane, the preferential permeation through the region would probably give rise to decreased conversion. In addition, the membrane used was able to maintain prolonged experiments over 100 hours under reaction at approximately 400 °C without any loss of mechanical integrity or catalytic activity.

Finally, the result of the selected VOC conversion confirms that the flow-through membrane reactor operation is a promising alternative using this simple but effective “reservoir technique”. The reservoir method combined with proper selection of the support resulted in high conversion and reduced precious metal content. This will reduce cost and enhance commercialization.

6 Conclusions and Recommendation for Future Work

The contributions of this study are drawn and recommendations for future study in this area are also made based on the results obtained from the experimental data.

6.1 Conclusions

- ❖ This study had demonstrated the attractiveness of tubular membrane reactor for separation and reaction. The membrane reactor designed was operational for high temperature as well as corrosion resistant.
- ❖ A defect on alumina support was successfully repaired after exposing the alumina support to boehmite solution, it was observed that a significant increase of CO₂/H₂ selectivity (1.3) was obtained at room temperature for the first dip crack repair was achieved. Subsequent dips however reduced the CO₂ selectivity over H₂. This behaviour is related to the transport regime in the membrane. It is demonstrated experimentally that during the 1st dip repair, surface diffusion of CO₂ in an alumina support with γ -Al₂O₃, can contribute substantially to the transport rate.
- ❖ An alumina support modified with silica exhibits higher CO₂ selectivity at pressures of up to 3.0 barg from other gas components. The higher CO₂ permeance rate was attributed to the adhesion of the silica on the alumina support which resulted with surface diffusion mechanism. A CO₂/CH₄ selectivity of 24.07 was also obtained at room temperature and 0.7 barg. Such a selectivity value could be useful in a small-scale carbon dioxide removal unit for natural gas treatment processes.
- ❖ It has been demonstrated that, H₂ gas permeation increased from 4.6 to 6.0 l/min at temperature range between 25 up to 300 °C. Also, H₂/He and H₂/N₂ selectivities attained values of 1.96 and 2.72 at 300 °C respectively. High temperature also favoured H₂ diffusion as the H₂ selectivity over He on the mesoporous membrane increased with almost 2 fold compared to the ideal Knudsen selectivity (1.4).
- ❖ Defect-free mesoporous silica membrane has also been developed on the alumina substrate by the dip-coating technique. The prepared membrane was defect free as confirmed by the propylene and nitrogen permeation data. The high propylene selectivity obtained from nitrogen at low pressure drop.
- ❖ Experimental procedure to implement VOCs destruction was developed. Experiments on the catalytic combustion of VOCs were conducted with alumina membrane reactor. VOC conversion was significantly achieved and the product yield CO₂ was successfully permeated through the Pt alumina membrane which is monitored using CO₂ analyser.

- ❖ The conversion enhancements over Pt catalyst were obtained at lowest reactant flow rates and moderate temperatures. Also, the maximum conversion obtained by the membrane reactor was comparable with some literature.
- ❖ The experimental study was to develop an understanding of some important factors that contribute to the influence of alumina membrane reactor for catalytic membrane reactor/seperator. This demonstrates that the use of a membrane reactor enhanced reactant conversion as well as higher product yield.

6.2 Recommendations for Future Work

The objective of this study have been met, although, there are always unforeseen aspects and outcomes which need to be looked at for future work in this area of research. For these reasons, the following recommendations are made;

- ❖ Further study on VOC abatement using hybrid systems is needed in order to reduce the operating costs as well as bringing profit from the emissions by altering the wastes to a valuable product which will actually bring new alternative to researchers.
- ❖ The use of simulation study is recommended for future study in order to accurately assess and validate the performance of this experimental design.

7 References

- Adewole, J. K., Ahmad, A. L., Ismail, S. & Leo, C. P. (2013). Current challenges in membrane separation of CO₂ from natural gas: a review. *International Journal of Greenhouse Gas Control*, 17, pp. 46-65.
- Adhikari, S. & Fernando, S. (2006). Hydrogen membrane separation techniques. *Industrial & Engineering Chemistry Research*, 45(3), pp. 875-881.
- Adom, P.K., Bekoe, W., Amuakwa-Mensah, F., Mensah, J. T., & Botchway, E. (2012). Carbon dioxide emissions, economic growth, industrial structure, and technical efficiency: Empirical evidence from Ghana, Senegal, and Morocco on the causal dynamics. *Energy*, 47(1), pp. 314-325.
- Aguado, S., Coronas, J. & Santamaría, J. (2005). Use of zeolite membrane reactors for the combustion of VOCs present in air at low concentrations. *Chemical Engineering Research and Design*, 83(3), pp. 295-301.
- Ahmad, A. L. & Mustafa, N. N. N. (2007). Sol–gel synthesized of nanocomposite palladium–alumina ceramic membrane for H₂ permeability: Preparation and characterization. *International Journal of Hydrogen Energy*, 32(12), pp. 2010-2021.
- Ahmad, A. L., Othman, M. R. & Mukhtar, H. (2004). H₂ separation from binary gas mixture using coated alumina-titania membrane by sol-gel technique at high-temperature region. *International Journal of Hydrogen Energy*, 29(8), pp. 817-828.
- Ahmadian, N. P., Babaluo, A. A., Jannatdoust, E., Peyravi, M. & Akhfash, A. M. (2011). An optimum routine for surface modification of ceramic supports to facilitate deposition of defect-free overlaying micro and meso (nano) porous membrane. *Iran. J. Chem. Eng. Vol.* 30(3), pp. 63-73.
- Asaeda, M. & S. Yamasaki. (2001). Separation of Inorganic/Organic Gas Mixtures by Porous Silica Membranes. *Sep. Purif. Tech.*, 25, pp. 151-159.
- Baker, R. (2001). Future directions of membrane gas-separation technology. *Membrane Technology*, 2001(138), pp. 5-10.
- Baker, R. W. (2001). Membranes for vapor/gas separation. *Membrane Technology and Research, Inc.*, pp. 1-25.

- Baker, R.W. (2004). Overview of membrane science and technology. *Membrane Technology and Applications, Second Edition*, pp. 1-14.
- Benard, S., Giroir-Fendler, A., Vernoux, P., Guilhaume, N. & Fiaty, K. (2010). Comparing monolithic and membrane reactors in catalytic oxidation of propene and toluene in excess of oxygen. *Catalysis Today*, 156(3), pp. 301-305.
- Benard, S., Ousmane, M., Retailleau, L., Boreave, A., Vernoux, P. & Giroir-Fendler, A. (2009). Catalytic removal of propene and toluene in air over noble metal catalyst¹. *Canadian Journal of Civil Engineering*, 36(12), pp. 1935-1945.
- Benito, J. M., Conesa, A., Rubio, F. & Rodr'iguez, M. A. (2005). Preparation and characterization of tubular ceramic membranes for treatment of oil emulsions. *Journal of the European Ceramic Society*, 25(11), pp. 1895-1903.
- Bessarabov, D. (1999). Membrane gas-separation technology in the petrochemical industry. *Membrane Technology*, 1999(107), pp. 9-13.
- Bose, A. C. (2009). *Inorganic membranes for energy and environmental applications*. Springer.
- Brunetti, A., Scura, F., Barbieri G. & Drioli E. (2010). Membrane technologies for CO₂ separation. *Journal of Membrane Science*, 359(1), pp. 115-125.
- Buzcu-Guven, B. & Harriss, R. (2012). Extent, impacts and remedies of global gas flaring and venting. *Carbon Management*, 3(1), pp. 95-108.
- Capannelli, G., Carosini, E., Cavani, F., Monticelli, O. & Trifiro, F. (1996). Comparison of the catalytic performance of V₂O₅/γ-Al₂O₃ in the oxidehydrogenation of propane to propylene in different reactor configurations: i) packed-bed reactor, ii) monolith-like reactor and iii) Catalytic Membrane Reactor. *Chemical engineering science*, 51(10), pp. 1817-1826.
- Carlos, F. & Joaquin, C. (1999). Permeation of gases in asymmetric ceramic membranes. *Chemical Engineering Education*. Available from: <http://ufdcimages. uflib.ufl.edu/AA/00/00/03/83/00141/AA000003830014100062.pdf> [Accessed October 20, 2014].
- Chadha, N. & Parmele, C. S. (1993). Minimize emissions of air toxics via process change. *Chemical Engineering Progress; (United States)*, 89(1), pp. 37-42.

- Chai, M., Machida, M., Eguchi, K. & Arai, H. (1994). Promotion of hydrogen permeation on metal-dispersed alumina membranes and its application to a membrane reactor for methane steam reforming. *Applied Catalysis A: General*, 110(2), pp. 239-250.
- Choma, J., Kloske, M. & Jaroniec, M. (2003). An improved methodology for adsorption characterization of unmodified and modified silica gels. *Journal of Colloid and Interface Science*, 266(1), pp. 168-174.
- Christopher M. C. (2003). *Engineering development of ceramic membrane reactor systems for converting natural gas to hydrogen and synthesis gas for liquid transportation fuels*. U.S. Dept. of Energy Hydrogen Program Annual Review: Air Products and Chemicals, Inc. Available from: http://www1.eere.energy.gov/hydrogenandfuelcells/pdfs/merit03/8_acpi_chris_chen.pdf [Accessed January 15, 2015].
- Cooley, R. (2002). Burning Questions Catalytic Oxidation Q and A. *ENVIRONMENTAL PROTECTION-WACO-*, 13(2), pp. 12-17.
- Coronas, J. & Santamaria, J. (1999). Catalytic reactors based on porous ceramic membranes. *Catalysis Today*, 51(3), pp. 377-389.
- Coronas, J., Menendez, M. & Santamaria, J. (1995). Use of a ceramic membrane reactor for the oxidative dehydrogenation of ethane to ethylene and higher hydrocarbons. *Industrial & Engineering Chemistry Research*, 34(12), pp. 4229-4234.
- Cui, Y., Kita, H., & Okamoto, K. I. (2004). Preparation and gas separation performance of zeolite T membrane. *Journal of Materials Chemistry*, 14(5), 924-932.
- Delagrangé, S., Pinard, L. & Tatibouet, J. M. (2006). Combination of a non-thermal plasma and a catalyst for toluene removal from air: Manganese based oxide catalysts. *Applied Catalysis B: Environmental*, 68(3), pp.92-98.
- Delimaris, D. & Ioannides, T. (2008). VOC oxidation over MnO_x-CeO₂ catalysts prepared by a combustion method. *Applied Catalysis B: Environmental*, 84(1), pp.303-312.
- Dittmeyer, R., Höllein, V. & Daub, K. (2001). Membrane reactors for hydrogenation and dehydrogenation processes based on supported palladium. *Journal of Molecular Catalysis A: Chemical*, 173(1), pp. 135-184.
- Everaert, K. & Baeyens, J. (2004). Catalytic combustion of volatile organic compounds. *Journal of Hazardous Materials*, 109(1), pp. 113-139.

Gluhoi, A. C., Bogdanchikova, N. & Nieuwenhuys, B. E. (2006). Total oxidation of propene and propane over gold-copper oxide on alumina catalysts: Comparison with Pt/Al₂O₃. *Catalysis Today*, 113(3), pp. 178-181.

Gobina, E. & Hughes, R. (1996). Reaction coupling in catalytic membrane reactors. *Chemical Engineering Science*, 51(11), pp. 3045-3050.

Gobina, E. (2006). *Apparatus and Method for Separating Gases*, United States Granted Patent No. US 7048778, May 23, 2006.

Gopalakrishnan, S. & Diniz da Costa, J.C. (2008). Hydrogen gas mixture separation by CVD silica membrane. *Journal of Membrane Science*, 323(1), pp. 144-147.

Gopalakrishnan, S., Yoshino, Y., Nomura, M., Nair, B. N. & Nakao, S-I. (2007). A hybrid processing method for high performance hydrogen-selective silica membranes. *Journal of Membrane Science*, 297(1), pp. 5-9.

Guanzhong, L., Shoucang, S. & Ren, W. (1996). Direct oxidation of methane to methanol at atmospheric pressure in CMR and RSCMR. *Catalysis Today*, 30(1), pp. 41-48.

http://edgar.jrc.ec.europa.eu/news_docs/jrc-2014-trends-in-global-co2-emissions-2014-report-93171.pdf (2014). *Trends in global CO₂ emissions: 2014 Report*. Netherlands: PBL and JRC. [Accessed on 01/05/2015].

Heck, R. M., Farrauto, R. J. & Gulati, S. T. (2010). Catalytic Air Pollution Control: Commercial Technology, 3rd Edition. *Platinum Metals Rev.*, 54(3), pp. 180-183.

Howard, B. H. & Morreale, B. D. (2008). Effect of H₂S on performance of Pd₄Pt alloy membranes. *Energy Materials*, 3(3), pp. 177-185.

Hsieh, H. P. (1996). *Inorganic Membranes for Separation and Reaction*. Elsevier. Amsterdam, The Netherlands.

Huang, P., Xu, N., Shi, J. & Lin, Y. S. (1997). Recovery of volatile organic solvent compounds from air by ceramic membranes. *Industrial & Engineering Chemistry Research*, 36(9), pp. 3815-3820.

Hubbell, B. J., Crume, R. V., Everts, D. M. & Cohen, J. M. (2010). Policy Monitor: Regulation and Progress under the 1990 Clean Air Act Amendments Rev. *Environ. Econ. Policy*, 4(1), pp. 122-138.

- Hwang, S-T. (2001). Inorganic membranes and membrane reactors. *Korean Journal of Chemical Engineering*, 18(6), pp. 775-787.
- Iojoiu, E. E., Walmsley, J., Raeder, H., Bredesen, R., Miachon, S. & Dalmon, J.-A. (2003). Comparison of different support types for the preparation of nanostructured catalytic membranes. *Reviews on Advanced Materials Science*, 5(3), pp. 160-165.
- Irusta, S., Pina, M. P., Menendez, M. & Santamaria, J. (1998). Development and application of perovskite-based catalytic membrane reactors. *Catalysis letters*, 54(1-2), pp. 69-78.
- Jackson, S. D., Willis, J., Mclellan, G. D., Webb, G., Keegan, M. B. T., Moyes, R. B., Simpson, S., Wells, P. B. & Whyman, R. (1993). Supported metal catalysts: preparation, characterization, and function: I. Preparation and physical characterization of platinum catalysts. *Journal of Catalysis*, 139(1), pp. 191-206.
- Jin, Z., Yiqun, F. & Nanping, X. (2010). Preparation and characterization of alumina membranes on capillary supports: effect of film-coating on crack-free membrane preparation. *Chinese Journal of Chemical Engineering*, 18(3), pp. 377-383.
- Julbe, A. & Ayral, A. (2007). Catalytic membrane reactors involving inorganic membranes, A short overview. *In the proceedings of The Second French-Serbian Summer University, held in Vrnjačka Banja, Serbia, from October the 7th to October the 13th, 2007*, pp. 30-43.
- Julbe, A., Farrusseng, D. & Guizard, C. (2001). Porous ceramic membranes for catalytic reactors—overview and new ideas. *Journal of Membrane Science*, 181(1), pp. 3-20.
- Kajama, M. N., Nwogu, N. C. & Gobina, E. (2014). Gas permeation study using porous ceramic membranes. *Energy and Environment Research*, 4(3), pp. 43-49.
- Kajama, M. N., Nwogu, N. C. & Gobina, E. (2014). Hydrogen separation using silica-based composite membranes. *Advanced Materials Research*. Trans Tech Publ. pp. 107-111.
- Kanezashi, M. & Asaeda, M. (2006). Hydrogen permeation characteristics and stability of Ni-doped silica membranes in steam at high temperature. *Journal of Membrane Science*, 271(1), pp. 86-93.
- Keizer, K., Uhlhorn, R. J. R., Van vuren, R. J. & Burggraaf, A. J. (1988). Gas separation mechanisms in microporous modified γ -Al₂O₃ membranes. *Journal of Membrane Science*, 39(3), pp. 285-300.

- Kentish, S. E., Scholes, C. A. & Stevens, G. W. (2008). Carbon dioxide separation through polymeric membrane systems for flue gas applications. *Recent Patents on Chemical Engineering*, 1(1), pp. 52-66.
- Khan, F. I. & Ghoshal, A. K. (2000). Removal of volatile organic compounds from polluted air. *Journal of Loss Prevention in the Process Industries*, 13(6), pp. 527-545.
- Kim, D. H., Kung, M. C., Kozlova, A., Yuan, S. D. & Kung H. H. 2004. Synergism between Pt/Al₂O₃ and Au/TiO₂ in the low temperature oxidation of propene. *Catalysis letters*, 98(1), pp. 11-15.
- Kim, Y-S., Kusakabe, K., Morooka, S. & Yang, S-M. (2001). Preparation of microporous silica membranes for gas separation. *Korean Journal of Chemical Engineering*, 18(1), pp. 106-112.
- Koros, W. J., Ma, Y. H. & Shimidzu, T. (1996). Terminology for membranes and membrane processes (IUPAC Recommendations 1996). *J. Membr. Sci.*, 120(2), pp. 149-159.
- Koutsonikolas, D., Kaldis, S., Sakellaropoulos, G. P., Van Loon, M. H., Dirrix, R. W. J. & Terpstra, R. A. (2010). Defects in microporous silica membranes: Analysis and repair. *Separation and Purification Technology*, 73(1), pp. 20-24.
- Kusakabe, K., S. Sakamoto, T. Saie, & S. Morooka. (1999). Pore Structure of Silica Membranes Formed by a Sol-Gel Technique Using Tetraethoxysilane and Alkyltriethoxysilanes. *Sep. Purif. Tech.*, 16, pp. 139-146.
- Kusakabe, K., S. Yoneshige, A. Murata, & S. Morooka. (1996). Morphology and Gas Permeance of ZSM-5 Type Zeolite Membrane Formed on a Porous α -Alumina Support Tube. *J. Membrane Sci.*, 116, pp. 39-46.
- Lambropoulos, A., Romanos, G., Steriotis, Th., Nolan, J., Katsaros, F., Kouvelos, E., Charalambopoulou, G. & Kanellopoulos, N. (2007). Application of an innovative mercury intrusion technique and relative permeability to examine the thin layer pores of sol-gel and CVD post-treated membranes. *Microporous and Mesoporous Materials*, 99(1), pp. 206-215.
- Lange, C., Storck, S., Tesche, B. & Maier, W. F. (1998). Selective hydrogenation reactions with a microporous membrane catalyst, prepared by sol-gel dip coating. *Journal of Catalysis*, 175(2), pp. 280-293.
- Lee, D. & Oyama, S. T. (2002). Gas permeation characteristics of a hydrogen selective supported silica membrane. *Journal of Membrane Science*, 210(2), pp. 291-306.

- Leenaars, A. F. M. & Burggraaf, A. J. (1985). The preparation and characterization of alumina membranes with ultra-fine pores: Part 3. The permeability for pure liquids. *Journal of Membrane Science*, 24(3), pp. 245-260.
- Lewis, A. E., Kershner, D. C., Paglieri, S. N., Slepicka, M. J. & Way, J. D. (2013). Pd-Pt/YSZ composite membranes for hydrogen separation from synthetic water-gas shift streams. *Journal of Membrane Science*, 437, pp. 257-264.
- Li, A., Zhao, H., Gu, J. & Xiong, G. (1997). Preparation of γ -Al₂O₃ composite membrane and examination of membrane defects. *Science in China Series B: Chemistry*, 40(1), pp. 31-36.
- Li, K. (2007). *Ceramic membranes for separation and reaction*. John Wiley & Sons. London, United Kingdom.
- Lin, Y-S., & Burggraaf, A.J. (1991). Preparation and characterization of high-temperature thermally stable alumina composite membrane. *Journal of the American Ceramic Society*, 74(1), pp. 219-224.
- Liotta, L. F., Ousmane, M., Di Carlo, G., Pantaleo, G., Deganello, G., Boreave, A. & Giroir-Fendler, A. (2009). Catalytic removal of toluene over Co₃O₄-CeO₂ mixed oxide catalysts: comparison with Pt/Al₂O₃. *Catalysis Letters*, 127(3-4), pp. 270-276.
- Liotta, L. F. (2010). Catalytic oxidation of volatile organic compounds on supported noble metals. *Applied Catalysis B: Environmental*, 100(3-4), pp. 403-412.
- Louise, G. (2012). *Doha: Latest figures show global CO₂ emissions are rising*. The Telegraph. Available from: http://www.telegraph.co.uk/earth/environment/climate_change/9717280/Doha-Latest-figures-show-global-CO2emissions-are-rising.html [Accessed 02/10 2013].
- Lu, G. Q., Diniz da Costa, J. C., Duke, M., Giessler, S., Socolow, R., Williams, R. H. & Kreutz, T. (2007). Inorganic membranes for hydrogen production and purification: a critical review and perspective. *Journal of Colloid and Interface Science*, 314(2), pp. 589-603.
- Luebke, D. R., Pennline, H. W. & Myers, C. R. (2005). Surface selective membranes for carbon dioxide separation. Conference Paper: 22nd Annual International Pittsburgh Coal Conference, Pittsburgh, PA, Sept. 12-15, 2005. University of Pittsburgh School of Engineering, Pittsburgh, PA, United States.

- Maira, A. J., Lau, W. N., Lee, C. Y., Yue, P. L., Chan, C. K. & Yeung, K. L. (2003). Performance of a membrane-catalyst for photocatalytic oxidation of volatile organic compounds. *Chemical Engineering Science*, 58(3), pp. 959-962.
- Marécot, P., Fakche, A., Kellali, B., Mabilon, G., Prigent, P. & Barbier, J. (1994). Propane and propene oxidation over platinum and palladium on alumina: Effects of chloride and water. *Applied Catalysis B: Environmental*, 3(4), pp. 283-294.
- Marks, J. R. & Rhoads, T. (1991). Planning saves time and money, when installing VOC controls. *Chemical Processing*, (5), pp. 42.
- Meinema, H. A., Dirrix, R. W. J., Brinkman, H. W., Terpstra, R. A., Jekerle, J. & Kösters, P. H. (2005). Ceramic membranes for gas separation- recent developments and state of the art. *Interceram*, 54(2), pp. 86-91.
- Moretti, E.C. (2002). Reduce VOC and HAP emissions. *Chemical Engineering Progress*, 98(6), pp. 30-40.
- Mukhopadhyay, N., Moretti, E. C. & Nilson, T. (1993). *Current and potential future industrial practices for reducing and controlling volatile organic compounds*. Center for Waste Reduction Technologies, American Institute of Chemical Engineers.
- Mulder, M. (1996). *Basic principles of membrane technology*. Springer Science & Business Media.
- Müller, H., Deller, K., Despeyroux, B., Peldszus, E., Kammerhofer, P., Kühn, W., Spielmannleitner, R. & Stöger, M. (1993). Catalytic purification of waste gases containing chlorinated hydrocarbons with precious metal catalysts. *Catalysis Today*, 17(1), pp. 383-390.
- Nice, K. & Bryant, C. W. (2000). How catalytic converters work. Available From: <http://www.howstuffworks.com/How> [Accessed 02/10 2013].
- Nwogu, N.C., Kajama, M. & Gobina, E. (2015). A study of gas diffusion characteristics on a micro porous composite silica ceramic membrane. *Composite Structures*, 134, pp.1044-1050.
- Nwogu, N.C., Gobina, E. and Kajama, M.N. (2013). Improved carbon dioxide capture using nanostructured ceramic membranes. *Low Carbon Economy*, 4(03), p.125-128.
- Nwogu, N. C., Gobina, E. & Kajama, M. N. (2013). Improved carbon dioxide capture using nanostructured ceramic membranes. *Low Carbon Economy*, 4(3), pp. 125-128.

- Ohwoka, A., Ogbuke, I. & Gobina, E. (2012a). Performance of pure and mixed gas transport in reconfigured hybrid inorganic membranes Pt. 1. *Membrane Technology*, 2012(6), pp. 7-12.
- Ohwoka, A., Ogbuke, I. & Gobina, E. (2012b). Performance of pure and mixed gas transport in reconfigured hybrid inorganic membranes Pt. 2. *Membrane Technology*, 2012(7), pp. 7-9.
- Ojala, S., Pitkäaho, S., Laitinen, T., Koivikko, N. N., Brahmi, R., Gaálová, J., Matejova, L., Kucherov, A., Päivärinta, S., Hirschmann, C., Nevanperä, T., Riihimäki, M., Pirilä, M. & Keiski, R. L. (2011). Catalysis in VOC abatement. *Topics in Catalysis*, 54(16-18), pp. 1224-1256.
- Okal, J. & Zawadzki, M. (2009). Catalytic combustion of butane on Ru/ γ -Al₂O₃ catalysts. *Applied Catalysis B: Environmental*, 89(1), pp. 22-32.
- Othman, M. R., Mukhtar, H. & Ahmad, A. L. (2004). Gas permeation characteristics across nano-porous inorganic membranes. *IJUM Engineering Journal*, 5(2), pp. 17-33.
- Pandey, P. & Chauhan, R. S. (2001). Membranes for gas separation. *Progress in Polymer Science*, 26(6), pp. 853-893.
- Papaefthimiou, P., Ioannides, T. & Verykios, X. E. (1997). Combustion of non-halogenated volatile organic compounds over group VIII metal catalysts. *Applied Catalysis B: Environmental*, 13(3), pp. 175-184.
- Patkar, A. N. & Laznow, J. (1992). Hazardous air pollutant control technologies. *Hazmat World*, 2, pp. 78.
- Paulis, M., Gand'ia, L.M., Gil, A., Sambeth, J., Odriozola, J. A. & Montes, M. (2000). Influence of the surface adsorption-desorption processes on the ignition curves of volatile organic compounds (VOCs) complete oxidation over supported catalysts. *Applied Catalysis B: Environmental*, 26(1), pp. 37-46.
- Paulis, M., Peyrard, H. & Montes, M. (2001). Influence of chlorine on the activity and stability of Pt/Al₂O₃ catalysts in the complete oxidation of toluene. *Journal of Catalysis*, 199(1), pp. 30-40.
- Peureux, J., Torres M., Mozzanega, H., Giroir-Fendler, A. & Dalmon, J-A. (1995). Nitrobenzene liquid-phase hydrogenation in a membrane reactor. *Catalysis Today*, 25(3), pp. 409-415.

- Picasso, G., Quintilla, A., Pina, M. P. & Herguidoet, J. (2003). Total combustion of methyl-ethyl ketone over Fe_2O_3 based catalytic membrane reactors. *Applied Catalysis B: Environmental*, 46(1), pp. 133-143.
- Pina, M. P., Irusta, S., Menéndez, M., Santamaría, J., Hughes, R. & Boag, N. (1997). Combustion of volatile organic compounds over platinum-based catalytic membranes. *Industrial & Engineering Chemistry Research*, 36(11), pp. 4557-4566.
- Pina, M. P., Menéndez, M. & Santamaria, J. (1996). The Knudsen-diffusion catalytic membrane reactor: an efficient contactor for the combustion of volatile organic compounds. *Applied Catalysis B: Environmental*, 11(1), pp. L19-L27.
- Poshusta, J.C., V.A. Tuan, E.A. Pape, R.D. Noble, & J.L. Falconer. (2000). Separation of Light Gas Mixtures Using SAPO-34 Membranes. *AIChE J.*, 46(4), pp. 779-789.
- Radic, N., Grbic, B. & Terlecki-Baricevic, A. (2004). Kinetics of deep oxidation of n-hexane and toluene over $\text{Pt}/\text{Al}_2\text{O}_3$ catalysts: Platinum crystallite size effect. *Applied Catalysis B: Environmental*, 50(3), pp. 153-159.
- Ramachandra, A. M., Lu, Y., Ma, Y. H., Moser, W. R. & Dixonet, A. G. (1996). Oxidative coupling of methane in porous Vycor membrane reactors. *Journal of Membrane Science*, 116(2), pp. 253-264.
- Ruddy, E. N. & Carroll, L. A. (1993). Select the best VOC control strategy. *Chemical Engineering Progress; (United States)*, 89(7).
- Rui, Z., Ji, H. & Lin, Y. S. (2011). Modeling and analysis of ceramic-carbonate dual-phase membrane reactor for carbon dioxide reforming with methane. *International Journal of Hydrogen Energy*, 36(14), pp. 8292-8300.
- Rusu, A. O. & Dumitriu, E. (2003). Destruction of volatile organic compounds by catalytic oxidation. *Environmental Engineering and Management Journal*, 2(4), pp. 273-302.
- Sanchez Marcano, J. G. & Tsotsis, T. T. (2002). *Catalytic membrane reactors and membrane reactors*. Wiley-VCH Verlag GmbH.
- Sanders, D. F, Smith, Z. P, Guo, R, Robeson, L. M, McGrath, J. E, Paul, D. R. & Freeman, B. D. (2013). Energy-efficient polymeric gas separation membranes for a sustainable future: A review. *Polymer*, 54(18), pp. 4729-4761.

- Santos, V. P. Carabineiro Sónia, A. C., Tavares, P. B., Pereira Manuel, F. R., Órfãoa José, J. M. & Figueiredo, J. L. (2010). Oxidation of CO, ethanol and toluene over TiO₂ supported noble metal catalysts. *Applied Catalysis B: Environmental*, 99(1), pp. 198-205.
- Saracco, G. & Montanaro, L. (1995). Catalytic ceramic filters for flue gas cleaning. 1. Preparation and characterization. *Industrial & Engineering Chemistry Research*, 34(4), pp. 1471-1479.
- Saracco, G., Specchia, S. & Specchia, V. (1996). Catalytically modified fly-ash filters for NO_x reduction with NH₃. *Chemical Engineering Science*, 51(24), pp. 5289-5297.
- Saracco, G. & Specchia, V. (1994). Catalytic inorganic-membrane reactors: present experience and future opportunities. *Catalysis Reviews—Science and Engineering*, 36(2), pp. 305-384.
- Saracco, G. & Specchia, V. (1995). Catalytic ceramic filters for flue gas cleaning. 2. Catalytic performance and modeling thereof. *Industrial & Engineering Chemistry Research*, 34(4), pp. 1480-1487.
- Saracco, G. & Specchia, V. (2000). Catalytic filters for the abatement of volatile organic compounds. *Chemical Engineering Science*, 55(5), pp. 897-908.
- Saracco, G., Veldsink, J. W., Versteeg, G. F. & Van Swaaij Wim, P. M. (1995). Catalytic combustion of propane in a membrane reactor with separate feed of reactants—I. Operation in absence of trans-membrane pressure gradients. *Chemical Engineering Science*, 50(12), pp. 2005-2015.
- Saracco, G., Veldsink, J. W., Versteeg, G. F. & Van Swaaij Wim, P. M. (1995). Catalytic combustion of propane in a membrane reactor with separate feed of reactants—II. Operation in presence of trans-membrane pressure gradients. *Chemical Engineering Science*, 50(17), pp. 2833-2841.
- Shah, S. H. Uemura, Y., Yusup, S. and Kusakabe, K. (2011). High temperature separation of hydrogen from mixture of gases by using microporous silica membranes. *Journal of Materials Science and Engineering B*, 1(1), pp. 90-96.
- Shakya, K., Deegan, C. & Hegarty, F. (2015). Determination of the frequency response of an End tidal CO₂ analyser. *The ITB Journal*, 4(2), p.5.

- Sinquin, G., Petit, C., Libs, S., Hindermann, J. P. & Kiennemann, A. (2001). Catalytic destruction of chlorinated C₂ compounds on a LaMnO_{3+δ} perovskite catalyst. *Applied Catalysis B: Environmental*, 32(1), pp. 37-47.
- Smart, S., Liu, S., Serra, J. M., Diniz da Costa, J. C., Iulianelli, A. & Basile A. (2013). *Porous ceramic membranes for membrane reactors*. Handbook of membrane reactors: fundamental materials science, design and optimisation. Woodhead Publishing. Cambridge, United Kingdom 1(8), pp. 298-336.
- Snape, C. E. Perry, R. Casero, P. Rubiera, F. Sakellaropoulos, G. P. Skodras, G. Pinto, F. Tennison, S. & Iaquaniello, G. (2012). Hydrogen separation in advanced gasification processes (Hydrosep). *Directorate-General for Research and Innovation*.
- Sotirchos, S. V. & Burganos, V. N. (1999). Transport of gases in porous membranes. *MRS Bulletin*, 24(03), pp. 41-45.
- Spivey, J. J. & Butt, J. B. (1992). Literature review: deactivation of catalysts in the oxidation of volatile organic compounds. *Catalysis Today*, 11(4), pp. 465-500.
- Splinter, A., Sturmman, J., Bartels, O. & Benecke, W. (2002). Micro membrane reactor: a flow-through membrane for gas pre-combustion. *Sensors and Actuators B: Chemical*, 83(1), pp. 169-174.
- Sun, Y. M. & Khang, S. J. (1988). Catalytic membrane for simultaneous chemical reaction and separation applied to a dehydrogenation reaction. *Industrial & Engineering Chemistry Research*, 27(7), pp. 1136-1142.
- Tahir, S. F. & Koh, C. A. (1999). Catalytic destruction of volatile organic compound emissions by platinum based catalyst. *Chemosphere*, 38(9), pp. 2109-2116.
- Tamaddoni, M., Sotudeh-Gharebagha, R., Nario, S., Hajihosseinzadeh, M. & Mostoufi, N. (2014). Experimental study of the VOC emitted from crude oil tankers. *Process Safety and Environmental Protection*, 92(6), pp. 929-937.
- Thomas, J. M., Thomas, W. J. & Salzberg, H. W. (1967). Introduction to the principles of heterogeneous catalysis. *Journal of the Electrochemical Society*, 114(11), pp. 279C.
- Tiscarño-Lechuga, F., Hill Jr, C. G. & Anderson, M. A. 1996). Effect of dilution in the experimental dehydrogenation of cyclohexane in hybrid membrane reactors. *Journal of Membrane Science*, 118(1), pp. 85-92.

Tonkovich, A. L. Y., Jimenez, D. M., Zilka, J. L. & Roberts, G. L. (1996). Inorganic membrane reactors for the oxidative coupling of methane. *Chemical Engineering Science*, 51(11), pp. 3051-3056.

Tonkovich, A.L.Y., Zilka, J. L., Jimenez, D. M., Roberts, G. L. & Cox, J. L. (1996). Experimental investigations of inorganic membrane reactors: a distributed feed approach for partial oxidation reactions. *Chemical Engineering Science*, 51(5), pp. 789-806.

Tough, I. (2014a). *Introduction to energy dispersive X-ray analysis*. Lecture notes, Robert Gordon University ed.

Tough, I. (2014b). *The variable pressure scanning electron microscope*. Lecture notes, Robert Gordon University ed.

Trimm, D. L. (1991). Thermal stability of catalyst supports. *Studies in Surface Science and Catalysis*, 68, pp. 29-51.

Tsotsis, T. T., Champagnie, A. M., Vasileiadis, S. P., Ziaka, Z. D. & Minet, R. G. (1993). The enhancement of reaction yield through the use of high temperature membrane reactors. *Separation Science and Technology*, 28(1-3), pp. 397-422.

Tsuru, T., Kan-no, T., Yoshioka, T. & Asaeda, M. (2003). A photocatalytic membrane reactor for gas-phase reactions using porous titanium oxide membranes. *Catalysis Today*, 82(1), pp. 41-48.

Uemiya, S. (2004). Brief review of steam reforming using a metal membrane reactor. *Topics in Catalysis*, 29(1-2), pp. 79-84.

Uhlhorn, R. J. R., Keizer, K. & Burggraaf, A. J. (1990). Gas transport and separation properties of ceramic membranes with pores of molecular dimensions. *International Congress on Membranes and Membrane Processes (ICOM'90), Chicago, IL*.

Uhlhorn, R. J. R., Keizer, K. and Burggraaf, A. J. (1992). Gas transport and separation with ceramic membranes. Part I. Multilayer diffusion and capillary condensation. *Journal of Membrane Science*, 66(2), pp. 259-269.

Uzio, D., Miachon, S. & Dalmon, J-A. (2003). Controlled Pt deposition in membrane mesoporous top layers. *Catalysis Today*, 82(1), pp. 67-74.

- Wall, Y., Braun, G. & Brunner, G. (2010). Gas transport through ceramic membranes under super-critical conditions. *Desalination*, 250(3), pp. 1056-1059.
- Way, J.D. & D.L. Roberts. (1992). Hollow Fiber Inorganic Membranes for Gas Separations. *Sep. Sci. Tech.*, 27(1), pp. 29-41.
- Weidenthaler, C. (2011). Pitfalls in the characterization of nanoporous and nanosized materials. *Nanoscale*, 3(3), pp. 792-810.
- Westermann, T. & Melin, T. (2009). Flow-through catalytic membrane reactors—principles and applications. *Chemical Engineering and Processing: Process Intensification*, 48(1), pp. 17-28.
- Wilburg, J. D. & Young, T. M. (1991). Innovations of catalytic combustion. *Innovations of Catalytic Combustion*. 7th-10th October. Honolulu, Hawaii: International Symposium on Environmental Control of Combustion Processes. pp. 1-11.
- William, J. C. & Lead, P. E. (1997). VOC control strategies in plant design. *Chemical Processing: Project Engineering Annual*, 44.
- www.eia.gov/forecasts/ieo/ (2014). *International energy outlook 2014*. Washington: U.S. Energy Information Administration. [Accessed on 12/10/2014].
- www.rgu.ac.uk/file/research-ethics-policy-pdf-146kb (2014). *RGU research ethics policy*. [Accessed on 03/11/2014].
- www.worldometers.info/world-population/?utm_expid=4939992-7.scuhn054Q5WX%20vFD9uRG9Xw.2 (2014). *World population*. Worldometers. [Accessed on 04/10 2014].
- [www.eia.gov/forecasts/ieo/pdf/0484\(2013\).pdf](http://www.eia.gov/forecasts/ieo/pdf/0484(2013).pdf) (2013). *International energy outlook 2013*. Washington: U.S Energy Information Administration. [Accessed on 01/04/2014].
- www.meca.org/galleries/files/hapwp.pdf (1995). *Catalytic oxidation for the control of hazardous organic air pollutants*. Washington DC: manufacturers of emission control association. [Accessed on 29/10/2013].
- Yamada, M., Fugii, K., Haru, H. & Itabashi, K. (1988). Preparation and catalytic properties of special alumina membrane formed by anodic oxidation of aluminum. *The Light Metal Educational Foundation, Inc., Report of the Research Group for Functionalizing of Aluminum and Its Surface Films*, pp. 175-182
- Yampolskii, Y. & Freeman, B. (2010). *Membrane gas separation*. Wiley Online Library.

- Yildirim, Y. & Hughes, R. (2002). The efficient combustion of o-xylene in a Knudsen controlled catalytic membrane reactor. *Process Safety and Environmental Protection*, 80(3), pp. 159-164.
- Yildirim, Y. & Hughes, R. (2003). An experimental study of CO₂ separation using a silica based composite membrane. *Process Safety and Environmental Protection*, 81(4), pp. 257-261.
- Yoshino, Y., Suzuki, T., Nair, B. N., Taguchi, H. & Itoh, N. (2005). Development of tubular substrates, silica based membranes and membrane modules for hydrogen separation at high temperature. *Journal of Membrane Science*, 267(1), pp. 8-17.
- Zalamea, S., Pina, M. P., Vilellas, A., Menéndez, M. & Santamaría, J. (1999). Combustion of volatile organic compounds over mixed-regime catalytic membranes. *Reaction Kinetics and Catalysis Letters*, 67(1), pp. 13-19.
- Zhang, L., Park, I. S., Shqau, K., Ho, W. W., & Verweij, H. (2009). Supported inorganic membranes: promises and challenges. *JOM*, 61(4), pp. 61-71.
- Zhu, J., Fan, Y. & Xu, N. (2011). Modified dip-coating method for preparation of pinhole-free ceramic membranes. *Journal of Membrane Science*, 367(1), pp. 14-20.